

The Electrochemical Detection and Characterisation of Single Nanoparticles

A thesis submitted for the degree of Doctor of Philosophy
in Physical and Theoretical Chemistry

Emma J. E. Stuart
Hertford College

August 2014

Abstract

This thesis presents experimental work with the primary aim of developing new approaches for the detection and characterisation of nanoparticles *via* electrochemical methods. The first chapter introduces the fundamental aspects of electrochemistry while the second chapter discusses the need for nanoparticle detection methods and the non-electrochemical and electrochemical techniques that are currently used in the measurement of nanoparticles.

A novel way to quantify silver nanoparticles in aqueous solution is proposed *via* nanoparticle-electrode impact experiments. In this technique a suitably potentiostatted electrode is immersed in a nanoparticle solution so as to bring about the oxidation or reduction of a single nanoparticle upon its collision with the electrode surface. This "direct" nanoparticle impact technique is then employed to detect laboratory synthesised silver nanoparticles in seawater. It is further shown that this method is capable of sizing silver nanoparticles contained in a commercially available cleaning product. Commercial silver nanoparticles are subsequently monitored *via* a sticking and stripping technique where homemade gold electrodes fabricated from CDs are immersed in a seawater sample spiked with nanoparticles prior to stripping voltammetry.

The reduction of hydrogen peroxide on the surface of silver nanoparticles impacting upon an electrode is also examined. This "indirect" nanoparticle detection method is shown to provide an accurate route to nanoparticle sizing. A Fickian model is subsequently proposed to describe nanoparticle transport to the substrate electrode in both direct and indirect nanoparticle detection techniques. The importance of determining the proportion of nanoparticles which adhere to the electrode surface upon impact is highlighted and the sticking coefficient of a gold nanoparticle at a carbon surface determined. This technique to monitor nanoparticle sticking is optimised by chemical modification of the substrate electrode in order to achieve a "sticky" surface improving the rate of silver nanoparticle sticking.

Finally, the nanoparticle collision method is shown to be applicable to C_{60} nanoparticles where their detection and sizing is achieved in non-aqueous conditions. The methods developed in this thesis make a significant contribution to the promising application of electrochemical techniques in the detection and characterisation of single nanoparticles.

Acknowledgements

First and foremost I would like to thank my supervisor, Professor Richard Compton, for welcoming me into his research group and for being just a door knock (and sometimes a long queue!) away when I have needed any help or advice over the last three years. Thank you for providing me with such amazing opportunities and experiences during my time here. Thanks must also go to Professor Martin Pumera who took me in when I found myself wondering the halls of a Singaporean university-I would not have found my way to the Compton group without you.

Thank you to all of the members of the Compton group, past and present, for making the lab such an enjoyable place to work in. In particular, thanks to the other members of my year group, Min, Eddy, Lin and Ying, with whom I have gone through this experience; their dinners, company and laughter has been an immeasurable support over the last three years-we have finally made it! To Neil and Kristina, the postdocs who have helped to supervise me, thank you for always being willing to answer my stupid questions (and for pretending that they weren't stupid)-your neverending positive attitudes and reassurance has been much appreciated. Thanks also to the now Dr Yige Zhou for introducing me to the wonders of impact experiments, I miss celebrating with you when we get spikes and then commiserating with you when we actually have to count them!

I am also very grateful to my college, Hertford, who have provided me with a home, lots of dinners, generous travel grants and even a job for the last year. Thank you Rich for putting up with me for these three years when I am sure others would have not and thanks also to my grandfather who has always been so supportive although I know he is secretly very pleased I have finally found myself a 'real' job!

Finally, to my parents, who have always worked so hard to give us such wonderful opportunities-thank you.

Contents

1 Fundamentals of Electrochemistry **3**
1.1 Electrolysis . . . 3
1.2 The Electrochemical Cell . . . 4
1.3 Faradaic and Non-Faradaic Processes . . . 5
1.4 The Electrical Double Layer . . . 6
1.5 Mass Transport . . . 7
1.6 Electrode Kinetics . . . 10
1.7 Experimental Techniques . . . 11
1.8 Microelectrodes . . . 13
Bibliography . . . 16

2 Nanoparticles: Emerging Contaminants **18**
2.1 Nanoparticles in the Environment and the Need for Monitoring . . . 19
2.2 Non-Electrochemical Approaches to Detect Nanoparticles and their Limitations . . . 21
2.3 Electrochemical Approaches to Detect Nanoparticles . . . 26
2.4 Outlook . . . 44
Bibliography . . . 45

3 Experimental Methods **50**
3.1 Chemical Reagents . . . 50
3.2 Nanoparticle Synthesis . . . 50
3.3 Electrochemical Methods . . . 53
3.4 Non-Electrochemical Methods . . . 57
Bibliography . . . 58

4 Determining Unknown Concentrations of Silver Nanoparticles *via* Anodic Particle Coulometry **59**
4.1 Introduction . . . 60
4.2 Experimental Procedure . . . 62
4.3 Results and Discussion . . . 63
4.4 Conclusions . . . 70
Bibliography . . . 71

5 Direct Electrochemical Detection and Sizing of Silver Nanoparticles in Seawater Media **73**
5.1 Introduction . . . 74

5.2 Experimental Procedure . . . 75
5.3 Results and Discussion . . . 78
5.4 Conclusions . . . 85
Bibliography . . . 85

6 Electrochemical Detection of Commercial Silver Nanoparticles: Identification, Sizing and Detection in Seawater Media 88
6.1 Introduction . . . 89
6.2 Experimental Procedure . . . 90
6.3 Results and Discussion . . . 92
6.4 Conclusions . . . 101
Bibliography . . . 102

7 Gold Electrodes from Recordable CDs for the Sensitive, Semi-Quantitative Detection of Commercial Silver Nanoparticles in Seawater Media 104
7.1 Introduction . . . 105
7.2 Experimental Procedure . . . 108
7.3 Results and Discussion . . . 112
7.4 Conclusions . . . 122
Bibliography . . . 123

8 Particle-impact Voltammetry: The Reduction of Hydrogen Peroxide at Silver Nanoparticles Impacting a Carbon Electrode 125
8.1 Introduction . . . 126
8.2 Experimental Procedure . . . 128
8.3 Results and Discussion . . . 129
8.4 Conclusions . . . 136
Bibliography . . . 137

9 A Fickian Model for Nanoparticle Transport and the Importance of Determining the Sticking Coefficient 139
9.1 Introduction . . . 140
9.2 Experimental Procedure . . . 141
9.3 Results and Discussion . . . 144
9.4 Conclusions . . . 156
Bibliography . . . 156

10 Improving the Rate of Silver Nanoparticle Adhesion to "Sticky Electrodes": Stick and Strip Experiments at a DMSA-modified Gold Electrode **158**
10.1 Introduction 159
10.2 Experimental Procedure 161
10.3 Results and Discussion 163
10.4 Conclusions 173
Bibliography 173

11 Electrochemical Observation of Single Collision Events: Fullerene Nanoparticles **175**
11.1 Introduction 176
11.2 Experimental Procedure 178
11.3 Results and Discussion 180
11.4 Conclusions 191
Bibliography 192

12 Conclusions **195**

Glossary

Roman Symbols

Symbol	Definition	Units
A_{e}	Electrode area	m^2
A_{NP}	Nanoparticle area	m^2
C	Concentration	$\mathrm{mol\ m}^{-3}$
C_{t}	Concentration at time, t	$\mathrm{mol\ m}^{-3}$
C_0	Concentration at t=0	$\mathrm{mol\ m}^{-3}$
D	Diffusion coefficient	$\mathrm{m}^2\ \mathrm{s}^{-1}$
D_{2D}	Two-dimensional diffusion coefficient	$\mathrm{m}^2\ \mathrm{s}^{-1}$
e	Elementary charge (1.602×10^{-19})	C
E	Applied potential	V
E_{exp}	Exposure potential	V
E^0_{f}	Formal potential	V
f_{s}	Frequency of impact spikes	s^{-1}
F	The Faraday constant (96485)	$\mathrm{C\ mol}^{-1}$
I	Current	A
j	Flux	$\mathrm{mol\ m}^{-2}\ \mathrm{s}^{-1}$
k	Rate constant	
k_{B}	The Boltzmann constant (1.380×10^{-23})	$\mathrm{J\ K}^{-1}$
k_{ox}	Heterogeneous rate constant for oxidation	$\mathrm{m\ s}^{-1}$
k_{red}	Heterogeneous rate constant for reduction	$\mathrm{m\ s}^{-1}$
k^0	Standard heterogeneous rate constant	$\mathrm{m\ s}^{-1}$
m	Number of moles	mol
M	Molar mass	$\mathrm{kg\ mol}^{-1}$
n	Number of electrons transferred	
N	Cumulative number of impact spikes	
N_{A}	The Avagadro constant (6.022×10^{23})	mol^{-1}
N_{ads}	Rate of atom adsorption	s^{-1}
N_{NP}	Number of atoms in a nanoparticle	
P_{ads}	Rate of nanoparticle adsorption	s^{-1}
Q	Charge	C
r	Radius	m
r_{e}	Electrode radius	m
r_{NP}	Nanoparticle radius	m
R	The Gas constant (8.314)	$\mathrm{J\ K\ mol}^{-1}$
R_{NP}	Nanoparticle cluster radius	m
s	Sticking coefficient	
S	Salinity	
t	Time	s
T	Temperature	K

Greek Symbols

Symbol	Definition	Units
α	Butler-Volmer transfer coefficient for reduction	
β	Butler-Volmer transfer coefficient for oxidation	
η	Viscosity	kg $m^{-1}s^{-1}$
γ	Surface energy	J m^{-2}
Γ	Surface coverage	mol m^{-2}
λ	Wavelength	m
ν	Scan rate	V s^{-1}
ρ	Density	kg m^{-3}
τ	Dimensionless time	
χ	Number of nanoparticles in a cluster	

Abbreviations

Abbreviation	Definition
AFM	Atomic Force Microscopy
AgNP	Silver Nanoparticle
APC	Anodic Particle Coulometry
CD	Compact Disc
CE	Counter Electrode
CPC	Cathodic Particle Coulometry
CV	Cyclic Voltammetry
DLS	Dynamic Light Scattering
GC	Glassy Carbon
ICP-MS	Inductively Coupled Plasma-Mass Spectrometry
IHP	Inner Helmholtz Plane
nano-C_{60}	C_{60} Nanoparticle
NHE	Normal Hydrogen Electrode
NP	Nanoparticle
NTA	Nanoparticle Tracking Analysis
OCP	Open Circuit Potential
OHP	Outer Helmholtz Plane
RE	Reference Electrode
SCE	Saturated Calomel Electrode
SEM	Scanning Electron Microscopy
TEM	Transmission Electron Microscopy
UV-VIS	Ultraviolet-Visible
WE	Working Electrode

Chapter 1

Fundamentals of Electrochemistry

This thesis is concerned with the use of electrochemistry for the detection and characterisation of nanoparticles. This chapter provides an elementary introduction to the fundamental understanding behind electrochemistry and the techniques that can be employed in order to study electrochemical reactions. Fuller discussions are available in numerous electrochemical textbooks[1–5] and are presented as required throughout the parts of this thesis dealing with experimental results and their interpretation.

1.1 Electrolysis

The term electrolysis refers to chemical changes that accompany Faradaic reactions at electrodes that are in contact with an electrolyte[1], for example the decomposition of A to B *via* the transfer of n electrons.

$$\mathrm{A} + n\mathrm{e}^- \leftrightharpoons \mathrm{B} \tag{1.1}$$

In 1834 Faraday studied the electrolysis of water and concluded that[6]:

> *"when subjected to the influence of the electric current, a quantity of [water] is decomposed exactly proportionate to the quantity of electricity which has passed"*

Therefore it is possible to study the extent of a chemical reaction by studying the

quantity of electricity, or charge Q, passed. The above statement can be expressed as equation 1.2[2] and is known as Faraday's law of electrolysis:

$$m = \frac{Q}{nF} \tag{1.2}$$

where the number of moles of formed product or consumed reactant is given by m and F is the Faraday constant (96485 C mol^{-1}). The Faraday constant is the value of the charge of 1 mole of electrons i.e. 1.602×10^{-19} C (e) $\times$ 6.022×10^{23} mol^{-1} (N_{A}) = F.

1.2 The Electrochemical Cell

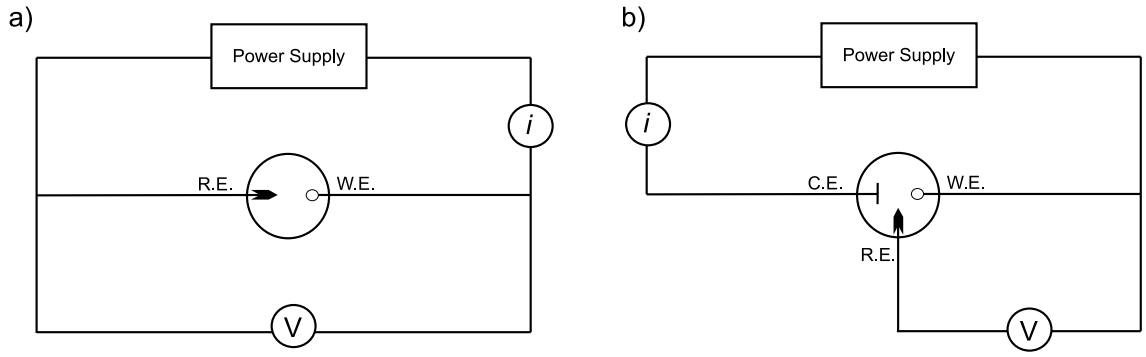


Figure 1.1: Schematic diagram of a) a two electrode cell and b) a three electrode cell showing the working electrode (W.E.), reference electrode (R.E.) and counter electrode (C.E.)[1].

Faraday studied the electrolysis of water using a two electrode cell where a power supply is used to apply a potential between two electrodes immersed in solution resulting in a flow of electrons through the external circuit as an electrochemical reaction occurs at the working electrode (figure 1.1a). This approach is valid for systems where the currents passed are very low, for example at a working electrode of micron dimensions[2, 3]. When this is not the case, current may be drawn through the reference electrode compromising

its composition and thereby its ability to hold a constant potential[2]. Therefore a third electrode, the counter electrode, must be introduced to pass an equivalent amount of current to that flowing through the working electrode to ensure the current passed at the working electrode-solution interface is measured with respect to the applied potential at the same electrode. A diagram of this three electrode set-up is shown in figure 1.1b.

1.3 Faradaic and Non-Faradaic Processes

1.3.1 Faradaic Processes

Faradaic processes are dictated by Faraday's law (equation 1.2) and therefore result from the transfer of electrons at the solution-electrode interface. A number of processes can influence the observed Faradaic current response for a simple electrode reaction, most importantly the mass transport of reactants and products to and from the electrode surface respectively and the rate of electron transfer across the electrode-solution interface. Faraday's law assumes that the flow of electrons through the external circuit results wholly from Faradaic processes. However, in reality, non-Faradaic processes can also occur when an electrode reaction takes place. The majority of electrochemical studies focus on Faradaic processes however if quantitative information is to be extracted from electrochemical data it is vital to consider that a proportion of the measured current may result from non-Faradaic contributions[1].

1.3.2 Non-Faradaic Processes

The term non-Faradaic process applies to any reaction where electrons do not cross the electrode-solution interface. Non-Faradaic current can result from adsorption and desorp-

tion at the electrode surface as well as changes in the solution composition at the interface when the potential of the electrode is changed. Contributions to the current response that are a result of these changes in solution composition at the electrode-solution interface are referred to as capacitative charging currents as reorganisation of charged species in the vicinity of the interface, known as the electrical double layer, occurs. A description of the electrical double layer can be found in section 1.4. The study of non-Faradaic currents that result from capacitative charging of the double layer is a rapidly developing research area with promising application in energy storage[7–10].

1.4 The Electrical Double Layer

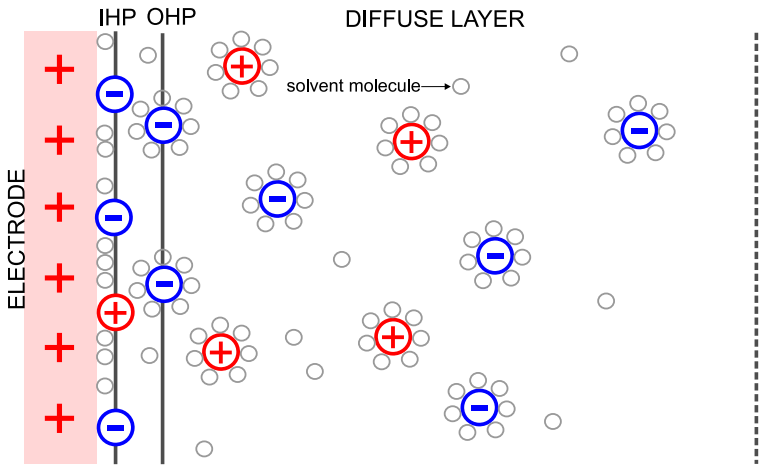


Figure 1.2: Schematic representation of the electrical double layer

When an electrode is immersed in solution and a potential is applied the ions and solution dipoles adjacent to the charged electrode surface are redistributed. This array of ions and orientated dipoles is termed the electrical double layer.

A number of models have been developed to describe the structure of the double layer with the most simplest being proposed by Helmholtz in [11] and [12]. This model was later improved by Gouy[13, 14] and Chapman[15] before being further developed by Stern[16]

and Grahame[17]. Figure 1.2 shows a schematic diagram of the double layer region. Closest to the electrode are ions and solvent molecules in solution that are specifically adsorbed at the surface where the position of their electrical centres is at a distance of x_1 from the electrode surface which is referred to as the inner Helmholtz plane (IHP). A specifically adsorbed ion is not solvated and binds strongly to the electrode surface, these ions can have either the same or opposite charge to the electrode surface[5]. The outer Helmholtz plane (OHP) is at a distance x_2 from the electrode surface and is the closest distance to which solvated ions can approach the electrode. These solvated ions are nonspecifically adsorbed and exist in the diffuse layer which ranges from the OHP to bulk solution[1]. The potential decreases linearly with distance from the electrode surface to the OHP at which point the decrease becomes exponential until bulk solution is reached.

1.5 Mass Transport

In order for an electrode reaction to occur, it is necessary for the reactant molecules in solution to be transported to the electrode interface from the bulk solution and the products to be transported in the opposite direction. This net movement of material is known as mass transport. There are three modes of mass transport: diffusion, convection and migration. Each of these processes are summarised below.

1.5.1 Diffusion

In order for diffusive flux to occur a concentration gradient is required. For an electrode reaction, when a suitable potential is applied, the reactant is consumed at the electrode surface reducing the concentration of this species in the vicinity of the electrode and

thereby providing the drive for diffusion from the bulk solution to the interface.

The number of moles passing through a unit area in a unit time is defined as the flux, j, which is directly proportional to the measured current, I:

$$j = \frac{I}{nFA_{\mathrm{e}}} \tag{1.3}$$

where A_{e} is the electrode area. The flux at a distance from the electrode surface, x, can be quantified by Fick's first law[18]:

$$j = -D\frac{\partial c}{\partial x} \tag{1.4}$$

where $\frac{\partial c}{\partial x}$ is the concentration gradient at x and D is the diffusion coefficient.

Fick's second law[18] is used to describe how the concentration of a species at x varies with time, t:

$$\frac{\partial c}{\partial t} = D\frac{\partial^2 c}{\partial x^2} \tag{1.5}$$

Equation 1.5 can be used to derive the Cottrell equation[19] which predicts the current response for a potential-step chronoamperometry experiment as described in section 1.7.2.

1.5.2 Convection

Convection refers to the movement of species caused by external mechanical forces acting upon a solution. There are two types of convection: natural convection and forced convection. Movement in solution by natural convection results from density and thermal gradients caused by a chemical change occurring at the electrode surface when a potential

is applied. This type of convection is unpredictable and can be the cause of experimental irreproducibility. In order to overcome this problem forced convection is often employed. The application of forced convection must be controlled and quantitative and can be achieved *via* stirring or sparging the solution with inert gas. Forced convection can also be used to deliver electroactive species to the electrode surface at a known rate with, for example, a rotating disc electrode[20–22].

1.5.3 Migration

The final mass tranport process, migration, only affects charged species. The movement of these charged species in solution occurs in the presence of an external electric field at the electrode-solution interfacial region resulting from a difference in potential between the electrode and solution. In order to eliminate the effects of migration, a concentration of supporting electrolyte that is much larger than that of the elecroactive species is used to ensure it is the electrolytic ions that undergo the majority of migratory movement as opposed to the electroactive species[4]. The supporting electrolyte also acts to compress the electrical double layer (section 1.4) to a region immediately adjacent to the electrode surface that is compatible with electron tunnelling (approximately 10-20 Å[2]) so that the potential difference from the electrode surface to bulk solution is also limited to this region and electrochemical rate constants (described in section 1.6) can be accurately determined.

1.6 Electrode Kinetics

Following the arrival of the electroactive species of interest from bulk solution to the electrode surface *via* mass transport, the rate at which electron transfer at the interface occurs needs to be considered.

Consider a typical one electron reaction:

$$\mathrm{A} + \mathrm{e}^- \underset{k_{\mathrm{ox}}}{\overset{k_{\mathrm{red}}}{\rightleftharpoons}} \mathrm{B} \tag{1.6}$$

where k_{red} and k_{ox} are the heterogenous rate constants for the reduction and oxidation respectively.

The Butler-Volmer equation[23, 24] is the most widely accepted model of electrode kinetics and predicts the rate constants to be potential dependent by:

$$k_{\mathrm{red}} = k^0 \exp\left[\frac{-\alpha F}{RT}\left(E - E^0_{\mathrm{f}}\right)\right] \tag{1.7}$$

$$k_{\mathrm{ox}} = k^0 \exp\left[\frac{+\beta F}{RT}\left(E - E^0_{\mathrm{f}}\right)\right] \tag{1.8}$$

where k^0 is the standard heterogenous rate constant, α and β are the transfer coefficients where typically $\alpha + \beta = 1$ and $E - E^0_{\mathrm{f}}$ is the "overpotential" where applied potential (E) is related to the formal potential (E^0_{f}).

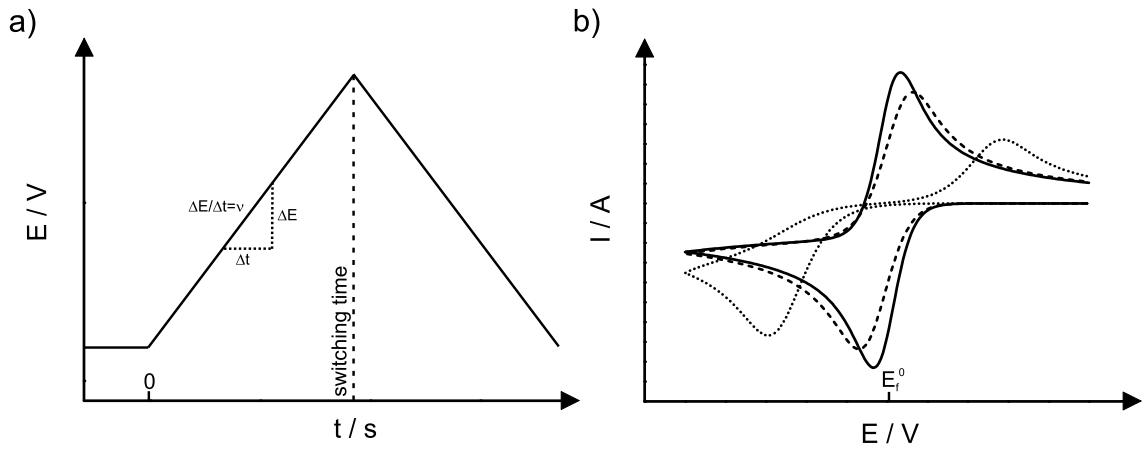


Figure 1.3: a) Potential *vs.* time sweep and b) resulting cyclic votltammetric profiles at a macroelectrode for a reversible (solid line), quasi-reversible (dashed line) and irreversible system (dotted line).

1.7 Experimental Techniques

1.7.1 Cyclic Voltammetry

In cyclic voltammetry a potential is applied to a working electrode and varied with time before the potential scan is reversed and swept in the opposing direction. Figure 1.3a shows how the slope of the potential-time profile relates to the scan rate, ν. The potential range scanned is selected to be one in which an oxidation or reduction reaction will occur. The current flow at the working electrode is measured as a function of the applied potential and current-potential curves, known as cyclic voltammograms, are obtained.

A typical cyclic voltammogram for a general reversible diffusional system ($A + e^- \rightleftharpoons B$) is shown in figure 1.3b (solid line). With reference to this voltammogram it can be seen that no electron transfer occurs at the starting potential as there is negligible current flow, the potential is then swept in the negative direction and as the electroactive species is reduced at the electrode surface an increase in the current results. The flux of material from the bulk solution to the interface increases as a concentration gradient is established

before the rate of mass transport reaches a maximum and the current decreases giving rise to the observed peak in the voltammogram. An analogous peak is seen in the reverse scan of the voltammogram as the formed product, B, is re-oxidised.

The three voltammetric profiles shown in figure 1.3b correspond to a reversible (solid line), quasi-reversible (dashed line) and irreversible (dotted line) system. Cyclic voltammetry clearly can be used to provide information on the reversibility of the electrode reaction. A system is classified as "reversible" if the electrode kinetics are sufficiently fast, and therefore the value for k^0 is large, in relation to the rate of mass transport (m_T). If the converse is true and $k^0 << m_T$ the system is said to be "irreversible". In the reversible case the oxidised and reduced species will be in equilibrium at the electrode surface so the anodic and cathodic peaks will be observed at potentials close to the formal potential, E^0_f, of the redox couple as shown in figure 1.3b. For an irreversible system these peaks are shifted to significantly different potentials from those in the reversible voltammogram as a large overpotential is required to drive the electrode reaction. A quasi-reversible system is intermediate to these two extreme cases.

This technique can also be used to quantify electrochemical rate constants[25] and determine if a system is diffusional or surface bound[26].

1.7.2 Chronoamperometry

Chronamperometric measurements involve the application of a large potential step at t=0 where the potential is changed from a value where no electrode reaction occurs (E_1) to one at which all of the electroactive species in the vicinity of the electrode is either oxidised or reduced (E_2) depleting its concentration at the electrode surface to zero (figure 1.4a). The resulting concentration gradient causes diffusion of electroactive species from the

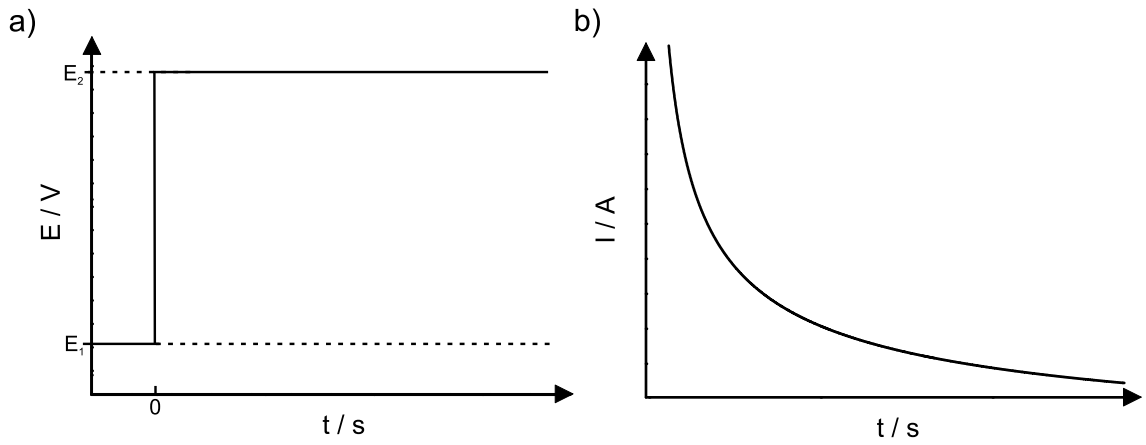


Figure 1.4: a) Application of a potential step at t=0 and b) resulting chronoamperomogram for a macroelectrode

bulk solution to the electrode-solution interface. With increasing time the diffusion layer becomes thicker, reducing the rate of diffusion to the electrode surface and a decrease in current is observed as shown in figure 1.4b.

Where diffusion to an electrode is linear i.e. at a macroelectrode the resulting current response from a potential step can be described by the Cotrrell equation[19]:

$$I = \frac{nFA\sqrt{DC}}{\sqrt{\pi t}} \tag{1.9}$$

where C is the concentration. The Cottrell equation states that the decay of current resulting from a potential step will be inversely proportional to the square root of time and will reach zero at infinite time.

1.8 Microelectrodes

Due to their small size, diffusion to microelectrodes is significantly different to that at a macroelectrode. Figure 1.5 demonstrates the convergent diffusion regime that dominates at a microdisc in comparison to linear diffusion at a larger macro-sized electrode.



Figure 1.5: Schematic diagram comparing linear and convergent diffusion

1.8.1 Voltammetry at Microelectrodes

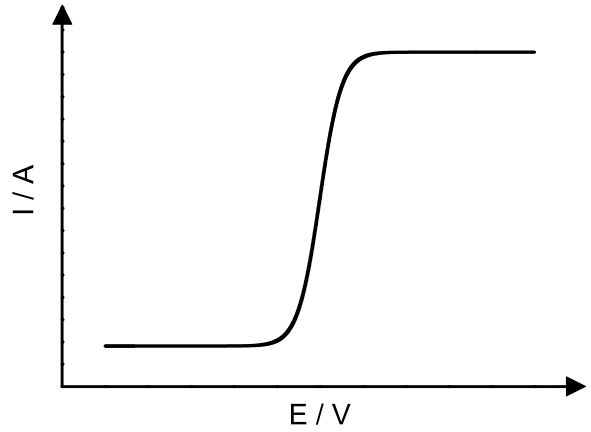


Figure 1.6: Cyclic voltammogram measured at a microelectrode

This changed diffusion regime has an appreciable influence on the appearance of cyclic voltammograms measured at a microelectode at sufficiently slow scan rates (figure 1.6) as opposed to voltammetric profiles observed at macroelectrode (figure 1.3b). As explained in section 1.7.1, the peak shaped response observed in voltammetric scans for a macroelectrode results from a fall off in the measured current as the electroactive species is depleted at the electrode-solution interface and the electrode reaction becomes limited by diffusion. At a microelectrde the convergent diffusion regime results in a faster flux of material to and from the electrode surface thereby steady state conditions are achieved in

a shorter time scale. In the resulting steady state voltammogram the reverse scan retraces the forward sweep.

The steady state current at a microelectrode is given by equation 1.10:

$$I = 4nFCDr_e \tag{1.10}$$

where r_e is the radius of the electrode.

If voltammetry at a microelectrode is scanned at sufficiently high scan rates anodic and cathodic peaks begin to appear in the observed voltammetric profile and the shape becomes similar to that shown for a macroelectrode in figure 1.3b[3, 27].

1.8.2 Chronoamperometry at Microelectrodes

When a potential step is applied to a microelectrode its behaviour can be described as Cottrellian at very short times where diffusion to the electrode surface is linear and the decay of current is proportional to $\frac{1}{\sqrt{t}}$ as dictated by equation 1.9. Here, the diffusion layer thickness is smaller than the electrode radius. However, with time, the diffusion layer expands hemispherically as a convergent diffusion regime is established and steady state conditions are reached.

Equation 1.11 describes the current response at a microdisc electrode after the application of a potential step[2].

$$I = 4nFCDr_e f(\tau) \tag{1.11}$$

A single expression $f(\tau)$ to describe the current-time transient over the entire time domain has been developed by Shoup and Szabo[28]:

$$f(\tau) = 0.7854 + 0.8863\tau^{-1/2} + 0.2146\exp(0.7823\tau^{-1/2}) \quad (1.12)$$

where $\tau = 4Dt/r_e^2$. This equation is regularly used in the analysis of chronomaperometric profiles measured at microdisc electrodes[29–31], more detail on the Shoup and Szabo expression can be found in chapter 4.

Bibliography

[1] A. J. Bard and L. R. Faulkner, *Electrochemical Methods: Fundamentals and Applications* (John Wiley & Sons, Inc., New York, 2001), second edition.

[2] R. G. Compton and C. E. Banks, *Understanding Voltammetry* (Imperial College Press, London, 2011), second edition.

[3] P. H. Reiger, *Electrochemistry* (Chapman & Hall, London, 1993), second edition.

[4] D. Pletcher, *A First Course in Electrode Processes* (The Electrochemical Consultancy, Romsey, 1991), first edition.

[5] C. M. A. Brett and A. M. O. Brett, *Electrochemistry:Principles, Methods and Applications* (Oxford University Press, Oxford, 1993), first edition.

[6] M. Faraday, *Philos. Trans. R. Soc. London* **124** (1834) 77–122.

[7] R. Holze and W. Vielstich, *Electrochim. Acta* **29** (1984) 607–610.

[8] J. Benson, S. Boukhalfa, A. Magasinski, A. Kvit and G. Yushin, *ACS Nano* **6** (2012) 118–125.

[9] H. Huang, C. Huang, C. Hsieh and H. Teng, *J. Mater. Chem. A* DOI:10.1039/C4TA01468E.

[10] P. S. Simon and Y. Gogotsi, *Nature Mat.* **7** (2008) 845–854.

[11] H. L. F. von Helmholtz, *Ann. Phys.* **165** (1853) 211–233.

[12] H. L. F. von Helmholtz, *Ann. Phys.* **243** (1879) 337–382.

[13] G. Gouy, *J. Phys.* **9** (1910) 457–467.

[14] G. Gouy, *Compt. Rend.* **149** (1910) 654–657.

[15] D. L. Chapman, *Philos. Mag.* **25** (1913) 475.

[16] O. Stern, *Z. Electrochem.* **30** (1924) 508–516.

[17] D. C. Grahame, *Chem. Rev.* **41** (1947) 441–501.

[18] A. Fick, *Poggendorff's Annel. Physik.* **94** (1855) 59–86.

[19] F. G. Cottrell, *Z. Physik. Chem.* **44** (1902) 385–431.

[20] J. J. Concepcion, R. A. Binstead, L. Alibabaei and T. J. Meyer, *Inorg. Chem.* **52** (2013) 10744–10746.

[21] J. Herranz, A. Garsuch and H. A. Gasteiger, *J. Phys. Chem. C* **116** (2012) 19084–19094.

[22] Y. Lu, Q. He and H. A. Gasteiger, *J. Phys. Chem. C* **118** (2014) 5733–5741.

[23] J. A. Z. Butler, *Trans. Faraday Soc.* **19** (1924) 729–733.

[24] T. Erdey-Gruz and M. Volmer, *Z. Physik. Chem.* **150** (1930) 203–213.

[25] C. Cannes, F. Kanoufi and A. J. Bard, *J. Electroanal. Chem.* **547** (2003) 83–91.

[26] L. M. Goncalves, C. Batchelor-McAuley, A. A. Barros and R. G. Compton, *J. Phys. Chem. C* **114** (2010) 14213–14219.

[27] J. Heinze and M. Storzbach, *Ber. Bunsenges. Phys. Chem.* **90** (1986) 1043–1048.

[28] D. Shoup and A. Szabo, *J. Electroanal. Chem. Interfacial Electrochem.* **140** (1982) 237–245.

[29] E. J. E. Stuart, Y. G. Zhou, N. V. Rees and R. G. Compton, *RSC Adv.* **2** (2012) 6879–6884.

[30] L. Xiong, E. O. Barnes and R. G. Compton, *Sens. Actuators, B* **200** (2014) 157–166.

[31] Y. Hishida, M. Nishi, Y. Baba and H. Ikeuchi, *Anal. Sci.* **22** (2006) 931–935.

Chapter 2

Nanoparticles: Emerging Contaminants

Nanoparticles result in the environment from natural sources and human manufacturing processes. It is important that these can be quantified given the uncertainties surrounding their effects on human health. This chapter summarises the non-electrochemical and electrochemical techniques that can be used to detect and measure nanoparticles. For the electrochemical detection of nanoparticles, the state of the art in stripping voltammetry of nanoparticles, nanoparticle-electrode impacts and nanoparticle detection at "sticky" surfaces are discussed. The work included in this chapter is based on a book chapter co-authored with Prof. R. G. Compton in a book titled 'Environmental Analysis by Electrochemical Sensors and Biosensors' authored by Prof. L. M. Moretto and Prof. K. Kalcher to be published by Springer Publishing. Advances made by others during the period of research covered by this thesis are included along with earlier work but the author's own contributions are detailed in the subsequent chapters.

2.1 Nanoparticles in the Environment and the Need for Monitoring

A nanoparticle is widely considered to be a particle with at least one dimension that is less than 100 nm[1]. This definition partially overlaps that of colloids which are dispersions in a fluid medium of particles between 1 nm and 1 µm in size. More usefully, the term nanoparticle often implies a particle of sufficiently small size in contrast to bulk media of the same chemical composition such that one or more of its properties (e.g. optical, electronic or mechanical properties) is size dependent.

Environmental nanoparticles primarily originate from natural sources or from human manufacturing activities. The former includes particles from forest fires or volcanic emissions and some of those made of humic materials as well as biological particles such as bacteria and viruses. The incidence of manufactured nanoparticles reflects the huge growth in the nanotechnology industries in recent years with continued expansion expected such that the US National Science Foundation predicts a global 1 trillion USD market with 2 million workers in the nanotechnology area by 2015[2] with broad and diverse applications in materials science, medicine, energy, communication and the environment[3]. Nanomaterials feature in consumer products such as electronic components, cosmetics, cigarette filters, anti-microbial and stain resistant fabrics[3]; more specifically as batteries, skin-care products, paints, wound dressings, food additives and toothpastes[4]. Indeed no less than 15 % of all global consumer products are estimated to be nano-enabled[5]. Nanoparticles have also been employed in environmental remediation to improve the quality of air, water and soils. The US Environmental Protection Agency allocated 1 billion USD for environmental remediation in 2009[3, 6], for example magnetic iron oxides have been used

to remove arsenic from drinking water. The ions adsorb onto the nanoparticle surface and then a magnetic field is used to separate this complex from the water[7]. Gold nanoparticles supported on alumina have been used to remove inorganic mercury from drinking water[8] whilst iron nanoparticles have been used to remove metals such as Cr(VI), U(IV and VI) and Co(II)[9–11]. The latter have also been used to degrade organic pollutants in the same way as TiO_2 nanoparticles[2].

Incidental nanoparticles are produced as a side product of anthropogenic processes such as in automobile exhausts. One interesting but unexpected source of incidental nanoparticles relates to the discovery that silver and copper metallic nanoparticles are formed spontaneously on the surface of manmade objects (made of Ag and Cu) that humans have long been in contact with and that macroscale objects represent a potential source of nanoparticles in the environment[12].

The most important environmental nanoparticles are carbon nanotubes (CNTs), fullerenes (such as C_{60}), nanowires, TiO_2, ZnO, CeO_2, SiO_2 (silica), iron oxides, alumina, hydroxyapatite and metallic nanoparticles such as Fe, Ag, Au[4]. World production of TiO_2 is estimated to be in excess of 40,000 tons per annum with most of the material being nano-sized[13].

Due to their size, nanoparticles can display significantly changed behaviour in comparison with their corresponding macroscopic materials. Most notably the reduced size leads to high surface area to volume ratios, high absolute surface areas and changed electronic properties arising from quantum effects leading to changed chemical and physical properties such as aggregation, electrical conductivity, heat conduction, catalytic activity, surface chemistry, mechanical strength and solubility[3].

An implication of the changed reactivity between the macro- and nano-scale is that the

documentation and understanding of the effects of nanoparticles on human health as well as on plants and other animals is at a relatively immature stage. There is evidence that nanoparticles are usually more toxic than larger particles of the same material[14, 15]. Origins of some nanotoxicity have been suggested to lie in the ability of, for example, Fe nanoparticles to generate radical species, coupling into the chemistry of reactive oxygen species and causing oxidative stress or removing anti-oxidants[16]. In other cases, the changed physical and chemical properties from the macroscale can make materials behave quite differently from their bulk analogues. In some cases positive effects, for example the beneficial role of CNTs on mustard plant growth, have been reported[17].

Given the absolute and increasing scale of production of nanomaterials allied to their uncertain effects on human health it is important that the presence of nanoparticles in the environment can be measured and monitored along with their chemical identification and concentration. The quantification of environmental nanoparticles represents a significant analytical challenge[13]. In the next section (2.2), existing non-electrochemical methods are summarised before their electrochemical alternatives and existing research in this area are reviewed in detail in section 2.3.

2.2 Non-Electrochemical Approaches to Detect Nanoparticles and their Limitations

There are a number of existing techniques that can be used to detect and measure nanoparticles such as inductively coupled plasma-mass spectrometry (ICP-MS)[18], dynamic light scattering (DLS)[19, 20], nanoparticle tracking analysis (NTA)[19, 21], transmission electron microscopy (TEM)[21, 22], disc centrifugation[23], atomic force mi-

croscopy (AFM)[24], tunable resistive pulse sensing[25], ultraviolet-visible (UV-VIS) spectroscopy[26] and scanning electron microscopy (SEM)[27].

In this section, the principles of three of the above techniques (SEM, DLS and NTA) are discussed along with their associated advantages and limitations. These specific techniques have been chosen as they are the nanoparticle characterisation methods employed in this thesis.

2.2.1 Scanning Electron Microscopy

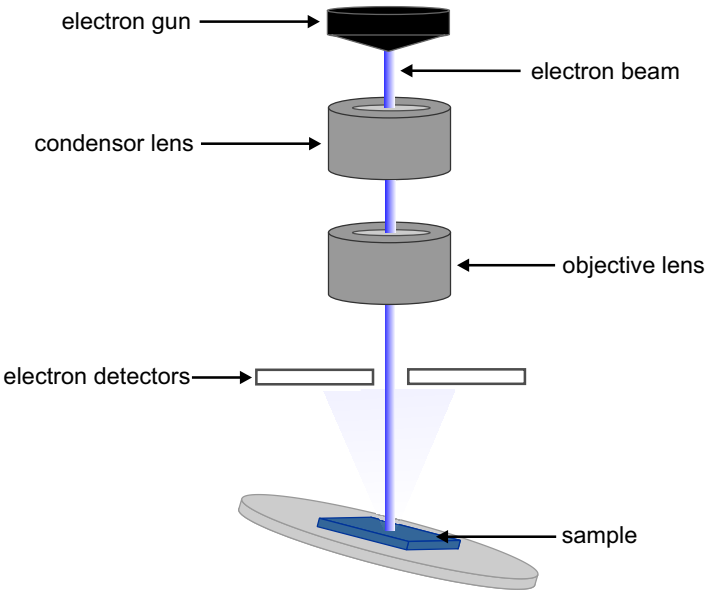


Figure 2.1: Schematic diagram showing the major components of a scanning electron microscope

SEM allows the user to determine the size and shape of nanoparticles, it can also be used to quantify nanoparticles in a sample. Furthermore, if SEM is combined with energy dispersive x-ray spectroscopy the composition of the sample can be established. In SEM electrons are utilised to generate an image. The principles behind this technique are shown in figure 2.1. An electron gun generates an electron beam which is focussed on the sample of interest using magnetic lenses. When the electron beam penetrates the

sample the electrons are scattered. Detectors within the microscope detect these scattered electrons and an image of the sample is generated. The sample is mounted on a holder which manipulates the sample to allow the electron beam to be scanned across the whole sample[28].

One of the major advantages of SEM is that it allows the particles to be visualised and it is therefore one of the only techniques that allows determination of nanoparticle shape. It also allows particle measurement on a particle-by-particle basis as opposed to analysing the whole sample at once, however this manual measurement of individual particles can sometimes result in poor representation of the whole nanoparticle population. Another issue with SEM is that the sample must be dry[28] meaning the nanoparticles cannot be measured whilst in solution. Often the nanoparticles are prone to change during sample preparation and tend to aggregate on the SEM holder. SEM is capable of measuring nanoparticles with a diameter not less than 1 nm[29].

2.2.2 Dynamic Light Scattering

DLS is a laser scattering technique that can be used to measure nanoparticles dispersed in solution. The suspension, in which the nanoparticles are moving *via* Brownian motion, is irradiated with a laser beam (λ=633 nm) which is scattered upon hitting a nanoparticle. The resulting Rayleigh scattering waves are detected by a photon detector. When large numbers of nanoparticles suspended in solution are irradiated with the laser there will be either a constructive or destructive interference of the scattered waves at the detector at a given time resulting in fluctuations in the measured light intensity[28]. It can be seen in figure 2.2 that larger nanoparticles will move through solution at a slower rate therefore the resulting fluctuations in light intensity will be less frequent than those measured for

smaller, faster moving particles.

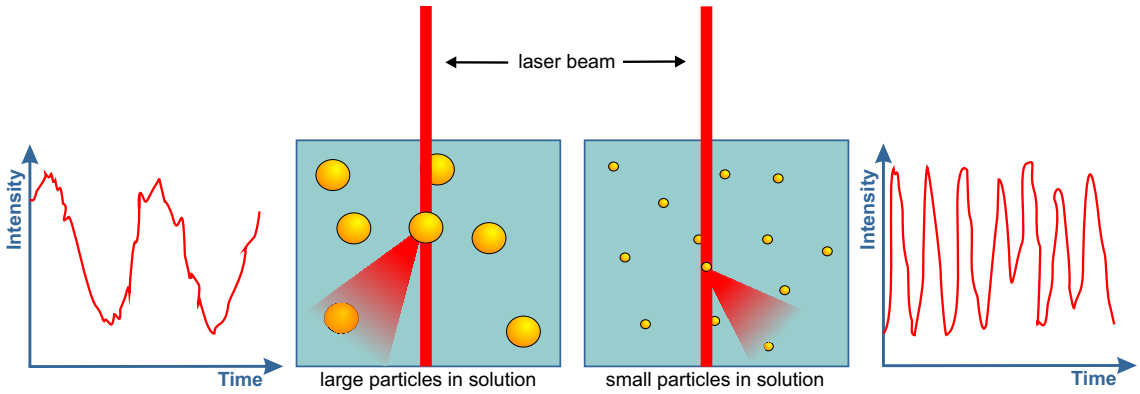


Figure 2.2: Schematic diagram of dynamic light scatting used to measure nanoparticles in solution

These measured intensity fluctuations therefore depend on the nanoparticle diffusion coefficient (D) and can be used to gain a value for the nanoparticle radius (r_{NP}) *via* the Stokes-Einstein equation (equation 2.1) if the nanoparticle is assumed to be spherical[28]:

$$D = \frac{k_{\mathrm{B}}T}{6\pi\eta r_{\mathrm{NP}}} \tag{2.1}$$

where k_{B} is the Boltzmann constant (J K^{-1}), T is the temperature (K) and η is the solution viscosity (kg m^{-1} s^{-1}).

The major advantage of DLS is that it can be used to analyse nanoparticles in solution where the nanoparticle radius determined is the hydrodynamic radius. While the measurements are very quick and straightforward to carry out, the sample is analysed as a whole which can result in poorly resolved nanoparticle size distributions. This technique also requires the user to have some knowledge of the sample which is being analysed as information regarding the physical properties of the particle and the solution in which it is suspended needs to be inputted. Furthermore, there are limitations associated with the particle suspension media as transparent solutions are required meaning that envi-

ronmental samples cannot be analysed without pretreatment. DLS can be used to size particles between 1 and 5000 nm[30], however it is unable to determine the concentration or identity of nanoparticles in a solution.

2.2.3 Nanoparticle Tracking Analysis

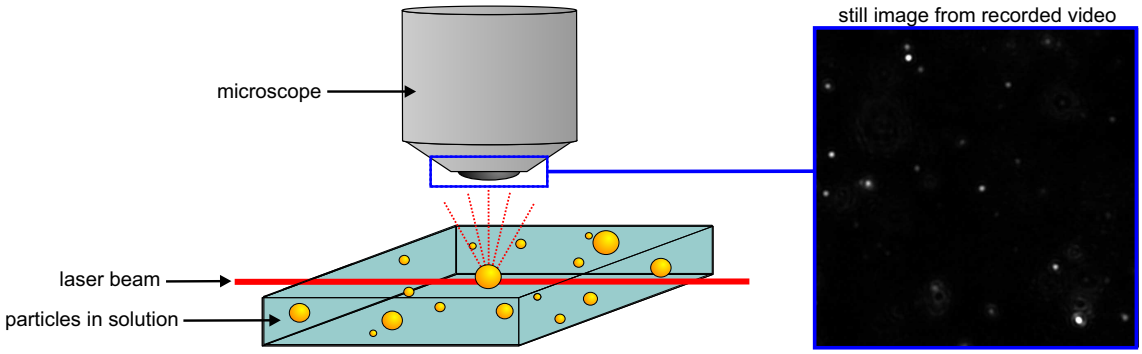


Figure 2.3: Schematic diagram demonstrating the principles of nanoparticle tracking analysis

NTA can be used to size and quantify nanoparticles in solution. It is a relatively new technique that is performed using an instrument purchased from NanoSight (Amesbury, UK). The nanoparticle suspension is inserted into the viewing chamber of the instrument which has a known capacity of 0.3 mL. As shown in figure 2.3 the suspension is irradiated with a laser beam (λ=638 nm) which is scattered by the nanoparticles in the chamber. A microscope with an incorporated digital video recorder is used to visualise and record a 30 s video of the light being scattered by the nanoparticles. The particles appear as bright spots against a black background in the recorded video (figure 2.3) which can be analysed by the NTA software suite. This software tracks the movement of each nanoparticle along a two-dimensional plane and a two-dimensional diffusion coefficient (D_{2D}) is calculated *via* equation 2.2[31]:

$$D_{2D} = \frac{\overline{(x,y)^2}}{4} \tag{2.2}$$

where $\overline{(x,y)^2}$ is the mean square displacement per unit time. Hence, equation 2.1 can be used to determine a value for the nanoparticle radius from the measured two-dimensional diffusion coefficient.

As with DLS, nanoparticles suspended in opaque solutions cannot be analysed and it is the hydrodynamic radius of the nanoparticle that is determined. There are also problems associated with the tracking of nanoparticles that move out of the measured 2D plane, however measurement of the nanoparticles on a particle-by-particle basis gives rise to particle-size distributions with a better resolution that DLS. As the volume of solution in the chamber is known, the concentration of nanoparticles in a solution can be established, however no information is available regarding nanoparticle identity. The minimum nanoparticle diameter that can be detected is 10 nm however this lower limit is dependent on the refractive index of the nanoparticle material[31].

In comparison with the above techniques, electrochemical methods are relatively under-explored but offer scope for chemical identification, low cost and ease of portability.

2.3 Electrochemical Approaches to Detect Nanoparticles

2.3.1 Stripping Voltammetry of Nanoparticles

The simplest approach to the electrochemical (voltammetric) analysis of nanoparticles is to first separate and isolate the nanoparticles from the sample of interest and then

immobilise them on a suitable substrate electrode and conduct stripping voltammetric analysis. This approach can be illustrated by the work of Giovanni and Pumera[32] on molybdenum metallic nanoparticle detection using cyclic and differential pulse voltammetry. They formed Mo nanoparticle modified glassy carbon (GC) electrodes by depositing a small amount of colloidal suspension on the surface of a GC electrode and then letting the solvent (dimethylformamide) evaporate to dryness. Voltammograms were then recorded in phosphate buffer of neutral pH and these are shown in figure 2.4. Clearly defined oxidation features are discernible, helping to identify the nanoparticles as Mo. A similar approach has been applied by the same group to Ni[33] and Ag[34] nanoparticles. Such analyses has potential applications in bioassays with the possibility that different nanoparticles can be used to label (tag) different species. For example CdS nanoparticles can be directly detected electrochemically in much the same way as Mo[35] and have been used to label DNA[36].

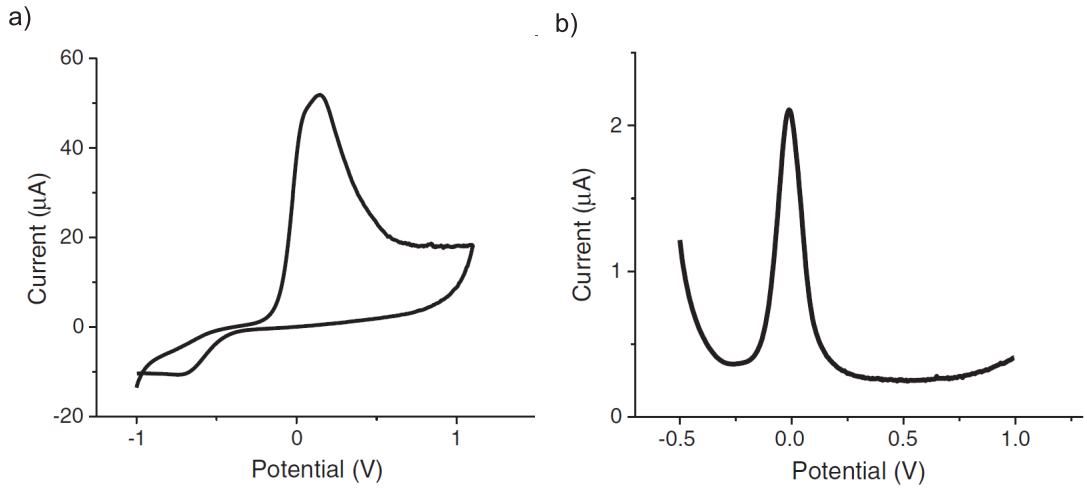


Figure 2.4: a) Cyclic voltammogram for a GC electrode modified with 0.25 µg of molybdenum nanoparticles recorded in 50 mM phosphate buffer (pH 7.4) at a scan rate of 100 mV s^{-1} b) Differential pulse voltammetric response for the oxidation of 0.1 µg of molybdenum nanoparticles in 50 mM phosphate buffer (pH 7.4). Reprinted from [32] with permission from Elsevier.

There are several reports that the electrochemical oxidation of nanoparticles can be

size dependent with both Ag[34, 37] and Pt nanoparticles studied[38]. Ivanova and Zamborini immobilised different sized citrate capped Ag nanoparticles ranging in size from 8 to 50 nm onto an amine-functionalised indium tin oxide (ITO) coated glass electrode *via* electrostatic attachment to the protonated amine group[37]. The largest diameter particles studied showed an oxidation potential in 0.1 M aqueous sulphuric acid at approximately 100 mV more positive than that of the smallest nanoparticles studied.

The size-dependency of the electrochemical oxidation of metal nanoparticles can be partially understood in the light of several different considerations[37–43]. First, data deriving from work on small silver clusters, Ag_n, formed in aqueous solution *via* pulse radiolysis coupled with other information such as mass spectroscopic equilibrium data and Gibbs energies of sublimation of silver has led to the estimation of the standard electrode potential of the redox couple.

$$Ag_n \leftrightharpoons Ag_{n-1} + Ag^+ + e^- \tag{2.3}$$

For large values of n the potential approaches that expected for the Ag/Ag^+ redox couple (+0.799 V). However at small values of n there is a strong size dependence[40] with a value of -1.8 V calculated for the special case of a single atom of silver (n=1)[39–41]. In between these limits the electrode potential varies as shown in figure 2.5 with a strong oscillation in the n=1-3 range - the silver atom being strongly electron donating while the dimer (n=2) is almost noble[41] (-0.1 V) with the trimer again having a very negative value. The ease of oxidation of Ag_n as n increases is evident in figure 2.5.

For larger clusters approaching nanoparticle dimensions Plieth[39] considered surface Gibbs energies reflecting the fact that metal atoms on the surface of a small particle are

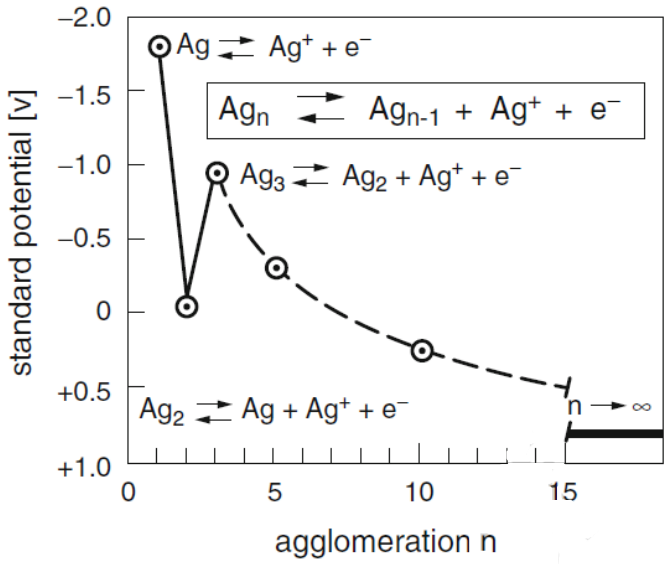


Figure 2.5: Variation of the standard electrode potential for the Ag/Ag^+ redox couple with agglomeration of silver atoms. Reprinted with permission from [40]. Copyright 1993 American Chemical Society.

in less energetically favourable positions compared to those in bulk material. He obtained the following equation for the difference in electrode potential between the dispersed (colloidal) metal as compared with the bulk material:

$$\Delta E \propto -\frac{\gamma}{r} \tag{2.4}$$

where the particles were considered to be spheres of radius r, γ is the surface energy (J m^{-2}) and the analysis was considered to apply to particles of approximately 0.7 nm or larger in radius (corresponding to 100 atoms or so). Application of the theory required knowledge of surface energy values and this limited its application to real systems. Figure 2.6 shows the results of some model calculations[39] and that significant shifts of redox potential can be seen for particles as large as 10 nm.

Developing from this type of approach Tang and colleagues[38] used first principle electronic structure calculations of the surface energy of Pt nanoparticles to develop size

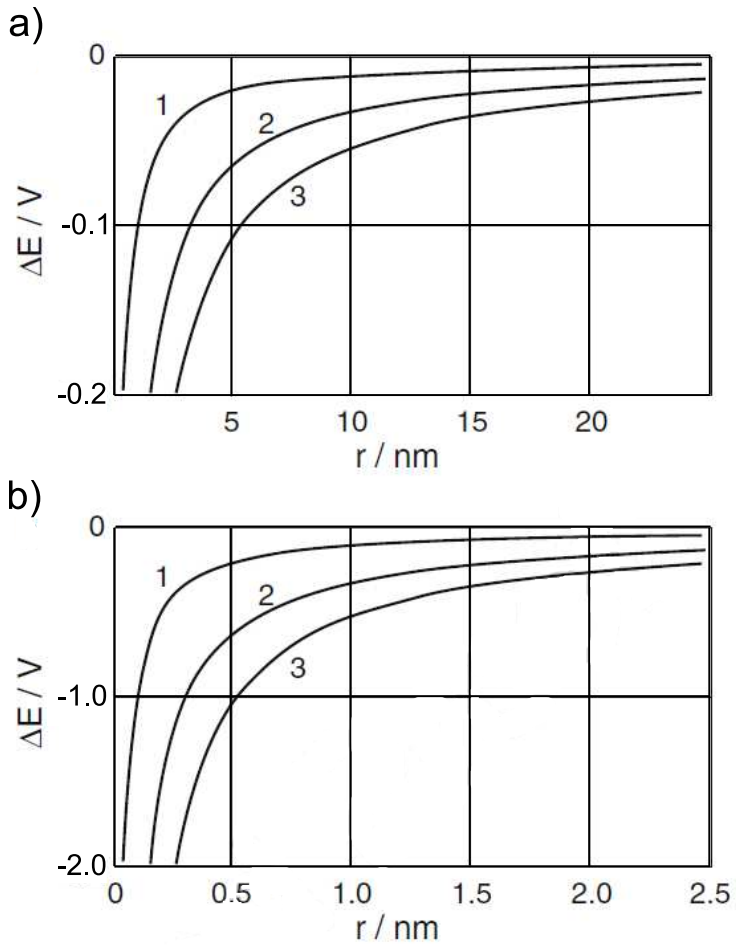


Figure 2.6: Cathodic shift in redox potential for a metal electrode as a function of particle size a) particle radius $r < 25\,\text{nm}$ b) particle radius $r < 2.5\,\text{nm}$ for surface energy values of 0.5 J m^{-2} (curve 1), 1.5 J m^{-2} (curve 2) and 2.5 J m^{-2} (curve 3). Adapted with permission from [39]. Copyright 1982 American Chemical Society.

dependent potential pH diagrams and to show, supported by experimental electrochemical scanning tunnelling microscopy, that Pt nanoparticles of diameter less than $\sim$4 nm dissolve oxidatively *via* the direct electrochemical dissolution shown in equation 2.5

$$\mathrm{Pt} \longrightarrow \mathrm{Pt}^{2+} + 2\,\mathrm{e}^{-} \tag{2.5}$$

whereas larger nanoparticles form oxide layers.

A further consideration pertaining to the size dependent electrochemical oxidation of metal nanoparticles supported on a conductive electrode surface relates to the size dependent concentration profiles of the metal ions produced during oxidation as they diffuse away from the electrode surface[42–44]. In order to identify the effects of diffusion on the voltammetric stripping signal from an electrode partially covered with nanoparticles (of a uniform size) being stripped, the formal potential for the oxidation was assumed constant in simulations made to isolate the effects of diffusion[42–44]. Under these conditions, theory predicts that for electrochemically irreversible kinetics (slow electron transfer requiring an overpotential) the peak potential will be independent of the metal coverage but will shift to more negative potentials as the nanoparticle radius shrinks in size. If a range of nanoparticle sizes is present then this is reflected by the broadening of the stripping peak as observed experimentally for Bi nanoparticles being stripped from the surface of a boron-doped diamond electrode[44].

In contrast for an electrochemically reversible stripping process it is predicted, again assuming no influence of particle size on the standard electrode potential of the stripping process, that assuming the diffusion layers surrounding each nanoparticle overlap so as to produce overall planar diffusion of the stripped ions away from the electrode, that

the peak potential will depend on the total metal coverage but not the nanoparticle size. In the opposite limit, where the diffusion layers do not overlap then particle size effects are predicted. Experiments reported for the electrochemically reversible stripping of silver nanoparticles supported on a basal plane pyrolytic graphite electrode showed the expected dependence on metal loading but not on particle size[43].

In summary, stripping voltammetry can be used to identify the presence of oxidisable nanoparticles so allowing fingerprinting and, with suitable calibration, their quantification although care is required in the interpretation of the peak potential with sensitivity to particle size and possible loadings.

2.3.2 Nanoparticle-Electrode Impacts

An alternative and at least in principle much simpler and easier electrochemical approach to that of the previous section, in which nanoparticles are sequentially isolated, immobilised on an electrode and then analysed *via* stripping voltammetry, is the direct study of the nanoparticles suspended in a solution phase into which an electrode under potentiostatic control is introduced. The movement of the nanoparticles in the solution is expected to approximate to Brownian which, from time to time, will bring the nanoparticles close to or in physical contact with the electrode to which they can either stick or rebound, unless the electrode is held at a potential corresponding to the oxidation or reduction of the nanoparticles or at least the surface of the nanoparticles. In the latter case, the nanoparticle collisions with the electrode are revealed by a pulse of current, as shown schematically in figure 2.7. These spikes can be used to identify the nanoparticles (by virtue of their onset potentials), measure their concentrations and to size them as discussed in more detail below. This type of measurement is currently subject to significant

levels of interest[45].

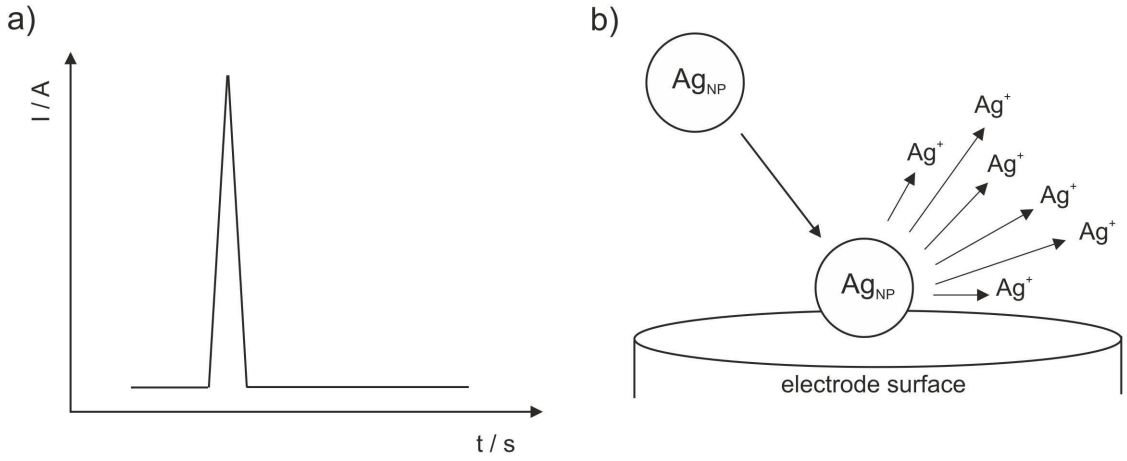


Figure 2.7: Schematic diagram of (a) a spike observed in the current-time transient when a silver nanoparticle collides with a potentiostatted electrode and is oxidatively destroyed (b)

The original work in this area was carried out by Heyrovsky and colleagues[46–49] using mercury electrodes to electro-reduce particles of metal oxides. They examined the voltammetry of polydisperse colloidal solutions of the oxides SnO_2, TiO_2 and Fe_2O_3 in aqueous solution. The voltammograms measured reflected the summation of the contribution of groups of particles of different sizes and they were able to voltammetrically determine the approximate composition of Fe(III) doped TiO_2 colloids[49]. The work was subsequently extended, again exclusively with mercury electrodes, to the reduction of oxide layers on the surfaces of metal powders (Cu, Fe, Ni, Mo, W)[50], on copper/copper oxide ultrafine powder[51] and finally on aluminium nanoparticles[52]. In [48] the authors report the reduction of protons in acid solutions occurring on the surface of TiO_2 particles for the duration of their impacts with the electrode surface (figure 2.8). This experiment is the forerunner of the indirect processes now studied more widely and discussed later in this chapter.

Innovative experiments were carried out by Scholz[53] in which the range of impact

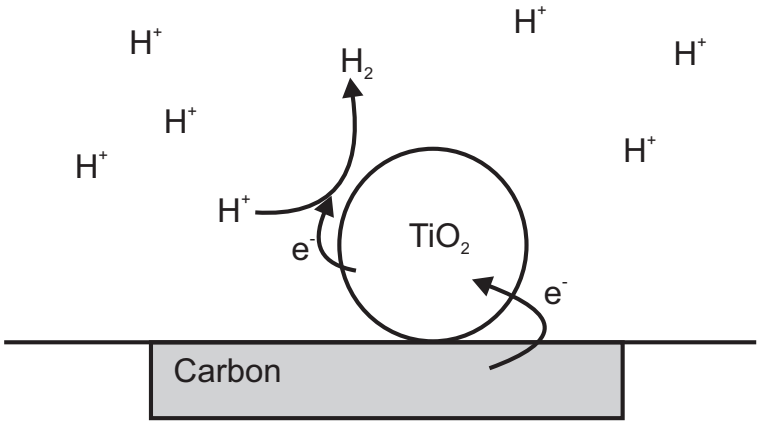


Figure 2.8: The indirect nanoimpact process studied by Heyrovsky et al. in [48] where protons are reduced on the surface of impacting TiO_2 particles. [45] Adapted by permission of The Royal Society of Chemistry.

experiments were usefully extended to study the collisions of liposomes with a mercury electrode in aqueous solution at pH 7. Sharp current transients, of 1-20 ms duration, were seen as the liposomes contacted, broke up and then spread over the electrode surface. However, unlike the experiments of Heyrovsky, the current spikes were deduced to be non-Faradaic in character with capacitative origins: the frequency of the transient signals was found to be a minimum at the potential of zero charge, pzc, and to increase with potentials negative or positive of the pzc. In subsequent work, the kinetics of liposome adhesion were explored and the impact of montmorillonite clay particles on a mercury electrode was also studied[54, 55].

Similar experiments were carried out using suspensions of oil droplets and solid particles in aqueous solutions induced into motion by power ultrasound and allowed to impact solid electrodes [56–59]. Current transients of microsecond duration were seen corresponding to the much faster speed of the impacting particles as compared to those in the Scholz experiments, leading to a greatly reduced contact time between particle and electrode. The amount of charge passed in the impact transients scaled with the size and conduc-

tivity of the impacting particle and the sign of the current transient inverted at the pzc of the substrate electrode as shown in figure 2.9. Charge transfer between the particle and the electrode and/or the deformed double layer and the electrode was inferred but at the microsecond timescales resulting from insonation it was concluded that Faradaic charge transfer was not operative and experiments using large insonated metal particles confirmed no such activity.

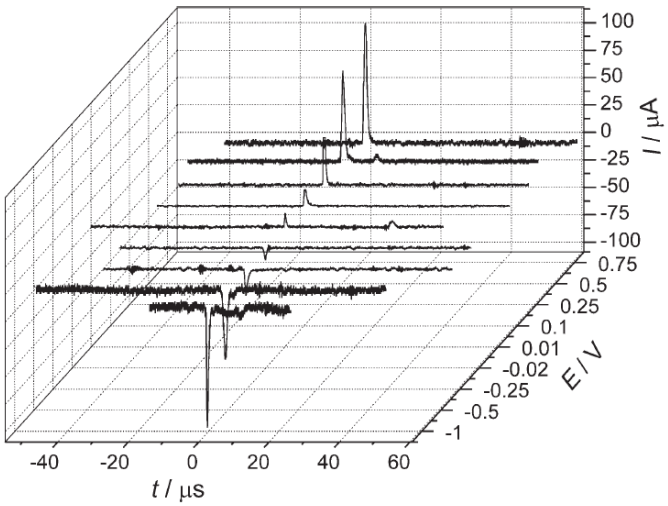


Figure 2.9: Current spikes observed for graphite powder (diameter 2-20 µm) impacting a gold microdisc electrode under sonication in 0.1 M perchloric acid. Reprinted with permission from [58]. Copyright 2004 American Chemical Society.

A significant advance was made in which similar experiments were performed using silver nanoparticles, AgNPs, but without insonation, rather using natural Brownian motion to give rise to an impact with the electrode surface[27]. Using a carbon electrode it was found that sharp current spikes of 1-10 ms durations were seen (figure 2.10a) when the electrode was potentiostatted at a value more positive than that required for the process in which the nanoparticles were oxidised to aqueous silver cations:

$$\mathrm{AgNP_{(s)}} - \mathrm{e^-} \longrightarrow \mathrm{Ag^+_{(aq)}} \tag{2.6}$$

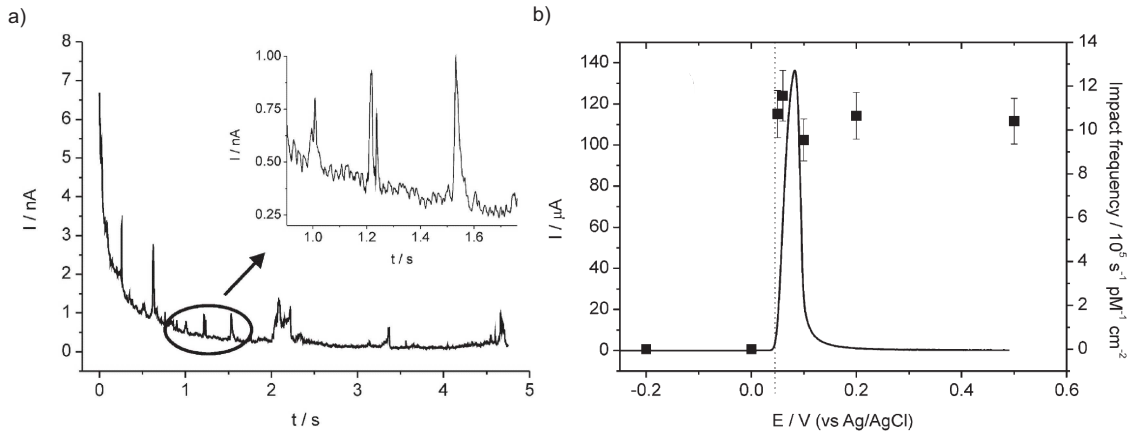


Figure 2.10: a) Impact spikes observed when silver nanoparticles are directly oxidised upon collision with a potentiostatted carbon microelectrode surface in 10 mM citrate/90 mM KCl b) Stripping voltammogram for a silver nanoparticle-modified GC electrode in 10 mM citrate/90 mM KCl (left axis) overlaid with the observed frequency of nano-impacts (right axis) at a carbon microelectrode in the same solution at varying potentials. Reproduced from [27]. Copyright 2013 WILEY-VCH Verlag GmbH and Co. KGaA, Weinhem.

The onset potential for the observation of the spikes corresponded closely to the peak potential recorded if the same silver nanoparticles were immobilised on a GC electrode (as in section 2.3.1) and subjected to anodic stripping analysis (figure 2.10b). Furthermore, in the former experiments, the frequency of the measured impacts scaled with the nanoparticle concentration in solution. Analogous experiments were conducted for the electro-oxidation of other metal nanoparticles; gold[60] and copper[61].

It is evident that such experiments can provide information about the chemical identity of the impacting nanoparticles by virtue of the onset potential for the appearance of oxidative spikes. However, it was additionally discovered that the oxidation of the nanoparticles is quantitative, so that all of the atoms in a particle become oxidised on impact even for a large nanoparticle approaching 100 nm in diameter[27, 62]. This was understood in terms of a model explicitly invoking Brownian motion interpreting the observed millisecond timescale current spikes as each resulting from a cluster of very rapidly consecutive encounters of the nanoparticle with the electrode, in each of which partial

oxidation of the nanoparticle takes place, but such as to bring about the overall complete oxidation of the nanoparticle[63]. Calculations suggested that it was unlikely that partially oxidised nanoparticles would survive on the observed millisecond timescale. It follows that the charge passed during the current spikes was directly and quantitatively linked with the number of atoms in the nanoparticles (*via* Faraday's law of electrolysis as described in chapter 1) and hence with nanoparticle size. The size of single silver nanoparticles determined *via* direct oxidative electrode impacts (anodic particle coulometry), where the nanoparticle radius has been inferred from the charge passed under the spikes on the assumption that the particle is spherical, and that measured from SEM was found to give excellent and quantitative agreement[27].

It was found that for silver and gold nanoparticles the electrochemical measurements revealed the presence of aggregation in solution[45, 60]. Figure 2.11 shows the atom counting and sizing for gold nanoparticles measured in 0.1 M aqueous HCl solution. The nanoparticles were sized as 20 nm in diameter *via* SEM; the electrochemistry shows the presence of some single nanoparticles (r_{NP}=10.5 $\pm$ 0.5 nm) as well as clusters of two or more nanoparticles so revealing the occurrence of aggregation of the nanoparticles in aqueous solution[60]. Similar observations were made for silver nanoparticles[45]. Thus anodic particle coulometry allows not only particle sizing (number of atoms, radius of the nanoparticle if assumed spherical) but also, in principle, the extent and rate of nanoparticle aggregation in real time. A further study found that it is possible to successfully achieve a slower rate of silver nanoparticle agglomeration/aggregation for a range of different sized particles when a high concentration of tri-sodium citrate is selected as the electrolyte thanks to its nanoparticle stabilising properties[64].

With the anodic particle coulometry method having been shown to be effective for

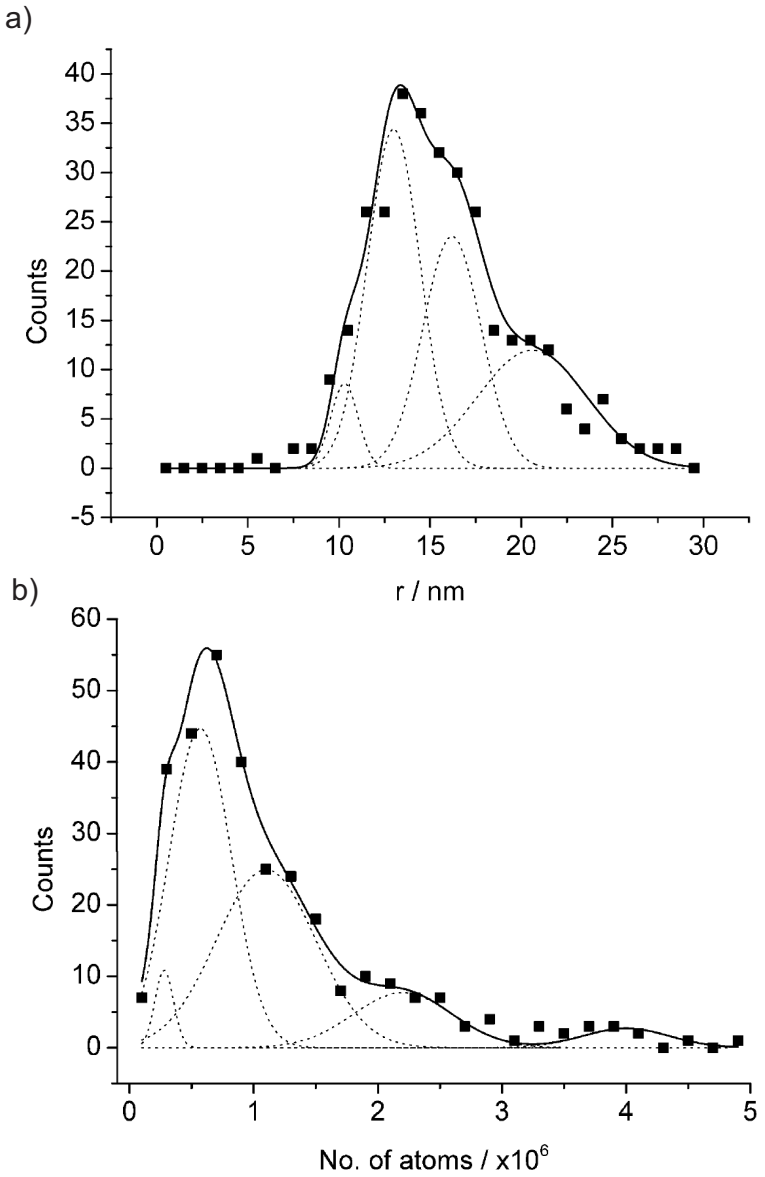


Figure 2.11: Size distribution for anodic particle coulometry measurements of gold nanoparticles expressed as a) radius (r) and b) the number of atoms in an impacting nanoparticle. [60] Reproduced by permission of The Royal Society of Chemistry.

the detection and sizing of a variety of metal nanoparticles, an obvious progression of this work and the earlier work performed by Heyrovsky[46–49] was to test the application of cathodic particle coulometry, where the nanoparticles are reduced upon contact with the electrode, for the detection of metal oxides. Fe_3O_4 nanoparticles were detected and sized using cathodic particle coulometry with SEM employed to confirm the accuracy of this electrochemical sizing method[65]. Furthermore, it was discovered that using both cathodic and anodic particle coulometry in conjunction with one another (figure 2.12) provides a suitably accurate and thorough nanoparticle characterisation method, rendering the use of optical techniques for verification of these electrochemical sizing methods redundant.

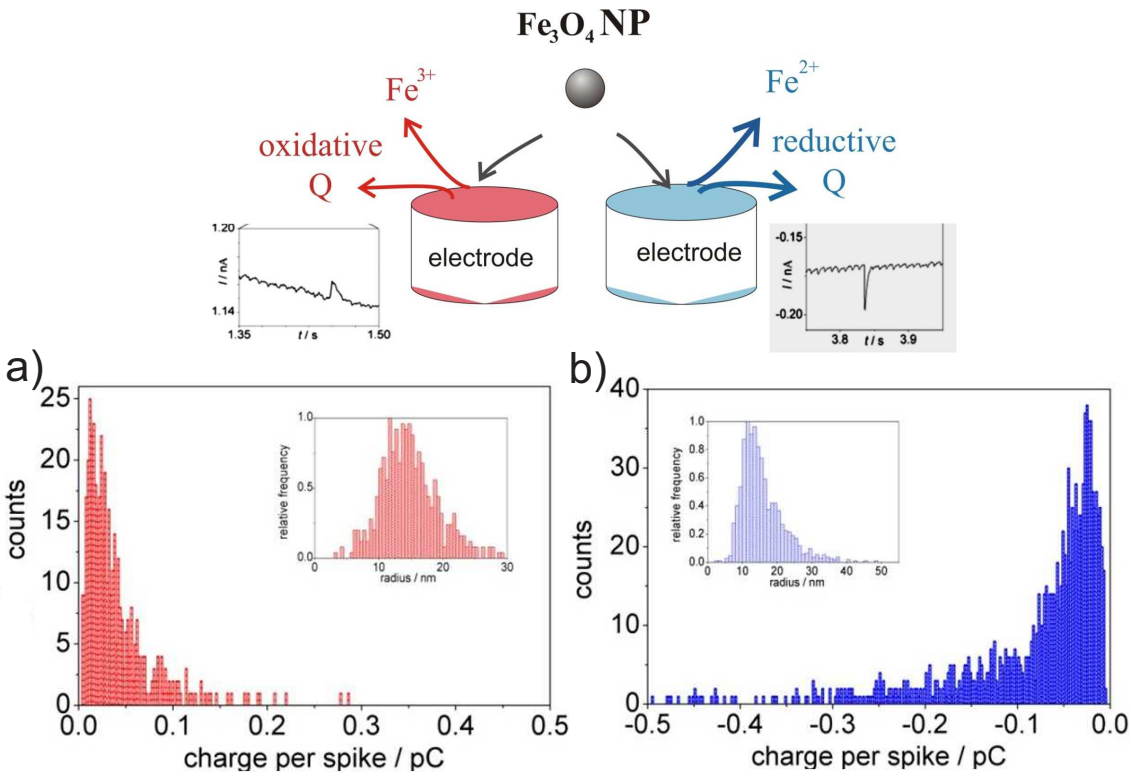


Figure 2.12: Schematic for the two electrochemical routes used to size Fe_3O_4 nanoparticles and the resulting charge and size (inset) distributions gained from a) anodic particle coulometry experiments and b) cathodic particle coulometry experiments. Reproduced from [65]. Copyright 2013 Tsinghua University Press and Springer-Verlag Berlin Heidelberg.

One type of nanoparticle that are particularly difficult to size using currently available techniques are organic nanoparticles. Experiments were conducted to investigate the suitability of cathodic particle coulometry as an alternative to existing techniques (e.g. SEM, TEM, DLS, ultracentrifugation) used for organic nanoparticle sizing, with indigo nanoparticles used as a model system [58]. Figure 2.13 shows the size distribution gained for the electro-reduction of indigo nanoparticles *via* cathodic particle coulometry in comparison with the size analysis of the same batch of nanoparticles determined using DLS. It can be seen that the resulting size distribution from both techniques are in excellent agreement, with the mean diameter of the indigo nanoparticles investigated being 68 nm.

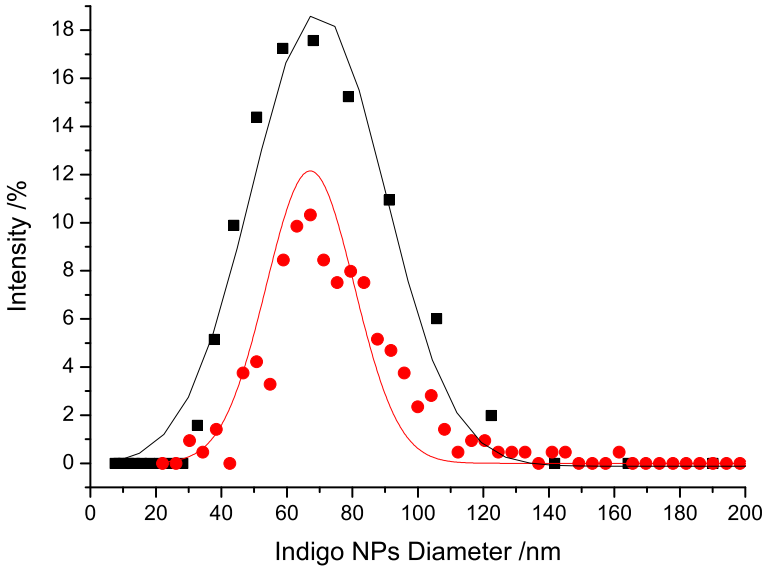


Figure 2.13: Overlaid distributions for indigo nanoparticle sizing measured *via* cathodic particle coulometry(red circle) and DLS(black square). Reproduced from [66]. Copyright 2013 WILEY-VCH Verlag GmbH and Co. KGaA, Weinhem.

The above impact experiments involve the exhaustive electro-oxidation or reduction of metal nanoparticles. An alternative non-destructive method for nanoparticle identification and sizing has been proposed[45, 60] in which the surface of metal nanoparticles such as silver or gold are tagged by the adsorptive attachment of redox active molecules onto the surfaces of the nanoparticles. The tagged nanoparticles are allowed to impact

an electrode surface just as in anodic particle coulometry except that now the electrode potential is held at a value such as to reduce or oxidise the tag. Typical tags might contain nitrophenyl[60] or ferrocenyl groups which respectively undergo reduction or oxidation in aqueous media. Thiol groups can be use to anchor the tags on silver or gold nanoparticle surfaces. In the case where a full monolayer of tag covers the nanoparticle surfaces, then the average charge passed under the spikes measured in an impact experiment provides information about the average surface area of the nanoparticles and hence, under the assumption that the particles are spherical, an indication of the nanoparticle size (radius). Radii inferred *via* this approach were in excellent agreement with those obtained for the same nanoparticles using anodic particle coulometry[67].

In the nanoparticle impact experiments discussed earlier the electron transfer to or from the nanoparticles is a direct transfer. Building on Heyrovsky's [35] observations of proton reduction on the surface of TiO_2 nanoparticles impacting mercury electrodes, considerable progress has been made on the study of the "indirect" electron transfers. Figure 2.14a schematically shows the concept underlying this experiment. As before, Brownian motion of nanoparticles brings them into contact with an electrode under potentiostatic control. Whilst a nanoparticle is in contact, usually for a period of 1-10 ms, it adopts the potential of the electrode so that if redox active molecules are present in solution they can undergo electrolysis on the surface of the nanoparticle. If the nanoparticle-electrode combination is carefully selected then at some potential values electrolysis can be exclusively confined to the nanoparticles. For the case of silver nanoparticles suspended in aqueous acid solution impacting a carbon electrode the reduction of protons on the impacting silver nanoparticles can be seen as current spikes at potentials less cathodic than that needed for their reduction on the underlying carbon electrode[68].

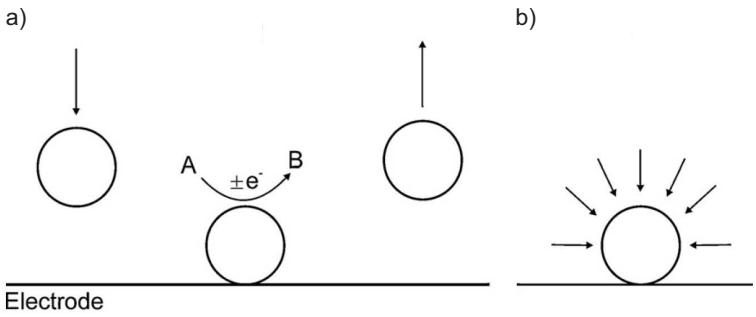


Figure 2.14: a) Schematic of an indirect process involving a redox reaction occurring on the surface of the nanoparticle when it is in contact with the electrode b) Upon impact convergent diffusion to the nanoparticle occurs almost instantaneously meaning a steady-state current is established for the electrocatalytic reaction occurring on the nanoparticle surface. Reprinted from [68] with permission from Elsevier.

The analysis of the potential dependence of the current spikes allows for the deduction of electron transfer kinetics of redox couples at single nanoparticles *via* appropriate modelling treating the impacted nanoparticle as a sphere on a flat surface (figure 2.14b). It has been recognised that the time needed to set up steady state electrolysis at the nanoparticle surface is tiny compared to the duration of the impacts so that the nanoparticle confined electrolysis can be accurately treated as being at steady state[68–70]. It should however be noted that some nanoparticles can stick to the electrode surface which thus gradually changes its chemical (and electrochemical) nature over the course of time; the sticking probability of silver nanoparticles has been measured[71]. Other chemical examples of these indirect processes include the oxidation of hydrazine on impacting platinum nanoparticles, water oxidation on iridium oxide nanoparticles and the oxidation of sodium borohydride on the surface of gold nanoparticles making contact with a platinum electrode[72].

Similar considerations, most notably treating the transport to an impacting sphere as being at steady state, also allow the modelling of the anodic particle coulometry type of impact experiment where the nanoparticle is exhaustively oxidised and in particular the

prediction of the onset potential for the appearance of current 'spikes'. Different behaviour is predicted for fast or slow (electrochemically reversible or irreversible) charge transfer kinetics[61, 69]. Copper[61] and nickel[69] nanoparticles showed slow electron transfer kinetics whereas silver nanoparticles showed reversible kinetics[69]. The latter observation explains the fact that the onset potential for the appearance of oxidation spikes for the silver nanoparticles approximately matches the peak potential in the stripping voltammetry when the same particles are immobilised on an electrode.

2.3.3 Nanoparticle Detection at Sticky Surfaces

For the application of the nanoparticle-electrode impact methods described in section 2.3.2 to environmental monitoring one major drawback is that it is likely the environmental samples to be tested would have to be isolated and transported to a laboratory before the nanoparticles within the selected sample can be detected *via* anodic or cathodic particle coulometry. Here, the user would run the risk of the nanoparticles within the sample changing (e.g. aggregating) before analysis can be performed. Therefore, an in-situ nanoparticle detection method is desirable for this type of field work. One such method is to immobilise nanoparticles in solution on an electrode surface under open circuit conditions before oxidatively stripping off the nanoparticles using stripping voltammetry to reveal the amount of nanoparticles that have adhered to the surface and therefore providing information on the concentration of nanoparticles in solution[73]. Again, the potential of the stripping peak can be used to identify the type of nanoparticles present.

It is possible to increase the adhesion extent and rate of nanoparticle adsorption on the electrode surface by modifying the surface so that it becomes "sticky". The electrochemical modification of a GC electrode surface with cysteine was found to increase

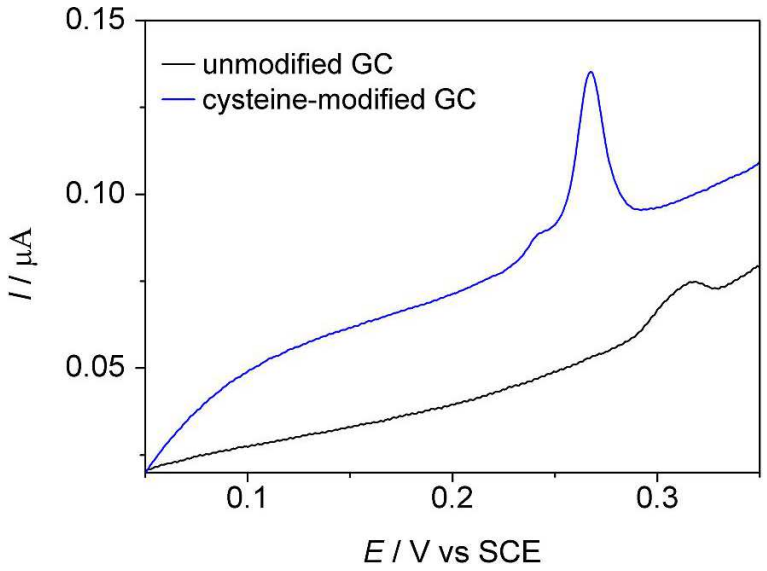


Figure 2.15: Anodic stripping voltammograms for the oxidation of silver nanoparticles that had become adhered to a cysteine modified GC electrode (blue line) and an unmodified GC electrode (black line) immersed in silver nanoparticle containing seawater at open circuit potential for 15 min under permanent agitation with nitrogen. Reproduced from [73] by permission of IOP Publishing.

the ability of silver nanoparticles in both 0.1 M $NaClO_4$ and seawater to stick onto the surface of an electrode with larger stripping peaks observed for the modified substrate in comparison those at an unmodified surface as shown in figure 2.15 [73]. The work in chapters 7 and 10 builds upon this preliminary sticking and stripping study.

2.4 Outlook

The study of nanoparticles is in its infancy and that is especially the case for the electrochemistry of these environmentally important species where measurements can be expected to reveal important information about the redox behaviour of nanoparticles as well as provide analytical methods for their characterisation. That said, to date, voltammetric methods have been developed for the identification of nanoparticles as well as offering the possibility for sizing them, monitoring their aggregation in real time and measuring their

concentrations. Already electrochemical methods are providing significant insights into the behaviour of naturally occurring environmental nanoparticles[74–78] and an explosion of growth in this area and related areas is to be expected in the near future. The following chapters of this thesis present experimental results for the detection of environmentally important nanoparticles using direct (anodic and cathodic particle coulometry) and indirect nanoparticle-electrode impact experiments as well as the nanoparticle sticking and voltammetric stripping technique.

Bibliography

[1] J. H. Duffus, M. Nordberg and D. M. Templeton, *Pure Appl. Chem.* **79** (2007) 1153–1344.

[2] A. Sanchez, S. Recillas, X. Font, E. Casals, E. Gonzalez and V. Puntes, *Trends Anal. Chem.* **30** (2011) 507–516.

[3] Z. Chen, A. M. Yadghar, L. Zhao and Z. Mi, *Toxicol. Environ. Chem.* **93** (2011) 1227–1250.

[4] H. Zanker and A. Schierz, *Annu. Rev. Anal. Chem.* **5** (2012) 107–132.

[5] P. Kumar, A. Kumar and J. R. Lead, *Environ. Sci. Technol.* **46** (2012) 7071–7072.

[6] B. Karn, T. Kuiten and M. Otto, *Environ. Health Perspect.* **117** (2009) 1813–1831.

[7] C. T. Yavuz, J. T. Mayo, W. W. Yu, A. Prakash, J. C. Falkner, S. Yean, L. Cong, H. J. Shipley, A. Kan, M. Tomson, D. Natelson and V. L. Colvin, *Science* **314** (2006) 964–967.

[8] K. Lisha, Anshup and T. Pradeep, *Gold Bull.* **42** (2009) 144–152.

[9] M. Dickinson and T. B. Scott, *J. Hazard. Mater.* **178** (2010) 171–179.

[10] Y. Xu and D. Zhao, *Water Res.* **41** (2007) 2101–2108.

[11] C. Uzum, T. Shahwan, A. Eroglu, I. Lieberwirth, T. Scott and K. Hallam, *Chem. Eng. J.* **144** (2008) 213–220.

[12] R. D. Glover, J. M. Miller and J. E. Hutchison, *ACS Nano* **5** (2011) 8950–8957.

[13] A. G. Howard, *J. Environ. Monit.* **12** (2010) 135–142.

[14] K. Donaldson, V. Stone, C. L. Tran, W. Kreyling and P. J. A. Borm, *J. Occup. Environ. Med.* **61** (2004) 727–728.

[15] P. J. Moos, K. Chung, D. Woessner, M. Honeggar, N. S. Cutler and J. M. Veranth, *Chem. Res. Toxicol.* **23** (2010) 733–739.

[16] E. Burello and A. P. Worth, *Nanotoxicology* **5** (2011) 228–235.

[17] A. Mondal, R. Basu, S. Das and P. Nandy, *J. Nanopart. Res.* **13** (2011) 4519–4528.

[18] R. Allabashi, W. Stach, A. de la Escosura-Muniz, L. Liste-Calleja and A. Merkoci, *J. Nanopart. Res.* **11** (2009) 2003–2011.

[19] K. E. Wilkinson, L. Palmberg, E. Witasp, M. Kupczyk, N. Feliu, P. Gerde, G. A. Seisenbaeva, B. Fadeel, S.-E. Dahln and V. G. Kessler, *ACS Nano* **5** (2011) 5312–5324.

[20] K. Prapainop, D. P. Witter and P. Wentworth, *J. Am. Chem. Soc* **134** (2012) 4100–4103.

[21] S. A. Orefuwa, M. Ravanbakhsh, S. N. Neal, J. B. King and A. A. Mohamed, *Organometallics* **33** (2014) 439–442.

[22] T. Morita and S. Lindsay, *J. Am. Chem. Soc.* **129** (2007) 7262–7263.

[23] M. Kamiti, D. Boldridge, L. M. Ndoping and E. E. Remsen, *Anal. Chem.* **84** (2012) 10526–10530.

[24] H. A. Bullen and S. J. Garrett, *Nano Lett.* **2** (2002) 739–745.

[25] D. Kozak, W. Anderson, R. Vogel, S. Chen, F. Antaw and M. Trau, *ACS Nano* **6** (2012) 6990–6997.

[26] W. Haiss, N. T. K. Thanh, J. Aveyard and D. G. Fernig, *Anal. Chem.* **79** (2007) 4215–4221.

[27] Y. G. Zhou, N. V. Rees and R. G. Compton, *Angew. Chem., Int. Ed.* **50** (2011) 4219–4221.

[28] P. Atkins and J. De Paula, *Atkins' Physical Chemistry* (Oxford University Press, Oxford, U.K., 2006), eighth edition.

[29] T. D. Allen, G. R. Bennion, S. A. Rutherford, S. Reipert, A. Ramalho, E. Kiseleva and M. W. Goldberg, *Scanning* **19** (1997) 403–410.

[30] J. Lim, S. Yeap, H. Che and S. Low, *Nanoscale Res. Lett.* **8** (2013) 381.

[31] B. Carr and Wright, *Nanoparticle Tracking Analysis* (NanoSight, Amesbury, U.K., 2013).

[32] M. Giovanni and M. Pumera, *Electrochem. Comm.* **13** (2011) 203–204.

[33] M. Giovanni, A. Ambrosi and M. Pumera, *Chem. - Asian J.* **7** (2012) 702–706.

[34] M. Giovanni and M. Pumera, *Electroanalysis* **24** (2012) 615–617.

[35] A. Merkoci, L. H. Marcolino-Junior, S. Marin, O. Fatibello-Filho and S. Alegret, *Nanotechnology* **18** (2007) 035502.

[36] S. Marin and A. Merkoci, *Nanotechnology* **20** (2009) 055101.

[37] O. S. Ivanova and F. P. Zamborini, *J. Am. Chem. Soc* **132** (2009) 70–72.

[38] L. Tang, X. Li, R. C. Cammarata, C. Friesen and K. Sieradzki, *J. Am. Chem. Soc.* **132** (2010) 11722–11726.

[39] W. J. Plieth, *J. Phys. Chem.* **86** (1982) 3166–3170.

[40] A. Henglein, *J. Phys. Chem.* **97** (1993) 5457–5471.

[41] A. Henglein, *Ber. Bunsenges Phys. Chem.* **81** (1977) 556–561.

[42] S. E. Ward Jones, F. G. Chevallier, C. A. Paddon and R. G. Compton, *Anal. Chem.* **79** (2007) 4110–4119.

[43] S. E. Ward Jones, F. W. Campbell, R. Baron, L. Xiao and R. G. Compton, *J. Phys. Chem. C* **112** (2008) 17820–17827.

[44] S. E. Ward Jones, K. E. Toghill, S. H. Zheng, S. Morin and R. G. Compton, *J. Phys. Chem. C* **113** (2009) 2846–2854.

[45] N. V. Rees, Y. Zhou and R. G. Compton, *RSC Adv.* **2** (2012) 379–384.

[46] M. Heyrovsky and J. Jirkovsky, *Langmuir* **11** (1995) 4288–4292.

[47] M. Heyrovsky, J. Jirkovsky and B. R. Muller, *Langmuir* **11** (1995) 4293–4299.

[48] M. Heyrovsky, J. Jirkovsky and M. Struplova-Bartackova, *Langmuir* **11** (1995) 4300–4308.

[49] M. Heyrovsky, J. Jirkovsky and M. Struplova-Bartackova, *Langmuir* **11** (1995) 4309–4312.

[50] A. Korshunov and M. Heyrovsky, *Electroanalysis* **18** (2006) 423–426.

[51] A. Korshunov and M. Heyrovsky, *J. Ele* **629** (2009) 23–29.

[52] A. Korshunov and M. Heyrovsky, *Electroanalysis* **22** (2010) 1989–1993.

[53] D. Hellberg, F. Scholz, F. Schauer and W. Weitschies, *Electrochem. Comm.* **4** (2002) 305–309.

[54] F. Scholz, D. Hellberg, F. Harnisch, A. Hummel and U. Hasse, *Electrochem. Comm.* **6** (2004) 929–933.

[55] D. Hellberg, F. Scholz, F. Schubert, M. Lovri, D. Omanovi, V. A. Hernndez and R. Thede, *J. Phys. Chem. B* **109** (2005) 14715–14726.

[56] C. E. Banks, N. V. Rees and R. G. Compton, *J. Electroanal. Chem.* **535** (2002) 41–47.

[57] C. E. Banks, N. V. Rees and R. G. Compton, *J. Phys. Chem. B* **106** (2002) 5810–5813.

[58] N. V. Rees, C. E. Banks and R. G. Compton, *J. Phys. Chem. B* **108** (2004) 18391–18394.

[59] A. D. Clegg, N. V. Rees, C. E. Banks and R. G. Compton, *ChemPhysChem* **7** (2006) 807–811.

[60] Y. G. Zhou, N. V. Rees, J. Pillay, R. Tshikhudo, S. Vilakazi and R. G. Compton, *Chem. Comm.* **48** (2012) 224–226.

[61] B. Haddou, N. V. Rees and R. G. Compton, *Phys* **14** (2012) 13612–13617.

[62] N. V. Rees, Y. Zhou and R. G. Compton, *ChemPhysChem* **12** (2011) 1645–1647.

[63] E. J. F. Dickinson, N. V. Rees and R. G. Compton, *Chem. Phys. Lett.* **528** (2012) 44–48.

[64] J. C. Lees, J. Ellison, C. Batchelor-McAuley, K. Tschulik, C. Damm, D. Omanovi and R. G. Compton, *ChemPhysChem* **14** (2013) 3895–3897.

[65] K. Tschulik, B. Haddou, D. Omanovic, N. V. Rees and R. G. Compton, *Nano Res.* **6** (2013) 836–841.

[66] W. Cheng, X. F. Zhou and R. G. Compton, *Angew. Chem., Int. Ed.* **52** (2013) 12980–12982.

[67] N. V. Rees, Y. Zhou and R. G. Compton, *Chem. Phys. Lett.* **525-526** (2012) 69–71.

[68] J. M. Kahk, N. V. Rees, J. Pillay, R. Tshikhudo, S. Vilakazi and R. G. Compton, *Nano Today* **7** (2012) 174–179.

[69] Y. Zhou, B. Haddou, N. V. Rees and R. G. Compton, *Phys. Chem. Chem. Phys.* **14** (2012) 14354–14357.

[70] K. R. Ward, N. S. Lawrence, R. S. Hartshorne and R. G. Compton, *J. Electroanal. Chem.* **683** (2012) 37–42.

[71] Y. G. Zhou, N. V. Rees and R. G. Compton, *Chem. Phys. Lett.* **514** (2011) 291–293.

[72] A. J. Bard, H. Zhou and S. J. Kwon, *Isr. J. Chem.* **50** (2010) 267–276.

[73] K. Tschulik, R. G. Palgrave, C. Batchelor-McAuley and R. G. Compton, *Nanotechnology* **24** (2013) 295502.

[74] E. Bura-Nakic, D. Krznaric, G. R. Helz and I. Ciglenecki, *Electroanalysis* **23** (2011) 1376–1382.

[75] E. Bura-Nakic, E. Viollier, D. Jezequel, A. Thiam and I. Ciglenecki, *Chem. Geol.* **266** (2009) 311–317.

[76] G. R. Helz, I. Ciglenecki, D. Krznaric and E. Bura-Nakic, *Voltammetry of Sulfide Nanoparticles and the FeS(aq) Problem*, volume 1071, chapter 14, 265–282 (2011).

[77] D. Krznaric, G. R. Helz, E. Bura-Nakic and D. Jurasin, *Anal. Chem.* **80** (2008) 742–749.

[78] E. Bura-Nakic, D. Krznaric, D. Jurasin, G. R. Helz and I. Ciglenecki, *Anal. Chim. Acta* **594** (2007) 44–51.

Chapter 3

Experimental Methods

This chapter details the chemical reagents and nanoparticle synthesis procedures used for the experiments presented in this thesis. A general overview of the experimental methods used throughout this thesis is also included while a detailed description of each experiment performed can be found in the relevant experimental sections of chapters 4-11.

3.1 Chemical Reagents

Table 3.1 details the chemical reagents used throughout this thesis along with their purities and suppliers.

3.2 Nanoparticle Synthesis

3.2.1 Silver Nanoparticle Synthesis

Metal nanoparticles are typically prepared *via* the reduction of a metal salt using a reducing agent that also acts to stabilise nanoparticles in solution. The method used for the synthesis of citrate capped silver nanoparticles studied in this thesis is adapted from the work of Pyatenko et al.[1].

Chemical Name	Formula	Purity	Supplier
Deionised water	H_2O	18.2 MΩ cm	Millipore
Silver nitrate	$AgNO_3$	$\geq$ 99.0 %	Sigma-Aldrich
Trisodium citrate	$Na_3C_6H_5O_7$	99 %	BDH
Silver nanoparticles	AgNP	-	synthesised
Sodium citrate monobasic	$NaC_6H_7O_7$	$\geq$ 99 %	Sigma-Aldrich
Acetonitrile	MeCN	$\geq$ 99.9 %	Sigma-Aldrich
Buckminsterfullerene	C_{60}	99.5 %	SES Research
Buckminsterfullerene nanoparticles	nano-C_{60}	-	synthesised
Gold nanoparticles	AuNP	-	Mintek
N-Methyl-2-pyrrolidone	C_5H_9NO	$>$ 99.5 %	Sigma-Aldrich
Sodium perchlorate	$NaClO_4$	$\geq$ 98.0 %	Sigma-Aldrich
Sodium chloride	NaCl	$\geq$ 99.0 %	Sigma-Aldrich
Potassium chloride	KCl	$>$ 99.0 %	Sigma-Aldrich
Hydrochloric acid	HCl	$\sim$ 37.0 %	Fisher Scientific
Nitric acid	HNO_3	70.0 %	Fisher Scientific
Sulphuric acid	H_2SO_4	$>$ 95.0 %	Fisher Scientific
Perchloric acid	$HClO_4$	70.0 %	Sigma-Aldrich
Tetra-n-butylammonium hexafluorophosphate	$C_{16}H_{36}F_6NP$	$>$ 99.0 %	Sigma-Aldrich
Sodium hydroxide	NaOH	$\geq$ 98.0 %	Sigma-Aldrich
Dimercaptosuccinic acid	$C_4H_6O_4S_2$	98.0 %	Sigma-Aldrich
Hydrogen peroxide	H_2O_2	14.1 %	Sigma-Aldrich
Ferrocene	$FeC_{10}H_{10}$	98.0 %	Sigma-Aldrich
Hexaammineruthenium(III) chloride	$RuN_6H_{18}Cl_3$	98.0 %	Sigma-Aldrich
Potassium ferricyanide	$K_3Fe(CN)_6$	99.0 %	Sigma-Aldrich
Potassium phosphate monbasic	KH_2PO_4	$\geq$ 98.0 %	Sigma-Aldrich
Potassium phosphate dibasic	K_2HPO_4	$\geq$ 98.0 %	Sigma-Aldrich
Potassium permanganate	$KMnO_4$	$>$ 99.0 %	Sigma-Aldrich

Table 3.1: List of chemical reagents used in this thesis

A 25 mL aliquot of a 10 mM silver citrate solution was placed in a flask containing 225 mL water. The solution was magnetically stirred and heated in the dark using an oil bath set to 110 °C until the boiling point was reached. Upon boiling, 5 mL of a trisodium citrate solution (1 g $Na_3C_6H_5O_7$/100 mL H_2O) was added to the flask and the mixture was left to boil for 1 h. After 1 h, the flask was placed in a cold water bath for approximately 5 min until the solution was cool. The nanoparticle suspension was stored away from light at room temperature. The concentration of silver nanoparticles in the synthesised stock suspension was determined *via* anodic stripping voltammetry (section 3.3.3) where a glassy carbon macroelectrode (r_e=1.5 mm) was modified with 2 µL of the silver nanoparticle suspension, dried under nitrogen or argon and then scanned to positive potentials in 0.1 M $NaClO_4$. The charge of the resulting stripping peak can then be used to quantify the number of nanoparticles on the electrode surface and therefore the concentration of silver nanoparticles in the synthesised suspension. Depending on the nanoparticle concentration required for experiments the silver nanoparticle suspension was then diluted with ultrapure water with a resistivity not less than 18.2 MΩ cm at 298 K.

3.2.2 C_{60} Nanoparticle Synthesis

A common synthesis method for organic nanoparticles is the reprecipitation method[2] where the species of interest is first dissolved in a solvent in which it is known to be soluble before transferring this solution to an agitated solvent in which the species is poorly soluble resulting in the formation of a colloidal solution. Due to the ease and reliability of this well established organic nanoparticle preparation technique it was selected for the synthesis of C_{60} nanoparticles, or nano-C_{60}. The method used here is based on the work by Zhang et

al[3], however the nanoparticles were reprecipitated in acetonitrile rather than water as in the nano-C_{60} synthesis reported by Alargova et al[4].

First, 17.2 mg C_{60} was dissolved in 20 mL N-Methyl-2-pyrrolidone (NMP) by stirring in the dark for 24 h. The C_{60} containing NMP solution was then added dropwise to 200 mL of stirring MeCN at a speed of 0.9 mL min^{-1}before continuing to stir for 30 min in the dark. The nanoparticle solution was passed through a 0.2 µm filter (Whatman International Ltd., Kent, U.K.) resulting in a transparent orange suspension of nano-C_{60} particles in 10 % NMP: 90 % MeCN. The nano-C_{60} particles were sized using DLS, as outlined in section 3.4.1, and found to be 16 nm in radius. The nanoparticle suspension was stored in the dark at room temperature until required. The concentration of nano-C_{60} was 0.1 mM, however this does not include the loss of material *via* filtration. For nanoparticle impact experiments where a low concentration of C_{60} particles is required the synthesised suspension was diluted with acetonitrile until the desired concentration was achieved.

3.3 Electrochemical Methods

3.3.1 Instrumentation

All electrochemical experiments were carried out using a computer controlled µ-Autolab type II potentiostat (EcoChemie, Utrecht, Netherlands). A standard three electrode set-up was used for all experiments reported in this thesis. Specific details regarding the electrode materials employed for each study can be found in the relevant experimental sections of chapters 4-11.

Table 3.2 summarises the various reference electrodes used in this thesis and their

Reference electrode material	E (V) vs. NHE[5, 6]	Supplier
Calomel (sat. KCl)	0.241	BASi, Japan
Silver chloride (sat. KCl)	0.197	eDAQ, Ireland
Mercurous sulphate (sat. KSO_4)	0.640	IJ Cambria Scientific, U.K.

Table 3.2: A list of reference electrodes employed and their potential against the normal hydrogen electrode (NHE)

Working electrode material	Radius (r_e)	Supplier
Glassy carbon	1.5 mm	CH Instruments, USA
Carbon fibre	6.9 µm, 5.9 µm, 5.5 µm, 4.8 µm	BASi, Japan
Gold	1.5 mm, 0.8 mm 0.5 mm, 4.2 µm	CH Instruments, USA

Table 3.3: A list of working electrodes employed and their associated radii

potential against the normal hydrogen electrode (NHE) while a list of working electrodes employed and their radii measured by electrochemical calibration is detailed in table 3.3. For all electrochemical experiments performed a graphite rod was used as the counter electrode.

3.3.2 Cyclic Voltammetry

Cyclic voltammetry was carried out using both macroelectrodes and microelectrodes. All voltammetric measurements were carried out in a Faraday cage to reduce noise. The potential window and scan rate measured for each voltammogram varied with the system studied, details of which can be found in the experimental sections of the following chapters.

The following is a schematic representation of the cell design for voltammetric measurements.

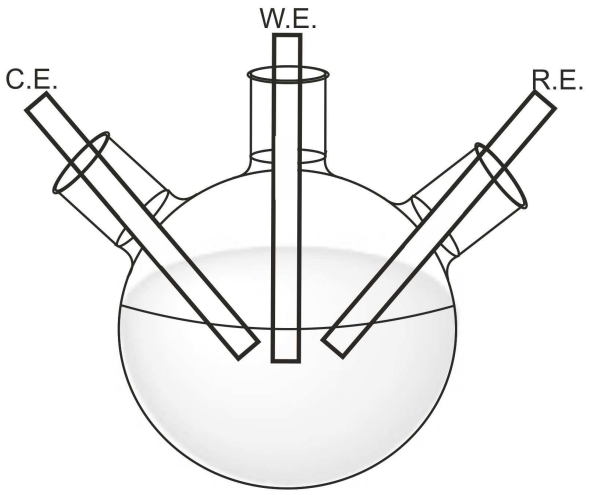


Figure 3.1: Diagram of the experimental set-up for cyclic voltammetry experiments showing the working, counter and reference electrodes (W.E, C.E. and R.E. respectively).

3.3.3 Anodic Stripping Voltammetry

The same experimental set-up detailed in section 3.3.2 was used for anodic stripping voltammetry.

3.3.4 Nanoparticle-Impact Experiments

Chonoamperometry was employed to observe nanoparticle-impact events. The duration of each chronoamperogram measured was 5 s and the sample time was 0.5 ms. All impact experiments were carried out within a double Faraday cage in order to minimise noise. Microelectrodes were also employed as the working electrode for all impact experiments performed. Figure 3.2 illustrates the electrochemical cell utilised which has a capacity of 25 mL.

A volume of electrolyte was added to the cell and the potential of the working electrode was set to one at which the nanoparticles to be added will undergo reduction or oxidation for the direct detection method, or one that will bring about the electrolysis of a solution

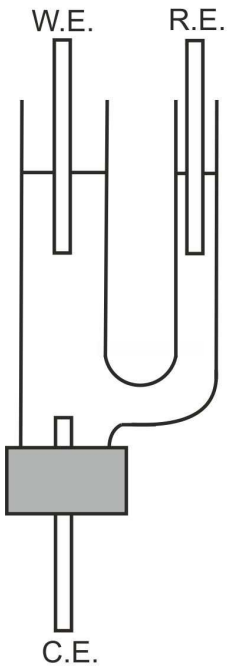


Figure 3.2: Diagram of the experimental set-up for nanoparticle-impact experiments showing the working, counter and reference electrodes (W.E, C.E. and R.E. respectively).

species on the nanoparticle surface if the indirect method is used. Chronoamperograms were recorded in the absence of nanoparticles to ensure no impact spikes were observed. An aliquot of nanoparticles was then added to the electrolyte and spikes in the current-time transient corresponding to nanoparticle-electrode collisions were observed. Either argon or nitrogen (oxygen-free, BOC gases plc) was bubbled through the solution at various points throughout the experiment, in between scans, to agitate the nanoparticles suspended in solution. The glass cell used for all experiments was cleaned using aqua regia to ensure complete removal of all nanoparticles.

To analyse the spikes observed in the current-time transients recorded OriginPro 8.5.1 and in-house developed software (SignalCounter) written by Dr Dario Omanovic at the Ruder Boskovic Institute in Zagreb, Croatia were used. The SignalCounter software uses a derivative transformation of the signal as the principal rule in the algorithm for spike recognition. A minimum height and the duration of the spike (threshold values) were

preselected in order to allow for the discrimination of small spikes from the noise. A visual inspection of spikes that had been automatically selected was performed and any spikes not identified automatically were then selected manually. The areas of the spikes were determined by means of the trapezoid rule. For two (or more) partly overlapped spikes a merged baseline was drawn and the corresponding area was assigned to each of the spikes respecting the minimum position between the spikes. Statistical analysis on the measured charge and nanoparticle size was performed with OriginPro 8.5.1.

3.4 Non-Electrochemical Methods

3.4.1 Dynamic Light Scattering

DLS measurements were performed using a Malvern Zetasizer Nano ZS (Malvern Instruments Ltd, Malvern, U.K.). Approximately 1 mL of a nanoparticle suspension that had been passed through a 0.2 µm filter (Whatman International Ltd., Kent, U.K.) was added to a glass cuvette before inserting the cuvette into the Zetasizer. The size of each nanoparticle suspension tested was measured three times to ensure reproducibility.

3.4.2 Nanoparticle Tracking Analysis

A NanoSight LM10 (NanoSight Limited, Amesbury, UK) was used to carry out NTA. A 300 µL sample of the nanoparticle solution to be studied was syringed into the viewing unit of the NanoSight and a red (638 nm) laser was used to illuminate the particles so they could be tracked. Measurements were recorded at 20 °C and the nanoparticles were tracked for a duration of 30 s. NanoSight NTA software was used to analyse the tracks of the nanoparticles in order to gain a particle size distribution.

3.4.3 Scanning Electron Microscopy

SEM imaging was performed by Dr Kristina Tschulik and Dr Kerstin Hennig at IFW Dresden, Germany. A LEO Gemini 1530 (Zeiss, Oberkochen, Germany) was employed for SEM imaging. A SEM holder that had been modified with a transmission electron microscopy grid was used for SEM experiments in order to minimise nanoparticle aggregation during sample preparation. Image J (Version 1.38) was used to analyse the nanoparticle size determined *via* SEM.

Bibliography

[1] A. Pyatenko, M. Yamaguchi and M. Suzuki, *J. Phys. Chem. C* **111** (2007) 7910–7917.

[2] H. Kasai, H. S. Nalwa, H. Oikawa, S. Okada, H. Matsuda, N. Minami, A. Kakuta, K. Ono, A. Mukoh and H. Nakanishi, *Jpn. J. Appl. Phys., Part 2* **31** (1992) L1132–L1134.

[3] S. A. Zhang, R. Sakai, T. Abe, T. Iyoda, T. Norimatsu and K. Nagai, *ACS Appl. Mater. Interfaces* **3** (2011) 1902–1909.

[4] R. G. Alargova, S. Deguchi and K. Tsujii, *J. Am. Chem. Soc* **123** (2001) 10460–10467.

[5] A. J. Bard and L. R. Faulkner, *Electrochemical Methods: Fundamentals and Applications* (John Wiley and Sons, New Jersey, 2001).

[6] D. J. G. Ives and G. J. Janz, *Potentials of Reference Electrode in Aqueous Solution at 25 C* (Academic, New York, 1961).

Chapter 4

Determining Unknown Concentrations of Silver Nanoparticles *via* Anodic Particle Coulometry

As discussed in chapter 2 there is an urgent need for suitable techniques that are capable of determining unknown concentrations of nanoparticles in solution. In this chapter it is shown that the recently developed technique known as anodic particle coulometry can be used to quantify silver nanoparticles suspended in an aqueous solution *via* the analysis of the cumulative number of nanoparticles impacting upon a carbon electrode over time. This analysis becomes more complex as the silver nanoparticles aggregate in solution during the experimental time-frame.

This work has been published in the *RSC Advances*[1] and was performed in collaboration with Dr. N. V. Rees who helped with the interpretation of experimental results and provided the data that was reinterpreted in figure 4.3.

4.1 Introduction

The development of suitable methods for nanoparticle quantification is necessary for assessing the hazards posed by the presence of nanoparticles in the environment[2]. Currently there is no standardised method to quantify nanoparticles[3, 4] and there are concerns surrounding the validity of literature reporting nanomaterial toxicity data due to limited information being provided on the concentration of nanomaterials employed in such studies[4, 5]. An accurate, reliable method to determine nanoparticle concentrations in solution would ensure ease of comparison between nanoparticle toxicity studies and allow the use of current data in models being developed to estimate the risks associated with exposure to nanomaterials[5].

One of the major problems associated with many existing techniques for nanoparticle quantification is that they need to be used in conjunction with specific separation or extraction methods in order to isolate the nanoparticles in a sample prior to determining nanoparticle concentrations[6, 7]. Electrochemical techniques offer a simpler and cheaper route to determining the concentration of nanoparticles within a sample without the need to separate the nanoparticles from solution, as well as having the potential to provide the user with multiple information regarding a specific nanoparticle sample (e.g. nanoparticle identity[1], size[8], aggregation behaviour[9, 10]) from just a single dataset.

A novel technique for the electrochemical detection of single nanoparticles in solution known as anodic particle coulometry has been introduced in chapter 2. This method monitors individual collision events between nanoparticles moving, *via* Brownian motion, in solution and a microelectrode that has been potentiostatted at a suitable oxidising potential so that destructive oxidation of the nanoparticle occurs upon impact. Therefore,

anodic particle coulometry requires a potential step to be applied to the microelectrode. Typically, the current-time transient resulting from a potential step at a microelectrode is given by:

$$I = 4nFCDr_{\mathrm{e}}f(\tau) \tag{4.1}$$

where n is the number of electrons transferred, F is the Faraday constant ($94\,685\,\mathrm{C\,mol^{-1}}$), C is the concentration (mol $\mathrm{m^{-3}}$), D is the diffusion coefficient ($\mathrm{m^2 s^{-1}}$), r_{e} is the radius of the microelectrode (m) and $f(\tau)$ is a function of time (s).

$f(\tau)$ can be given by the Shoup and Szabo equation[11] as introduced in chapter 1 where at short times the flux to the electrode surface is linear and Cottrellian behaviour is seen where $I \propto Cr_{\mathrm{e}}^2\ (D/t)^{1/2}$ whilst for longer times convergent diffusion is established ($I \propto Cr_{\mathrm{e}}D$). This equation is accurate to within 0.6%:

$$f(\tau) = 0.7854 + 0.8863\tau^{-1/2} + 0.2146\exp(0.7823\tau^{-1/2}) \tag{4.2}$$

where $\tau = 4Dt/r_{\mathrm{e}}^2$. The Shoup and Szabo equation is commonly used for fitting chronoamperometric measurements as it can provide the user with information regarding unknown values for (nC) and D. In this chapter, an integrated form of the Shoup and Szabo equation is fitted to experimentally determined plots of the cumulative number of nanoparticle-electrode impact events as a function of time measured *via* anodic particle coulometry, and as D can be determined using the Stokes-Einstein equation, a concentration value, C, for the nanoparticles in solution can be gained.

It has been shown in [8] that the frequency of spikes observed is proportional to the concentration of nanoparticles contained in the solution of interest. However, the use

of anodic particle coulometry to gain quantitative information regarding nanoparticle concentration has, until now, remained unexplored. Applying the proposed method to determine the concentration of aggregating nanoparticles is more complex as the nanoparticle concentration that is determined is that in solution at the time the potential step is applied. In this chapter silver nanoparticles are studied. Silver nanoparticles are prone to aggregation[9] thereby it is also demonstrated how this method can be used to determine the original concentration of nanoparticles dispersed into solution, that is the silver nanoparticle concentration pre-aggregation.

4.2 Experimental Procedure

4.2.1 Silver Nanoparticle Synthesis

The silver nanoparticles used were synthesised *via* the method described in section 3.2.1. The silver nanoparticles were characterised using anodic particle coulometry in [8] to be 13 nm in radius, a size that was supported with SEM imaging (r_{NP}=14 ± 2 nm).

4.2.2 Anodic Particle Coulometry

The experimental set-up described in section 3.3.4 was used for anodic particle coulometry experiments. The reference and counter electrodes used were a saturated calomel electrode (SCE) and graphite rod respectively while the working electrode used was a carbon fibre microelectrode (r_e=6.9 µm). The working electrode was polished using 3.0, 1.0 and 0.1 µm diamond spray respectively and then sonicated in water for 1 min. Following this, the electrode was immersed in a solution of 10 mM $NaC_6O_7H_7$/90 mM KCl that had been thoroughly degassed with argon to which 56 pM of silver nanoparticles had been added

and potentiostatted to +0.3 V *vs.* SCE. Analysis of the oxidative impact spikes observed *via* anodic particle coulometry and fitting with the integrated flux equation was performed using OriginPro 8.5.1.

4.2.3 Anodic Stripping Voltammetry

Anodic stripping voltammetry was carried out using the set-up detailed in 3.3.3. The working electrode was a glassy carbon (GC) electrode (r_e=1.5 mm) while the reference and counter electrodes employed were the same as in section 4.2.2. The working electrode was polished using three grades of diamond spray (3.0, 1.0 and 0.1 µm) before sonicating in water for 1 min. The electrode was then modified by dropcasting 2 µL of the synthesised silver nanoparticle suspension on the surface before drying under argon and scanning to positive potentials in an oxygen-free 0.1 M $NaClO_4$ solution.

4.3 Results and Discussion

Anodic particle coulometry was used to monitor stochastic silver nanoparticle collisions in 10 mM $NaC_6O_7H_7$/90 mM KCl at a carbon fibre microelectrode (r_e=6.9 µm) as in [8]. It is known from the work of Zhou et al. that the oxidation potential of silver nanoparticles in 10 mM $NaC_6O_7H_7$/90 mM KCl is 0.09 V *vs.* SCE[8]. Hence, for anodic particle coulometry experiments in this study the carbon fibre microelectrode was suspended in a solution of 10 mM $NaC_6O_7H_7$/90 mM KCl and potentiostatted at a higher potential than that of silver nanoparticle oxidation (+0.3 V *vs.* SCE). The 5 s chronomaperograms recorded showed no impact events (figure 4.1, dotted line) however when an aliquot of the synthesised silver nanoparticle suspension was added to the electrolyte solution so that the concentration

of nanoparticles in solution was equal to 56 pM, oxidative impact spikes were immediately observed in the current-time scans (figure 4.1, solid line). Each impact spike results from the destructive oxidation of a silver nanoparticle upon collision with the potentiostatted carbon electrode.

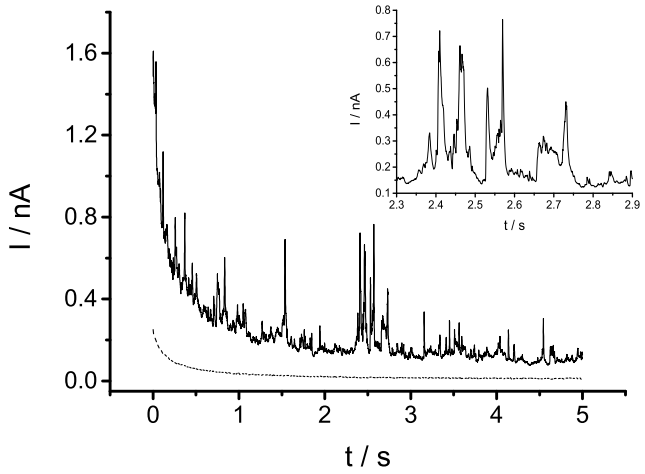


Figure 4.1: Typical chronoamperometric profile for a carbon fibre microelectrode (r_e=6.9 µm) potentiostatted at +0.3 V *vs.* SCE in a solution of 10 mM $NaC_6O_7H_7$/90 mM KCl with (solid line) and without (dotted line) 56 pM silver nanoparticles added. Inset shows a zoomed image of the oxidative impact spikes observed in the presence of silver nanoparticles caused by nanoparticle-electrode collisions.

Oxidative impact spikes were observed in each of the first 20 chronoamperometric scans which were recorded over 8 min. It was clear upon observation of these chronoamperometric scans that the frequency of spikes observed during each 5 s measurement decreased over time. This reduced occurrence of impact events can be explained by aggregation of the silver nanoparticles upon dispersion into the electrolyte solution. Silver nanoparticle aggregation has been studied in detail previously using anodic particle coulometry in the same electrolyte[9] with the nanoparticles having been found to increase in size from 13 nm to 29 nm in radius over a 2 h time duration. The affect of aggregation on the number of spikes observed per scan can be observed in figure 4.2 where the cumulative

number of spikes is plotted against time for scans measured at various time points post silver nanoparticle dispersion. It can be seen that the number of impact spikes observed per scan decreases from 82 to 36 to 27 for scans recorded at 1, 4 and 8 min after the nanoparticles had been dispersed in the electrolyte.

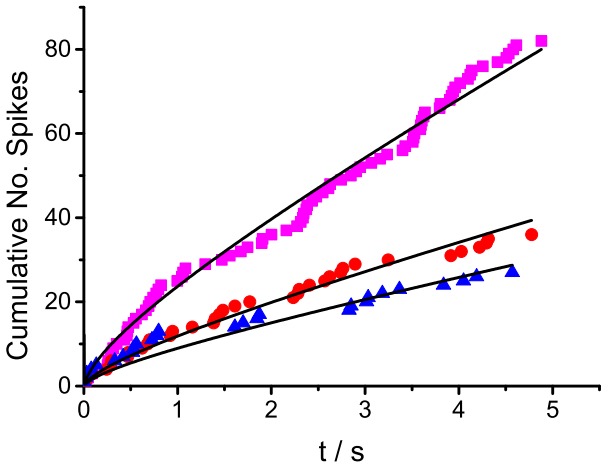


Figure 4.2: Fitting of equation 4.3 to plots of the cumulative number of spikes observed in a chronomaperometric scan for measurements performed 1 (pink square), 4 (red circle) and 8 min (blue triangle) post silver nanoparticle dispersion into 10 mM $NaC_6O_7H_7$/90 mM KCl. A fixed D value of 1.5×10^{-7} cm^2s^{-1} was used for all fittings shown.

The concentration of silver nanoparticles in solution at the time of scanning can be determined by fitting equation 4.3 to the plots shown in figure 4.2.

$$N = N_A C r_e^3(\tau + 1.437\tau^{1/2} + 6.57 \times 10^{-2} ln\tau - 3.35 \times 10^{-3}\tau^{-1} + 3.43 \times 10^{-3}\tau^{-1/2} + 3.49 \times 10^{-4}\tau^{-3/2} \quad (4.3)$$

Equation 4.3 is determined by converting the current, I, given by equation 4.1, to the number of silver nanoparticles impacting per second by introducing the Avagadro

constant, N_A, and the electrode area, and then integrating with respect to time (using a series expansion to 5 terms to simplify the exponential term).

The fitting of equation 4.3 to experimental data for the cumulative number of impact spikes observed over a 5 s measurement is shown by the black lines in figure 4.3. The increased occurrence of spikes observed at the start of the chronomaperometric scans measured during anodic particle coulometry experiments, as demonstrated by the apparent levelling off in the cumulative number of spikes in figure 4.3, is supported by this integrated flux equation. To determine a value for the nanoparticle concentration, C, at the time of scanning the values for D and r_e were fixed. The value for r_e (6.9 µm) was obtained *via* electrochemical calibration of the carbon microelectrode using the well established redox couple $Fe(CN)_6^{3-}/Fe(CN)_6^{4-}$ while the Stokes-Einstein equation (equation 4.4) was used for the determination of D for an individual nanoparticle (r_{NP}=13 nm)[12]:

$$D = \frac{k_B T}{6\pi\eta r_{NP}} \tag{4.4}$$

where k_B is the Boltzmann constant and η is the dynamic viscosity of the solvent. As $D \propto \chi^{-1/2}$ where χ is the number of nanoparticles in an aggregate, or cluster, it is approximated that the D value calculated using equation 4.4 (1.5×10^{-7} cm^2s^{-1}) is constant for the small clusters of silver nanoparticles formed over the short time duration (8 min) of the anodic particle coulometry experiment to simplify the fitting of equation 4.3 to experimental data. The fitting of equation 4.3 gives C values for silver nanoparticles in solution of 36 ± 6 pM, 21 ± 5 pM and 17 ± 4 pM for scans recorded 1, 4 and 8 min post nanoparticle dispersion into the electrolyte. Again, the decreasing concentration values observed with time suggests that the silver nanoparticles are aggregating in solution.

Thus, applying equation 4.3 for the quantification of nanoparticles in solution can also provide in-situ information on the state of nanoparticle aggregation.

Having determined the concentration of silver nanoparticles in solution at specific time intervals, C_{t}, it is possible to determine the starting concentration of silver nanoparticles, C_0, using:

$$C_{\mathrm{t}} = \frac{C_0}{\chi_{\mathrm{t}}} \tag{4.5}$$

where χ_t is the number of nanoparticles in a cluster at a time, t.

In previous work performed by Rees et al[9], using anodic particle coulometry to monitor silver nanoparticle aggregation in the same electrolyte used here, the size of the nanoparticle clusters were measured as a function of time over a period of 120 min. The radius of a nanoparticle cluster, R_{NP}, is related to the number of nanoparticles in the cluster *via*:

$$\chi = \left(\frac{R_{\mathrm{NP}}}{r_{\mathrm{NP}}}\right)^3 \tag{4.6}$$

It is possible to reinterpret the data presented by Rees et al. in [9] using equation 4.6 in terms the number of nanoparticles contained within a cluster as a function time (figure 4.3).

Using the plot shown in figure 4.3 it is possible to determine the empirical expression:

$$ln\chi = 0.42lnt + 0.50 \tag{4.7}$$

By substituting equation 4.5 into this expression (4.7) it is possible to empirically

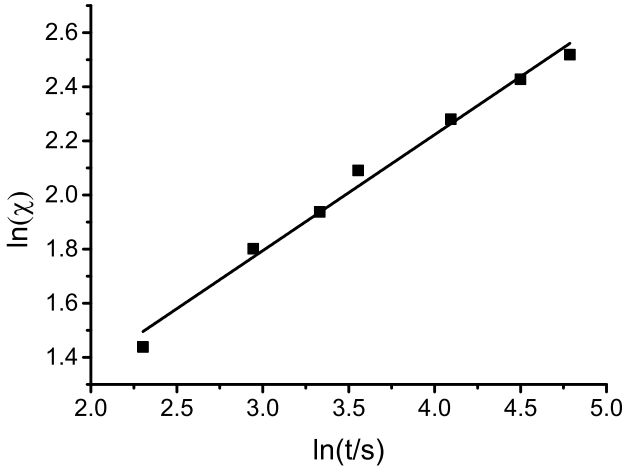


Figure 4.3: A plot of $\ln(\chi)$ *vs.* $\ln(t)$ determined using data from [9] and equation 4.6 in order to show how silver nanoparticle cluster size changes with time. Plot gradient=0.42 and y-intercept=0.50.

determine how the concentration of silver nanoparticles decreases with time as a result of aggregation using equation 4.8:

$$lnC_{\mathrm{t}} = -0.42lnt + (lnC_0 - 0.50) \tag{4.8}$$

Using this empirical expression, the starting concentration of silver nanoaparticles in solution, C_0, can be determined by employing equation 4.3 to plots of the cumulative number of impact spikes *vs.* time to determine the concentration of nanoparticles at specific time points since dispersion, C_{t}. A plot of $\ln(C_{\mathrm{t}})$ *vs.* $\ln(t)$ is shown in figure 4.4 where when multiple scans have been measured per minute a mean value is taken of the determined values for C_{t} in order to yield a single data point with an associated error. The application of expression 4.8 to the plot in figure 4.4 gives a C_0 value of $57 \pm 10\,\mathrm{pM}$.

To verify the accuracy of the above method for determining unknown concentrations of nanoparticles in solution and, for this system, the nanoparticle concentration pre-aggregation, an independent electrochemical method was used. For this method, a $2\,\mu\mathrm{L}$

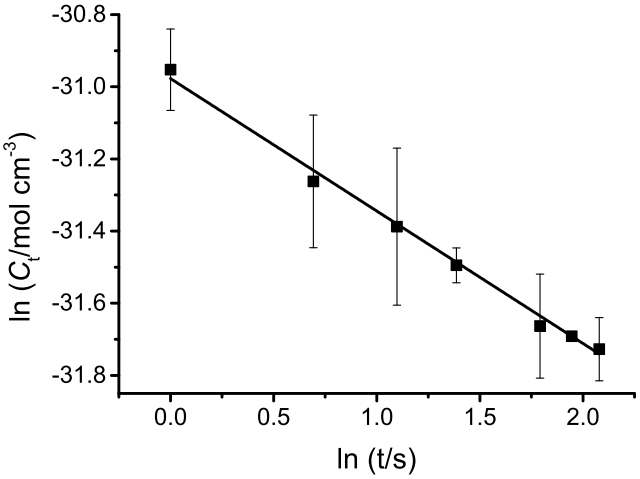


Figure 4.4: A plot of $\ln(C_t)$ *vs.* $\ln(t)$ where the C_t values are determined *via* the fitting of equation 4.3 to experimental data using a fixed D value of 1.5×10^{-7} cm^2 s^{-1}. Plot gradient=-0.39 and y-intercept=-31.0.

aliquot of the synthesised silver nanoparticle suspension was deposited onto a GC macroelectrode surface (r_e=1.5 mm) and scanned in the anodic direction in 0.1 M $NaClO_4$ until the immobilised silver nanoparticles had been oxidatively stripped off the electrode surface. An example stripping voltammogram is shown in figure 4.5. The area of the observed stripping peak can then be integrated to give the charge passed during the oxidative process. Using the molar mass (107.87 g mol^{-1}) and density (10.49 g cm^{-3}) of silver and the known size of the suspended silver nanoparticles (r_{NP}=13 nm) the number of silver nanoparticles deposited in the aliquotted volume can be calculated from the charge and thus the concentration, C_0, can be determined. A mean concentration value of C_0=55.7 $\pm$ 8.9 pM was determined from five oxidative stripping experiments. The good agreement between this concentration value and that obtained *via* analysis of the number of impact spikes observed using anodic particle coulometry (57 $\pm$ 10 pM) proves that the proposed method for determining unknown concentrations of nanoparticles in solution *via* anodic particle coulometry is both feasible and accurate.

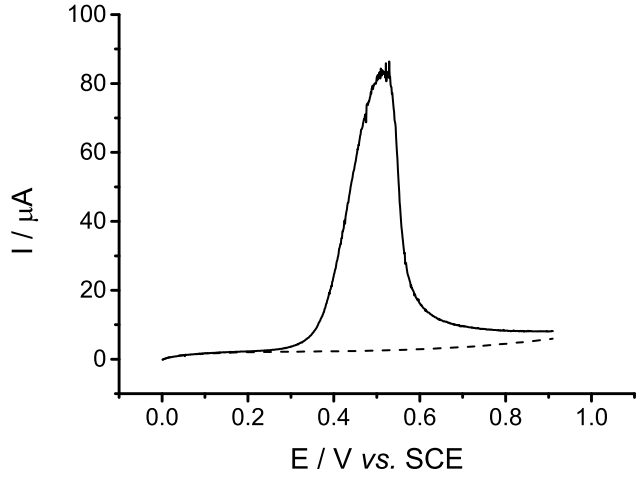


Figure 4.5: Anodic stripping voltammogram for a GC macroelectrode (r_e=1.5 mm) modified with 2 µL of the synthesised silver nanoparticle suspension (solid line) and the bare GC macroelectrode (dashed line) scanned in 0.1 M $NaClO_4$ at a scan rate of 200 mV s^{-1}.

4.4 Conclusions

This chapter has outlined the use of a new methodology by which to analyse results gained *via* anodic particle coulometry in order to determine unknown concentrations of silver nanoparticles in solution. Changes in the concentration of silver nanoparticles caused by nanoparticle aggregation can also be monitored using this method and an empirical expression that can be used to determine the starting concentration of silver nanoparticles in solution has been presented.

It is important to note that the empirical expression shown in equation 4.8 is only applicable to the size and type of nanoparticle studied in this chapter. The capping agent on the surface of the nanomaterial and type of electrolyte into which the nanoparticle is dispersed will also have a significant affect on aggregation behaviour and thus the expression used to determine C_0 from experimental data. However, as long as the type of nanoparticle, and its aggregation behaviour, is known this new methodology could be applied to other nanoparticle systems. Consequently, it has been shown that this tech-

nique is suitable for the determination of unknown concentrations of nickel nanoparticles which are known to be non-aggregating[1]. Recently, Barnes et al. have built upon the work outlined in this chapter and in [13] by developing a model that considers the effects of near wall hindered diffusion of nanoparticles in solution impacting upon an electrode to simulate the experimental anodic particle coulometry of nickel nanoparticles. It has also been found that equation 4.3 is useful for the calculation of suitable nanoparticle concentrations required in nanoparticle impact experiments[14].

With concerns surrounding the presence of nanoparticles in the environment [15, 16], anodic particle coulometry could potentially be used to determine unknown concentrations of nanoparticles in authentic environmental samples. In matrices with a high ionic strength, such as seawater, silver nanoparticles are known to be susceptible to aggregation therefore it is particularly useful that the methodology proposed in this chapter is applicable to aggregating systems.

Bibliography

[1] E. J. E. Stuart, Y. G. Zhou, N. V. Rees and R. G. Compton, *RSC Adv.* **2** (2012) 6879–6884.

[2] A. G. Howard, *J. Environ. Monit.* **12** (2010) 135–142.

[3] M. Li, S. Guha, R. Zangmeister, M. Tarlov and R. Zachariah, *Langmuir* **57** (2011) 14732–14739.

[4] S. J. Klaine, P. J. J. Alvarez, G. E. Batley, T. F. Fernandes, R. D. Handy, L. D. Y., S. Mahendra, M. J. McLaughlin and J. R. Lead, *Environ. Toxicol. Chem.* **27** (2008) 1825–1851.

[5] H. S. A. C. Members, *Hazardous Substances Advisory Committee Opinion on Nanoscience* (available from: www.nanotechnproject.org/inventories/consumer/, 2012).

[6] T. M. Benn and P. Westerhoff, *Environ. Sci. Technol.* **42** (2008) 4133–4139.

[7] J. Chao, J. Liu, S. Yu, Y. Feng, Z. Tan, R. Liu and Y. Yin, *Anal. Chem.* **83** (2011) 6875–6882.

[8] Y. G. Zhou, N. V. Rees and R. G. Compton, *Angew. Chem., Int. Ed.* **50** (2011) 4219–4221.

[9] N. V. Rees, Y. G. Zhou and R. Compton, *ChemPhysChem* **12** (2011) 1645–1647.

[10] D. F. Qiu, S. Wang, Y. Q. Zheng and Z. X. Deng, *Nanotechnology* **24** (2013) 505707.

[11] D. Shoup and A. Szabo, *J. Electroanal. Chem. Interfacial Electrochem.* **140** (1982) 237–245.

[12] K. A. Dill and S. Bromberg, *Molecular Driving Forces* (Garland Science, New York, 2002).

[13] E. O. Barnes, Y. G. Zhou, N. V. Rees and R. G. Compton, *J. Electroanal. Chem.* **691** (2013) 28–34.

[14] J. Ellison, C. Batchelor-McAuley, K. Tschulik and R. G. Compton, *Sens. Actuators, B* **200** (2014) 47–52.

[15] J. Fabrega, S. N. Luoma, C. R. Tyler, T. S. Galloway and Lead, *Environ. Int.* **37** (2011) 517–531.

[16] S. Yu, Y. Ying and J. Liu, *Environ. Sci.: Processes Impacts* **15** (2013) 78–92.

Chapter 5

Direct Electrochemical Detection and Sizing of Silver Nanoparticles in Seawater Media

The previous chapter reported on the use of a novel electrochemical technique known as anodic particle coulometry for determining the concentration of synthetic silver nanoparticles dispersed in an electrolyte solution. This chapter reports on proof-of-concept measurements using this anodic particle coulometry technique relating to the impact of nanoparticles with an electrode potentiostatted at a value corresponding to the oxidation of silver nanoparticles in *authentic seawater media*. The charge associated with the oxidation reveals the number of atoms in the nanoparticle and thus its size and state of aggregation providing information of importance for the possible toxicological implications of the presence of silver nanoparticles in the environment.

This work has been published in *Nanoscale*[1] and was carried out in collaboration with Dr. N. V. Rees and Dr. J. T. Cullen from the University of Victoria, BC, Canada. Dr. J. T. Cullen advised on oceanographic sampling and Dr. N. V. Rees helped to plan experiments, both Dr. J. T. Cullen and Dr. N. V. Rees contributed to scientific discussions.

5.1 Introduction

With the number of commercially available products containing silver nanoparticles continuing to rise and the potentially harmful environmental consequences posed by their inevitable release into natural waters[2–6] an accurate method capable of directly detecting these widely used nanoparticles in the environment is required.

In 2011 a novel nanoparticle detection and sizing technique, anodic particle coulometry, involving the observation of Faradaic charge transfer associated with the quantitative destructive oxidation of nanoparticles colliding with an electrode surface was reported for the first time[7]. Chapter 4 investigated the use of anodic particle coulometry for the accurate determination of silver nanoparticle concentrations in solution using the integrated form of the Shoup and Szabo equation and showed how aggregation of the silver nanoparticles can be monitored[8]. Not only is it possible to utilise this method for nanoparticle detection and quantification, it has also been shown that this method demonstrates selectivity in mixed nanoparticle systems as the onset of the current-time transients caused by nanoparticle collisions is potential dependent[9]. Importantly, anodic particle coulometry in principle exhibits portability advantages making it suitable for use in the field and could potentially be used for studies involving the release of silver nanoparticles into the environment from commercially available products. In this chapter, the possible application of anodic particle coulometry to environmental testing is investigated with a proof-of-concept study performed in which anodic particle coulometry is employed to detect laboratory synthesised citrate capped silver nanoparticles that have been dispersed in an authentic seawater sample.

One of the benefits of anodic particle coulometry that is of major importance for envi-

ronmental monitoring is its ability to determine the persistence of single nanoparticles in aqueous samples *via* determination of nanoparticle size from the charge transferred during a nanoparticle-electrode impact[8]. It was shown in chapter 4 that silver nanoparticles have a tendency to aggregate in aqueous solution[8] but how does this behaviour change when they are exposed to environmental conditions? With the biocidal nature of silver nanoparticles being particle-size dependent the degree of aggregation has possible implications on their hazardous effect on aquatic ecosystems[10]. Hitherto, researchers have combined two or more of the following techniques to detect, size and estimate the degree of silver nanoparticle aggregation in natural waters: DLS[6, 11–14], SEM[11], AFM[12], flow-field flow fractionation[13], UV-VIS absorbance measurements[6, 12], single particle ICP-MS[15], NTA[15] and TEM[6, 13, 14].

Determining the suitability of the anodic particle coulometry method to fieldwork of this type involves adding a known concentration of synthetic citrate capped silver nanoparticles to seawater samples collected in Saanich Inlet, a fjord located in southern British Columbia, Canada. The results of these proof-of-concept measurements reveal that anodic particle coulometry is indeed a suitable method for both the detection and characterisation of silver nanoparticles in natural water samples. This specific method additionally reveals that silver nanoparticles aggregate in seawater.

5.2 Experimental Procedure

5.2.1 Seawater Sampling

Water column observations and seawater samples from Saanich Inlet, an anoxic fjord in British Columbia, Canada were collected onboard the University of Victoria research ves-

sel M.S.V. John Strickland on June 13, 2012. The temperature, salinity and dissolved oxygen in the inlet were measured using a Sea-Bird 19plus CTD (Conductivity, Temperature and Depth) equipped with a dissolved oxygen sensor (SBE43). Seawater samples were obtained using 5 L Niskin bottles (General Oceanics, Miami, FL USA) attached to a stainless steel hydrowire that were tripped with Teflon coated messengers. Seawater was collected from the Niskin bottles directly into trace metal clean 250 mL low density polyethylene bottles that were immediately refrigerated and returned to the laboratory for subsequent analyses. The pH of the seawater sample after purging was found to be 8.28 and the samples were upturned in order to resuspend any settled particulate matter before use.

5.2.2 Silver Nanoparticle Synthesis

Citrate capped silver nanoparticles were synthesised as described in chapter 3 and were found *via* anodic particle coulometry to have a mean radius of 13 nm, a size that was supported with SEM imaging (r_{NP}=14 ± 2 nm).

5.2.3 Electrochemical Methods

Anodic Stripping Voltammetry

The experimental set-up used is described in chapter 3. A glassy carbon (GC) macroelectrode (r_{e}=1.5 mm) was used as the working electrode along with a saturated calomel (SCE) reference electrode and a graphite rod counter electrode. The GC macroelectrode was surface modified with silver nanoparticles by depositing 2 µL of the silver nanoparticle suspension onto the electrode surface before allowing it to dry under a nitrogen

atmosphere. The modified electrode was then immersed in a seawater sample that had been degassed thoroughly with nitrogen and an oxygen-free atmosphere was maintained throughout the duration of the experiment. The GC macroelectrode was polished using 3.0, 1.0 and 0.1 µm diamond spray respectively on hard polishing pads prior to sonicating in water for 1 min and drying with nitrogen.

Anodic Particle Coulometry

For nanoparticle impact experiments a carbon microelectrode (r_e=5.94 µm), a SCE or saturated silver/silver chloride (Ag/AgCl) electrode and a graphite rod were employed as the working, reference and counter electrodes respectively. Before commencing anodic particle coulometry experiments the natural seawater samples and NaCl solutions were degassed thoroughly with nitrogen and a nitrogen blanket was maintained during the experiment. Throughout the anodic particle coulometry experiment the solution was regularly bubbled with the nitrogen gas supply to agitate the nanoparticles in solution. Diamond spray (3.0, 1.0 and 0.1 µm) was used to polish the carbon microelectrode between experiments. After polishing, the microelectrode was sonicated in water for 1 min before drying with nitrogen. OriginPro v.8.5.1 was used to both analyse the impact spikes and to carry out Gaussian deconvolution of the size distributions.

5.3 Results and Discussion

5.3.1 Determining the Silver Nanoparticle Oxidation Potential in Seawater

The first step was to determine the oxidation potential of silver nanoparticles in seawater. To do this a GC macroelectrode (r_e=1.5 mm diameter) that had been surface modified with 1.5×10^{-15} mol silver nanoparticles was scanned to positive potentials using anodic stripping voltammetry in a seawater sample taken at a depth of 205 m (see figure 5.1). The peak potential was +0.03 V *vs.* SCE which is in agreement with previously reported measurements for the oxidation of silver nanoparticles in the presence of chloride ions as shown in reaction 5.1[16].

$$\mathrm{AgNP_{(s)} + Cl^-_{(aq)} \longrightarrow AgCl_{(s)} + e^-} \tag{5.1}$$

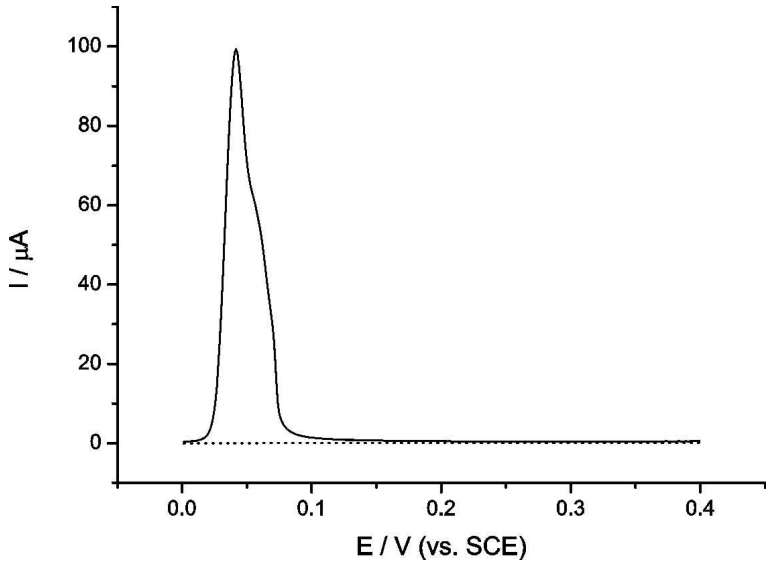


Figure 5.1: Stripping voltammogram of a bare GC macroelectrode (dotted line) and a GC macroelectrode modified with 1.5×10^{-15} mol silver nanoparticles (solid line) scanned in seawater at a scan rate of 20 mV s^{-1}.

5.3.2 Silver Nanoparticle Detection in Seawater *via* Anodic Particle Coulometry

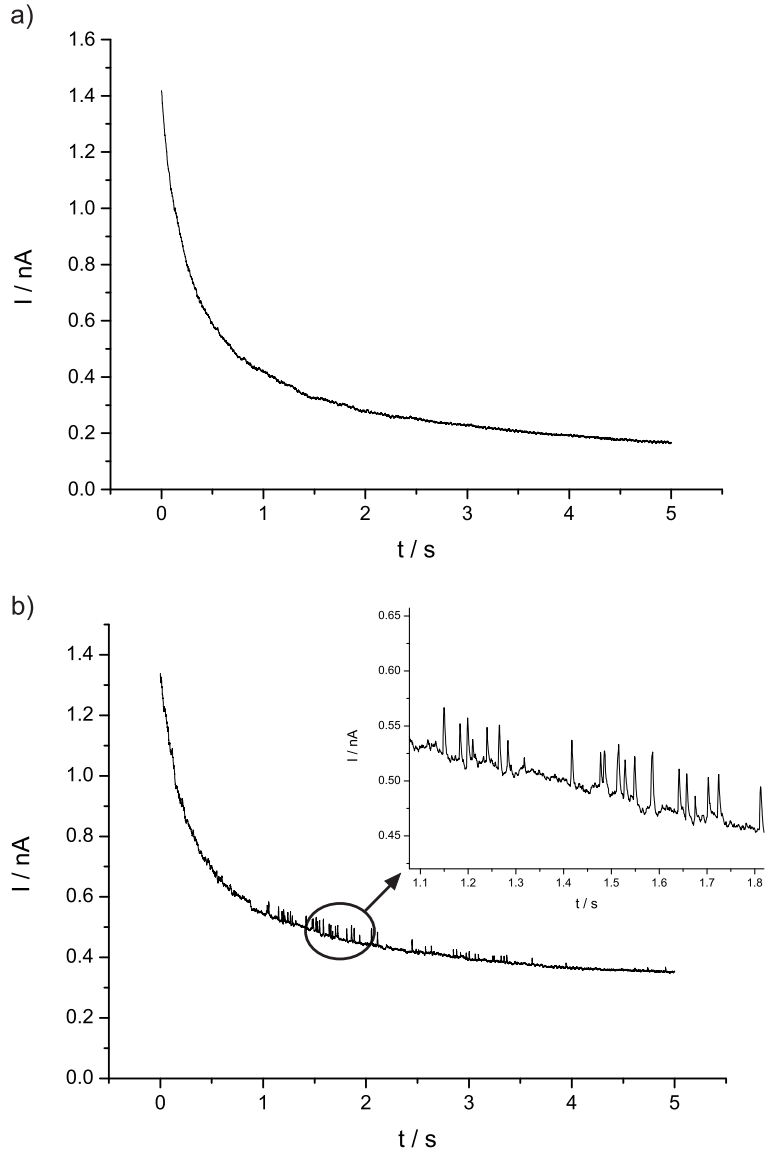


Figure 5.2: a) Current-time transient for a carbon microelectrode (r_e=5.94 µm) in seawater media held at E=+0.3 V *vs.* SCE. b) Oxidative impact spikes observed in a current-time transient for a carbon microelectrode (r_e=5.94 µm) in seawater media with 58.9 pM citrate-capped silver nanoparticles (r_{NP}=13 nm) added.

A carbon microelectrode (r_e=5.94 µm) was potentiostatted in the seawater sample at a potential more positive than that required to oxidise the nanoparticles in seawater as determined in section 5.3.1 and no impact spikes were observed (figure 5.2a). An aliquot

of silver nanoparticles was then added so that the concentration of nanoparticles in the cell was 58.9 pM and oxidative impact spikes were observed in the current-time transient, as shown in figure 5.2b.

With each spike observed allowing us to detect individual nanoparticle electrode collision events, it is also possible to gain quantitative information regarding the number of atoms in each silver nanoparticle (N_{NP}) and therefore the extent of aggregation by integrating the charge (Q) under each of oxidative impact spikes observed in the current-time transient and using equation 5.2:

$$Q = eN_{\mathrm{NP}} \tag{5.2}$$

where e is the elementary charge (1.602×10^{-19} C).

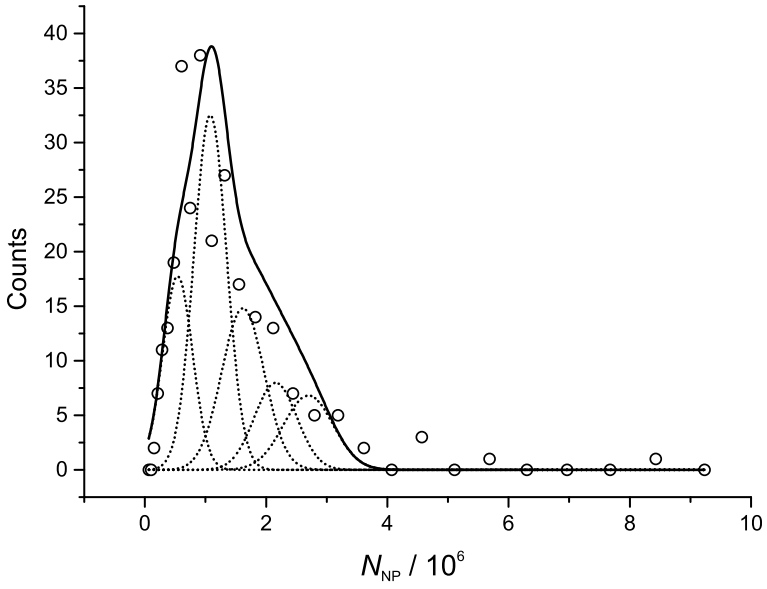


Figure 5.3: Size distribution of silver nanoparticles in seawater as determined from anodic particle coulometry showing deconvolution into five Gaussian subdistributions

Figure 5.3 shows the size distribution of nanoparticles in terms of the number of atoms making up each nanoparticle inferred from the charge passed during the observed nanopar-

ticle impacts using equation 5.2. With the average size of the laboratory synthesised silver nanoparticles utilised in this study having previously been determined *via* anodic particle coulometry to be 13 nm in radius[7], it can be estimated that a single silver nanoparticle of this size contains approximately 0.54×10^6 atoms. Therefore, figure 5.3 shows that the nanoparticles are extensively aggregated in solution since the majority of particles possess a larger number of atoms than that for a single silver nanoparticle. Preliminary deconvolution of the anodic particle coulometry distribtutuion in figure 5.3 into subdistributions arbitrarily using five Gaussian distributions revealed significant contributions from not only single nanoparticles but also aggregates of 2, 3, 4 and 5 nanoparticles corresponding to 1.08×10^6, 1.62×10^6, 2.16×10^6 and 2.70×10^6 atoms respectively. Therefore, anodic particle coulometry distribution data of silver nanoparticles in seawater suggests that over the timescale studied (42 min), silver nanoparticles are prone to aggregation. Five size classes were fitted as it is clear that very few impact spikes correspond to colliding nanoparticles beyond the size of five nanoparticle aggregates ($> 2.70 \times 10^6$ atoms). Further detailed studies focussing of silver nanoparticle aggregation have since been performed[17].

It is likely that the behaviour of silver nanoparticles in seawater is mostly controlled by the major ionic components of seawater which, at salinity S=35, are sodium (469.06 mmol kg^{-1}), magnesium (52.82 mmol kg^{-1}), calcium (10.28 mmol kg^{-1}), potassium (10.21 mmol kg^{-1}) cations and chloride (545.86 mmol kg^{-1}), sulphate (28.24 mmol kg^{-1}) and bicarbonate (1.80 mmol kg^{-1}) anions; sodium and chloride ions are the dominant components[18]. The salinity of seawater is determined by measuring its conductance, for example a seawater sample of salinity S=35 has an equivalent conductance of 32.4356 g KCl in 1 kg of solution at 1 atm pressure and 15 °C[18].

5.3.3 Silver Nanoparticle Detection in NaCl *via* Anodic Particle Coulometry

From salinity measurements of the seawater at the location and depth where sampling occurred (salinity=31.3, depth=205 m), the chloride concentration was determined to be equivalent to 487 mM[18]. Therefore, the next step was to perform the nanoparticle collision experiment under exactly the same conditions reported above for the seawater sample but this time replacing the seawater sample in which the anodic particle coulometry experiment was performed with 487 mM NaCl. A current-time transient showing an example of the oxidative impact spikes observed when silver nanoparticles were dispersed in a solution of 487 mM NaCl can be seen in figure 5.4b. As with the anodic particle coulometry experiment performed in seawater media no impact spikes were observed in the absence of silver nanoparticles (figure 5.4a). Impact spikes were recorded over a period of 47 min.

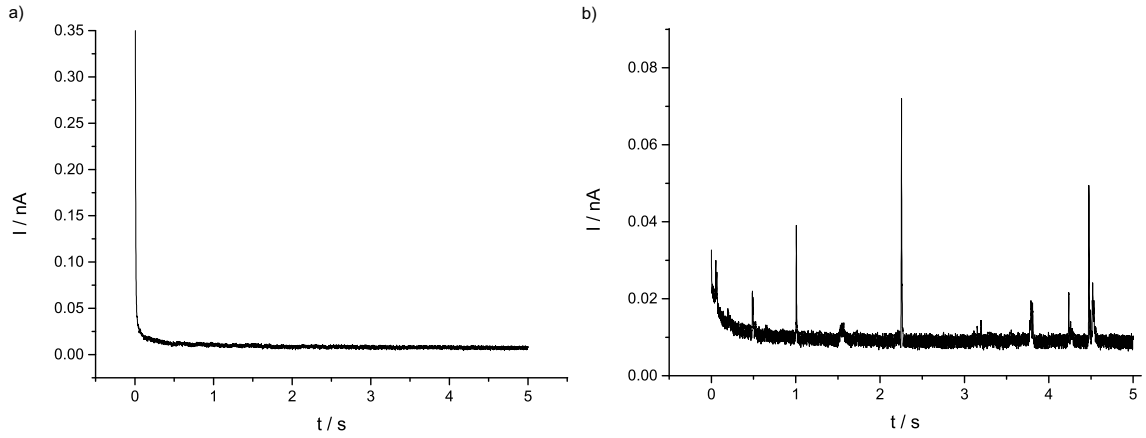


Figure 5.4: a) Current-time transient for a carbon microelectrode (r_e=5.94 µm) in 487 mM NaCl held at E=+0.3 V *vs.* SCE.b) Oxidative impact spikes observed in a current-time transient for a carbon microelectrode (r_e=5.94 µm) in a silver nanoparticle containing 487 mM NaCl solution.

As before, the size distribution of impacting nanoparticles was plotted (figure 5.5a) and contributions from the same five nanoparticle sizes observed in the seawater sample using arbitrary Gaussian deconvolution also appeared to be prevalent in 487 mM NaCl.

With aggregation occurring to a similar extent in this salt concentration we can conclude that the ionic strength of seawater is responsible for the observed silver nanoparticle aggregation in the seawater sample tested.

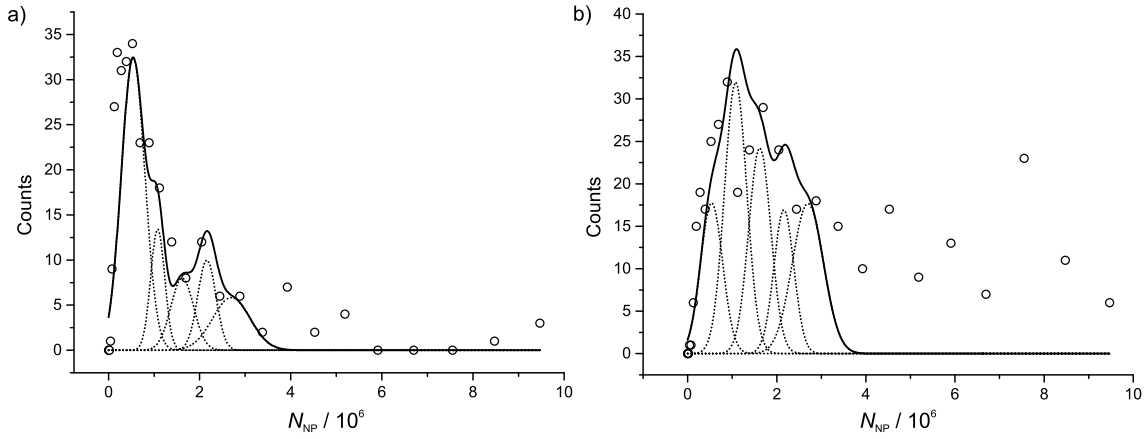


Figure 5.5: Anodic particle coulometry distribution of silver nanoparticles showing Gaussian sub-distributions representing aggregates of up to five nanoparticles in size in solutions of a) 487 mM NaCl and b) 100 mM NaCl.

Interestingly, when the same collision experiment was repeated in a lower salt concentration (100 mM NaCl) over a timescale of 42 min and an anodic particle coulometry distribution was plotted for the number of atoms (N_{NP}) in each impacting nanoparticle as inferred from equation 5.2 (figure 5.5b), it was apparent that the nanoparticles were aggregating at a faster rate at this lower ionic strength. It can be seen that this size distribution can be preliminarily deconvoluted into the same arbitrary sub-distributions for aggregates composed of up to five nanoparticles as before but it is clear that beyond nanoparticle cluster sizes of 2.70×10^6 atoms larger sized aggregates were also formed in solution which were not present at similar timescales in solutions of higher ionic strength i.e. in the seawater and pure 487 mM NaCl samples.

Note that moderately high concentrations of electrolyte are generally thought to encourage aggregation of silver nanoparticles[5, 6, 19]. This is in agreement with the Der-

jaguin, Landau, Verwey and Overbeek (DLVO) theory for particle interactions which states that an increase in ionic strength will result in the promotion of nanoparticle aggregation as the repulsion between like charged particles will be screened by ions in solution. However, a number of flaws have been identified in traditional DLVO theory, of most relevance here is the disregard for dispersion interactions[20]. Specifically Bostrm et al. have demonstrated the importance of dispersion forces in colloidal systems, noting a significant change in the force between charged interfaces when dispersion forces of counter ions were considered at salt concentrations of 100 mM and an even greater effect was observed when the concentration was increased to 300 mM[20]. As a result it has been suggested that classical DLVO theory is inadequate for systems where the salt concentration is 100 mM or higher[20].

The slower rate of aggregation of silver nanoparticles observed in the more concentrated NaCl solution tested might be explained by the significant ionic dispersion forces that will be dominant at these salt concentrations. Another possible reason behind the inconsistencies with DLVO theory observed here is that both of the NaCl concentrations tested are of high ionic strength. If silver nanoparticle aggregation at significantly lower NaCl concentrations had been examined (e.g. 0.1 mM) it may have been possible to observe DLVO behaviour. However, in order to ensure full support in the anodic particle coulometry experiments the electrolyte concentrations could not be reduced below 100 mM.

5.4 Conclusions

This chapter builds upon work on the detection of silver nanoparticles *via* anodic particle coulometry reported in [7, 8] and on the study presented in chapter 4. A significant motivation behind developing novel techniques for the detection, characterisation and quantification of nanoparticles is the growing prominence of these nanomaterials and the lack of suitable techniques currently available to analyse such materials. Increasing concerns regarding the leaching of nanomaterials from consumer products into the environment and the unknown toxicological implications associated with their presence in natural waters act as an additional driving force to further develop such nanoparticle detection techniques so as to employ them in the detection of nanoparticles contained in environmental matrices. The proof-of-concept measurements detailed in this chapter reveal the potential possessed by anodic particle coulometry for both the detection and characterisation of silver nanoparticles in the environment.

Anodic particle coulometry has been shown to be suitable for the detection of a number of different nanoparticle materials including gold[21], iron oxide[22], nickel[9] and organic[23] nanoparticles dispersed in typical laboratory electrolytes (potassium chloride, phosphate buffer and hydrochloric acid). Having demonstrated in this chapter that anodic particle coulometry can be applied to the detection of silver nanoparticles in seawater media it is anticipated that the detection and sizing of alternative nanoparticle types in seawater may also be feasible including mixtures of nanoparticles[9] within environmental samples.

Bibliography

[1] E. J. E. Stuart, N. V. Rees, J. T. Cullen and R. G. Compton, *Nanoscale* **5** (2013) 174–177.

[2] T. M. Benn and P. Westerhoff, *Environ. Sci. Technol.* **42** (2008) 4133–4139.

[3] A. Hinther, S. Vawda, R. C. Skirrow, N. Veldhoen, P. Collins, J. T. Cullen, G. van Aggelen and C. C. Helbing, *Environ. Sci. Technol.* **44** (2010) 8314–8321.

[4] P. V. Asharani, Y. L. Wu, Z. Gong and S. Valiyaveettil, *Nanotechnology* **19** (2008) 255102.

[5] L. Stebounova, E. Guio and V. Grassian, *J. Nanopart. Res* **13** (2011) 233–244.

[6] A. M. E. Badawy, T. P. Luxton, R. G. Silva, K. G. Scheckel, M. T. Suidan and T. M. Tolaymat, *Environ. Sci. Technol.* **44** (2010) 1260–1266.

[7] Y. G. Zhou, N. V. Rees and R. G. Compton, *Angew. Chem., Int. Ed.* **50** (2011) 4219–4221.

[8] N. V. Rees, Y.-G. Zhou and R. G. Compton, *ChemPhysChem* **12** (2011) 1645–1647.

[9] E. J. E. Stuart, Y. G. Zhou, N. V. Rees and R. G. Compton, *RSC Adv.* **2** (2012) 6879–6884.

[10] J. M. Zook, R. I. MacCuspie, L. E. Locascio, M. D. Halter and J. T. Elliot, *Nanotoxicology* **5** (2011) 517–530.

[11] B. J. R. Thio, M. O. Montes, M. A. Mahmoud, D.-W. Lee, D. Zhou and A. A. Keller, *Environ. Sci. Technol.* **46** (2012) 6985–6991.

[12] S. L. Chinnapongse, R. I. MacCuspie and V. A. Hackley, *Sci. Total Environ.* **409** (2011) 2443–2450.

[13] S. A. Cumberland and J. R. Lead, *J. Chromatogr., A* **1216** (2009) 9099–9105.

[14] A. M. E. Badawy, K. G. Scheckel, M. Suidan and T. Tolaymat, *Sci. Total Environ.* **429** (2012) 325–331.

[15] J. Farkas, H. Peter, P. Christian, J. A. G. Urrea, M. Hassellv, J. Tuoriniemi, S. Gustafsson, E. Olsson, K. Hylland and K. V. Thomas, *Environ. Int.* **37** (2011) 1057 – 1062.

[16] H. S. Toh, C. Batchelor-McAuley, K. Tschulik and R. G. Compton, *Analyst* **138** (2013) 4292–4297.

[17] J. Ellison, K. Tschulik, E. J. E. Stuart, K. Jurkschat, D. Omanovic, M. Uhlemann, A. Crossley and R. G. Compton, *ChemistryOpen* **2** (2013) 69–75.

[18] S. R. Emerson and J. I. Hedges, *Chemical Oceanography and the Marine Carbon Cycle* (Cambridge University Press, United Kingdom, 2011), fourth edition.

[19] M. G. Espinoza, M. L. Hinks, A. M. Mendoza, D. P. Pullman and K. I. Peterson, *J. Phys. Chem. C* **116** (2012) 8305–8313.

[20] M. Bostrom, D. R. M. Williams and B. W. Ninham, *Phys. Rev. Lett.* **87** (2001) 168103.

[21] Y. G. Zhou, N. V. Rees, J. Pillay, R. Tshikhudo, S. Vilakazi and R. G. Compton, *Chem. Comm.* **48** (2012) 224–226.

[22] K. Tschulik, B. Haddou, D. Omanovic, N. V. Rees and R. G. Compton, *Nano Res.* **6** (2013) 836–841.

[23] W. Cheng, X. F. Zhou and R. G. Compton, *Angew. Chem., Int. Ed.* **52** (2013) 12980–12982.

Chapter 6

Electrochemical Detection of Commercial Silver Nanoparticles: Identification, Sizing and Detection in Seawater Media

In the previous chapter it was reported that nanoparticle-impact experiments can be used to detect laboratory synthesised silver nanoparticles in seawater media. In this chapter, the electrochemistry of silver nanoparticles contained in a consumer product is studied. The redox properties of silver particles in a commercially available disinfectant cleaning spray are investigated *via* cyclic voltammetry before nanoparticle-impact experiments are performed to detect single particles in both a typical aqueous electrolyte and authentic seawater media. It is shown that nanoparticle-impact voltammetry is a promising method for the detection of nanoparticles that have leached into the environment from consumer products which is an important development for the determination of risks associated with the incorporation of nanotechnology into everyday products.

This work was carried out in collaboration with Dr K. Tschulik and Dr J. T. Cullen from the University of Victoria, BC, Canada. Dr K. Tschulik helped with the interpretation of experimental results and Dr J. T. Cullen advised on oceanographic sampling. The results included in this chapter have been published in *Nanotechnology*[1].

6.1 Introduction

Proof-of-concept measurements reported in the previous chapter have revealed that anodic particle coulometry is a suitable method for detecting nanoparticles in seawater media[2]. However, this in situ particle-electrode impact method has only been used for detecting synthetic silver nanoparticles synthesised in the laboratory using the method described by Pyatenko et al.[2–4]. In order to assess the consequences of the inevitable leaching of nanoparticles[5–7] from consumer products such as cleaning products, medical dressings and sportswear[8], in which manufacturers have introduced silver nanoparticles in order to utilise their bactericidal properties[9, 10], it is vital to develop an instrument capable of detecting and measuring the engineered nanomaterials contained in such products in the aquatic environment[11, 12]. It likely to be the types of nanoparticles originating from consumer goods that will leach into the environment as opposed to those synthesised in the laboratory.

There have been a number of papers published investigating the degree to which nanoparticles are released from consumer products such as nanosilver containing textiles[13, 14], washing machines[15] and socks[16]. Techniques typically used in these studies to detect silver nanoparticles include ICP-MS[15], electron microscopy[13, 15, 16] and NTA[15]. The former two techniques are ex situ whilst the latter provides indirect information *via* the measurement of diffusion coefficients in a restricted range of solutions. In contrast anodic particle voltammetry gives a direct measurement of the number of atoms in each impacting nanoparticle as outlined in chapter 5.

In this chapter the use of anodic particle coulometry for the detection of silver nanoparticles contained in a commercially available disinfectant product is reported. The product

studied in this investigation is a colloidal silver spray recommended for sanitising drinking water and disinfecting utensils and surfaces used for food and drink preparation. This is the first time nanoparticles contained in a consumer product have been detected using this electrochemical technique. This novel method of detection and sizing has been validated with NTA and is also shown to be suitable in environmental media.

6.2 Experimental Procedure

6.2.1 Reagents

Commercial Silver Nanoparticles

Higher Nature colloidal silver spray was purchased from OneClickPharmacy (oneclick-pharmacy.com). The product label states that the spray contains high stability active colloidal silver with a small particle size (0.0006 to 0.005 µm) at 10 parts per million.

Seawater Sampling

Seawater samples were collect from Saanich Inlet, British Coulombia, Canada as described in 5.2.1.

6.2.2 Electrochemical Methods

Cyclic Voltammetry

For cyclic voltammetry measurements a glassy carbon (GC) macroelectrode (r_e=1.5 mm) was used as the working electrode, a saturated calomel electrode (SCE) as the reference electrode while a carbon rod acted as a counter electrode. The GC macroelectrode was

modified by spraying varying amounts of the colloidal silver spray directly from the spray nozzle attached to the colloidal silver spray bottle onto the surface of the electrode and drying under nitrogen between each spray to speed up the drying process. Solutions were degassed thoroughly with nitrogen before scanning and a nitrogen blanket was maintained above the solution throughout the experiment. After each voltammetric scan the electrode was polished using three grades of diamond spray (3.0, 1.0 and 0.1 µm) before sonicating in water for 1 min and drying with nitrogen.

Anodic Particle Coulometry

Anodic particle coulometry experiments were performed with the same reference and counter electrode used for the voltammetric measurements above but the working electrode utilized was a carbon microelectrode (r_e=5.94 µm). The working electrode was polished as described above for the GC macroelectrode. The system was thoroughly degassed with nitrogen before scanning and an oxugen-free environment was maintained for the experiment. Once the nanoparticles had been dispersed in the electrolyte, the solution was agitated using the nitrogen flow at regular intervals throughout the experiment. SignalCounter was employed to count and size the nanoparticle-electrode impact spikes observed and OriginPro v.8.5.1 (www.OriginLab.com) was used to generate the size distributions.

6.2.3 Nanoparticle Tracking Analysis

NTA was performed as described in section 3.4.2. The concentration of nanoparticles in the colloidal spray was low so no dilution of the sample was required and the required 300 µL sample could be taken directly from the commerical spray bottle and inserted using

a syringe into the NanoSight viewing unit. Analysis of the data gained *via* nanoparticle tracking analysis was performed by the NanoSight software suite and the size distributions plotted using Origin v.8.5.1.

6.3 Results and Discussion

6.3.1 Cyclic Voltammetry of Commercial Silver Nanoparticles

First, cyclic voltammetry was used to examine the electrochemistry of the colloidal silver nanoparticles in 0.1 M $NaClO_4$, with the aim being to determine the silver nanoparticle oxidation potential required for impact experiments. Different loadings were studied by spraying the colloidal silver spray directly onto the surface of the working electrode multiple times. The modified glassy carbon electrode was then scanned in the positive direction, revealing a silver oxidation peak at around +0.4 V (reaction 6.1), before applying negative potentials at a scan rate of 200 $mV\,s^{-1}$(figure 6.1a). The reverse peak observed is most likely due to the silver ions formed being reduced back onto the electrode surface.

$$AgNP_{(s)} - e^- \longrightarrow Ag^+_{(aq)} \tag{6.1}$$

Increased loading onto the electrode surface caused the silver oxidation peak to grow, the area of which was integrated to gain a value for the charge, Q, transferred during this oxidation process. Figure 6.1b shows that an approximately linear relationship is observed between the number of times the GC electrode was sprayed with the colloidal silver spray and the charge of the silver oxidation peak for up to five spray loadings before the measured charge appears to begin to level off when the electrode was modified with

ten sprays of the colloidal silver. Loading experiments were repeated a second time and reproducibility is demonstrated by the error bars in figure 6.1b. The variation observed is due to the modification process as non-exact volumes are released from the spray nozzle due to the product normally being used for non-scientific purposes. On some occasions two merged oxidation peaks were observed suggesting that silver chloride was sometimes formed (reaction 6.2); with the most likely source of chloride in this case being trace quantities from the SCE reference electrode.

$$\mathrm{AgNP_{(s)}} + \mathrm{Cl^-_{(aq)}} \longrightarrow \mathrm{AgCl_{(s)}} + \mathrm{e^-} \tag{6.2}$$

It is important to note that the stripping of silver nanoparticles from the electrode surface is a one electron process regardless of one or two peaks being observed.

Another interesting observation that can be made from figure 6.1 is the increase in the peak potential of the silver oxidation peak with increased loading onto the electrode surface. The same phenomenon was reported by Ward Jones et al. when stripping silver nanoparticles in the same electrolyte[17]. Ward Jones et al. explained this trend in terms of overlapping diffusion layers of nanoparticles being oxidised; when a large number of metal nanoparticles are present on the surface of the electrode, the diffusion layers will overlap, slowing the rate of stripping and shifting the peak potential in the positive direction[17].

The next step was to determine if the same experiments could be carried out in authentic environmental media, in this case seawater. Once again, various loadings of the colloidal silver spray were introduced onto the electrode surface and voltammetric profiles were gained at a scan rate of $20\,\mathrm{mV\,s^{-1}}$(see figure 6.2a). As before, it was found that the

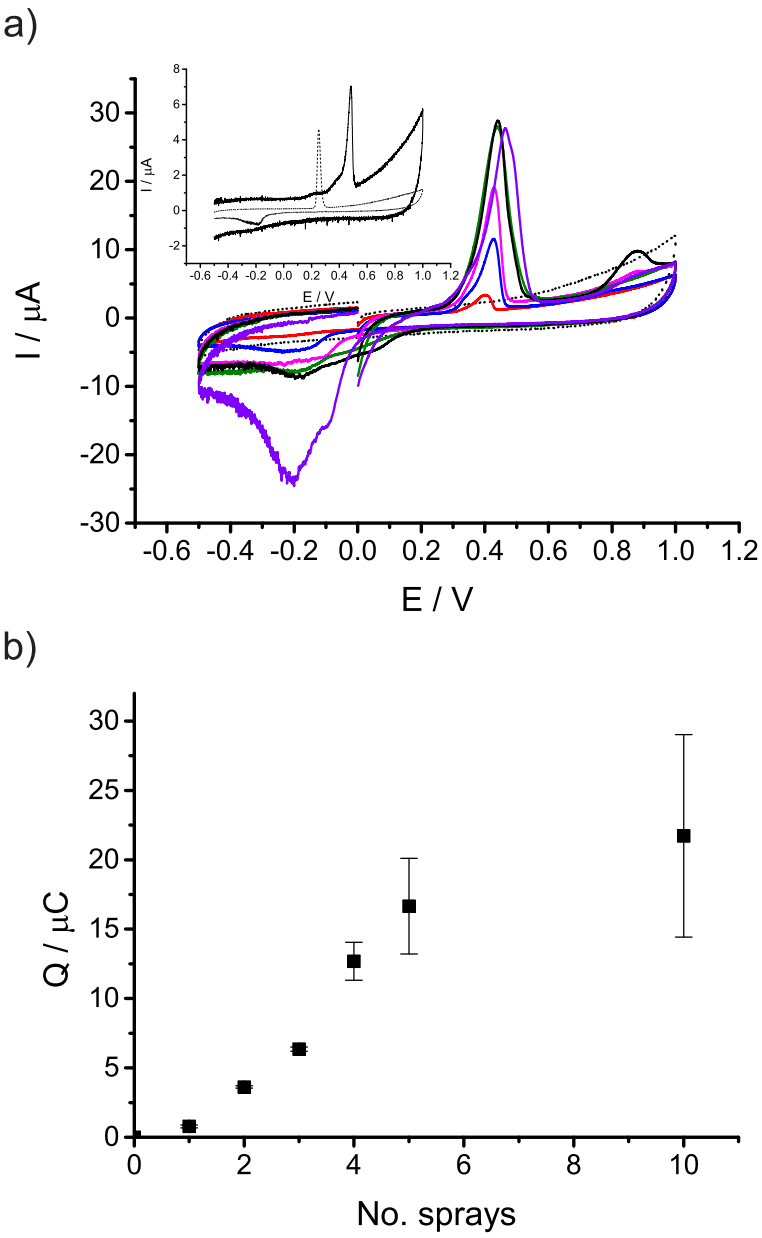


Figure 6.1: a) Voltammetric profiles for different loadings of colloidal silver spray on the surface of a GC macroelectrode (r_e=1.5 mm) in 0.1 M $NaClO_4$ at a scan rate of 200 mV s^{-1}. The bare GC electrode (dotted black line) was modified by spraying the surface 1 (red line), 2 (blue line), 3 (pink line), 4 (green line), 5 (black line) and 10 (purple line) times. Inset shows cyclic voltammograms for a GC electrode modified with 1 spray of colloidal silver at a scan rate of 20 mV s^{-1} (dotted black line) and 200 mV s^{-1} (black line) b) Plot of charge transferred, Q, during the oxidation of silver particles in the spray against the number of times the electrode was modified with the silver colloidal spray.

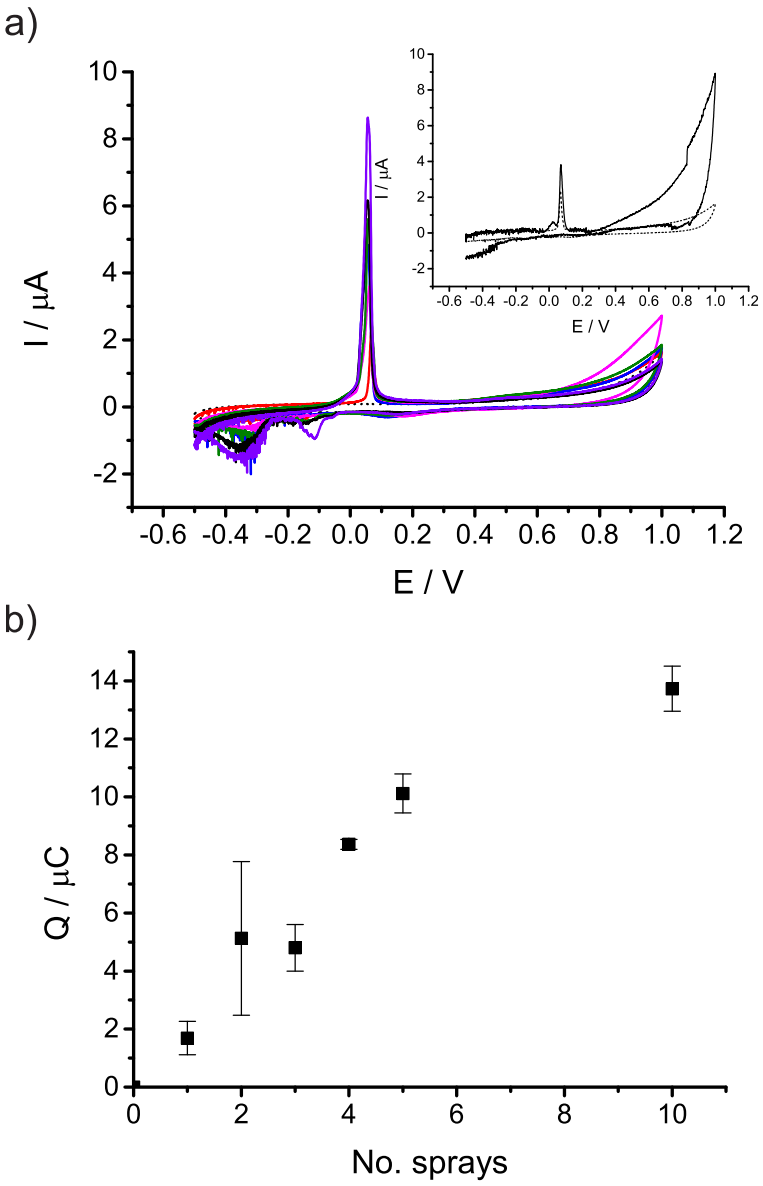


Figure 6.2: a) Cyclic voltammograms for different loadings of colloidal silver spray on the surface of a GC macroelectrode (r_e=1.5 mm) in authentic seawater media at a scan rate of 20 mV s^{-1}. The bare GC electrode (dotted black line) was modified by spraying the surface 1 (red line), 2 (blue line), 3 (pink line), 4 (green line), 5 (black line) and 10 (purple line) times. Inset shows cyclic voltammograms for a GC electrode modified with 1 spray of colloidal silver at a scan rate of 20 mV s^{-1}(dotted black line) and 200 mV s^{-1} (black line) b) Plot of charge transferred, Q, during the oxidation of silver particles in the spray in the seawater sample against the number of times the electrode was modified with the silver colloidal spray.

charge transfer during the oxidation of silver particles in the authentic seawater samples increased linearly with increased loading of up to five sprays of the silver nanoparticle spray onto the electrode surface, shown in figure 6.2b. Experiments were repeated once and as with the same process in 0.1 M $NaClO_4$ two oxidation peaks were occasionally observed.

When comparing the voltammetric profiles of the silver spray modified glassy carbon macroelectrode in 0.1 M $NaClO_4$ (figure 6.1a) against the scans for the same experiment performed in authentic seawater media (figure 6.2a), it is clear that the silver nanoparticle oxidation peak shifts to a more negative potential in the seawater sample. It is likely that part of this potential shift is due to the slower scan rate used for voltammetric measurements in seawater but the chloride concentration in seawater could also be a contributing factor. To test whether the high chloride concentration in the seawater media is the cause for this observed potential shift, cyclic voltammograms were recorded for a glassy carbon macroelectrode modified with one spray of colloidal silver in $NaClO_4$, authentic seawater media and 487 mM NaCl at a scan rate of $20\,mV\,s^{-1}$ (figure 6.3). This concentration of NaCl was chosen as the same concentration of chloride is present in the seawater sample tested in this study, the chloride concentration was calculated from the salinity value (S=31.3) measured at the depth (175 m) and location from where the sample was taken. It can be seen that while the oxidation of silver particles contained in the spray occurs at +0.25 V in $NaClO_4$, the same process in the seawater sample and 487 mM NaCl occurs approximately 200 mV more negative. With roughly the same peak potential observed for the oxidation in 487 mM NaCl and the seawater, it can be concluded that it is indeed the high chloride concentration in the seawater sample that is responsible for the observed shift in potential.

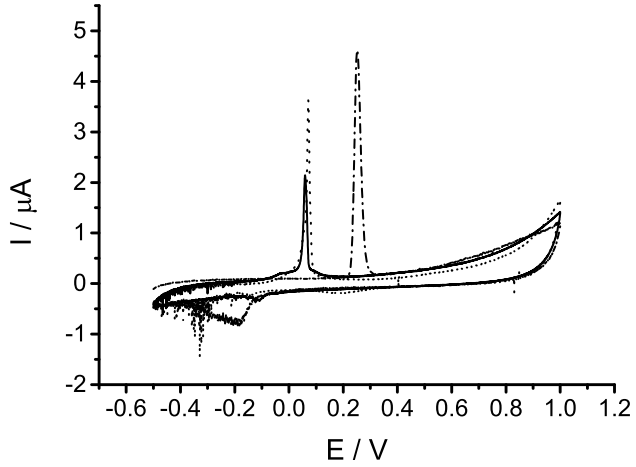


Figure 6.3: Voltammograms for a colloidal silver spray modified GC electrode (r_e=1.5 mm) in 0.1 M $NaClO_4$ (dot dash dot line), authentic seawater media (dotted line) and 487 mMl (solid line) at a scan rate of 20 mV s^{-1}.

6.3.2 Anodic Particle Coulometry of Commercial Silver Nanoparticles

Having carried out voltammetry studies for the colloidal silver spray and establishing the potential at which the silver particles contained in the spray were oxidised in both 0.1 M $NaClO_4$ and seawater media, the next step was to determine whether anodic particle coulometry could be used to directly detect the silver nanoparticles in this consumer product.

For anodic particle coulometry experiments in 0.1 M $NaClO_4$, an oxidising potential of +0.6 V *vs.* SCE was applied to the working electrode and 1 mL of the colloidal silver spray solution was added to a cell containing 20 mL of electrolyte. This potential was chosen as it is past the potential required to oxidise the silver particles contained in the spray (see figure 6.1a), therefore ensuring silver nanoparticles will be oxidised upon impact. Oxidative current transients (spikes) with durations of approximately 12 ms as shown in figure 6.4 were observed in the chronoamperograms recorded, with each spike

being caused by the destructive oxidation of one nanoparticle that occurs upon collision with the potentiostatted electrode. The same procedure was used for impact experiments in seawater media, although the oxidising potential applied this time was lower (+0.3 V *vs.* SCE) due to the oxidation of the silver particles occurring at a lower potential in seawater than in 0.1 M $NaClO_4$. Once again, after addition of the colloidal silver, spikes in the current-time transients were seen (figure 6.4b).

As each spike is caused by the destructive oxidation of a nanoparticle, the charge, Q, transferred during each collision can be determined, by integrating the area under each oxidative spike, and used to determine the number of atoms, N_{NP}, making up the impacting nanoparticles with equation 6.3

$$Q = eN_{\mathrm{NP}} \tag{6.3}$$

where e is the elementary charge (1.602 x 10^{19} C).

Size distributions for the silver particles in this commercially available product in both 0.1 M $NaClO_4$ and seawater media determined by anodic particle coulometry are shown in Figure 6.5. With the nanoparticle size being given in terms of the number of atoms (N_{NP}) contained in each nanoparticle, it was important to choose a suitable bin size for the distribution plots in order to accurately represent the number of atoms contained in each silver nanoparticle while at the same time performing a reasonable statistical analysis on the data. For these reasons a bin size of 0.05×10^6 was employed in the distributions.

The majority of impacting nanoparticles measured in 0.1 M $NaClO_4$ were found to be made up of 0.325×10^6 silver atoms, which if the nanoparticle is assumed to be spherical can be approximated to give a radius of 11 nm. In the authentic seawater sample most

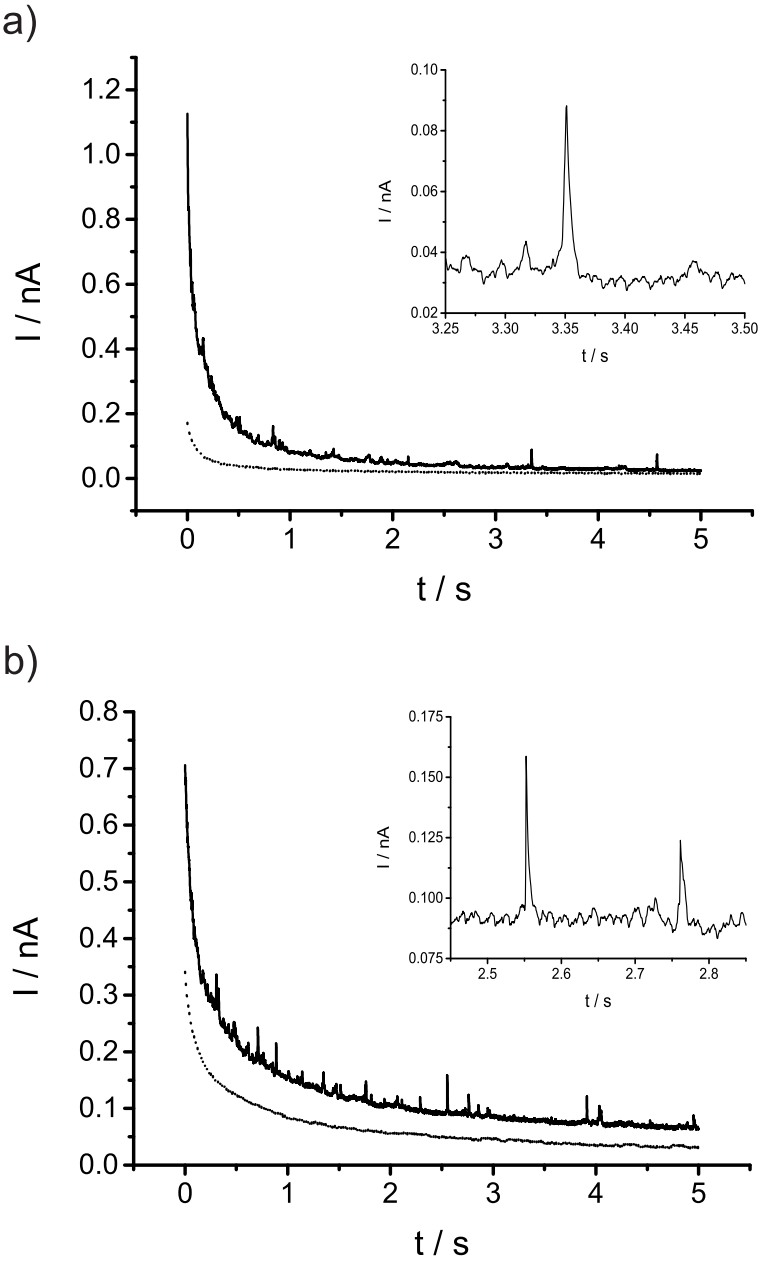


Figure 6.4: a) Chronoamperograms recorded for 5 s after a potential step of +0.6 V *vs.* SCE had been applied to a carbon microelectrode (r_e=5.94 µm) in a 0.1 M $NaClO_4$ solution before (dotted line) and after (solid line) addition of colloidal silver spray b) Chronoamperograms recorded for 5 s after potentiostatting a carbon microelectrode (r_e=5.94 µm) at +0.3 V *vs.* SCE in authentic seawater media before (dotted line) and after (solid line) addition of colloidal silver spray.

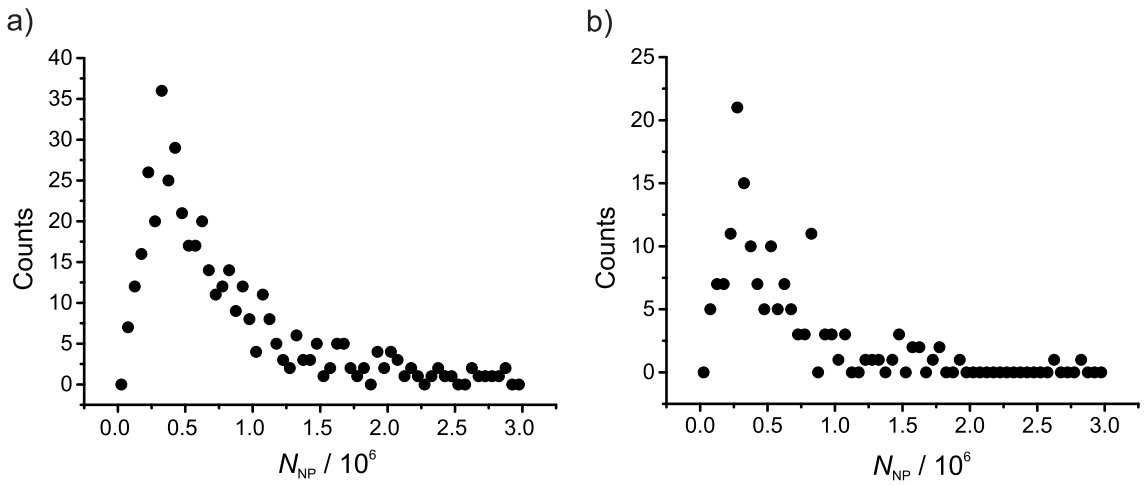


Figure 6.5: Size distribution for the number of atoms (N_{NP}) making up silver nanoparticles contained in a commercially available colloidal silver spray cleaning product determined *via* anodic particle coulometry in a) a solution of 0.1 M $NaClO_4$ and b) authentic seawater media.

colliding nanoparticles possessed 0.275×10^6 atoms relating to a radius of 10.3 nm.

Having sized the silver particles contained in the colloidal silver spray from the charge of the spikes observed in anodic particle coulometry it was necessary to carry out independent sizing analysis *via* NTA to determine the accuracy of our nanoparticle sizing method. NTA measurements were performed by taking a sample of the colloidal silver spray and tracking the silver particles contained in the spray over a 30 s timescale. Figure 6.6 shows the size distribution for the nanoparticle radius determined *via* anodic particle coulometry in both 0.1 M $NaClO_4$ and seawater overlaid with the distribution determined by NTA for the silver particles taken directly from the spray solution. A bin size of 1 nm was chosen for the size distributions gained from both anodic particle coulometry and NTA measurements. Both methods are shown to be in good agreement confirming the accuracy of anodic particle coulometry for sizing nanoparticles contained in a consumer product.

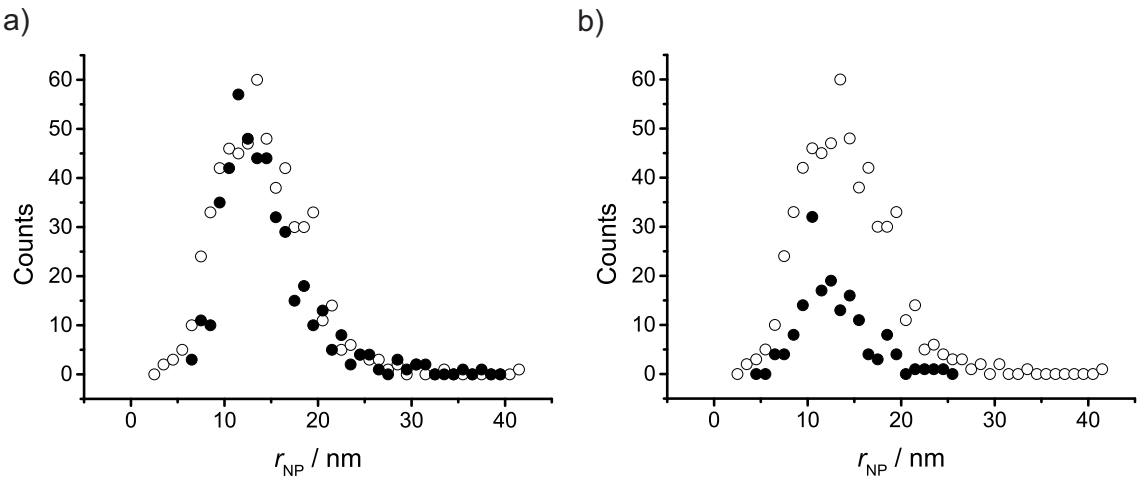


Figure 6.6: a) Radius (r_{NP}) distribution of silver nanoparticles in a colloidal silver spray determined *via* anodic particle coulometry (•) in a solution of 0.1 M $NaClO_4$ overlaid with a radius (r_{NP}) distribution for the same particles carried out by nanoparticle tracking analysis (○) b) Radius (r_{NP}) distribution of colloidal silver particles in a cleaning product determined *via* anodic particle coulometry (•) in authentic seawater media overlaid with a radius (r_{NP}) distribution for the same particles carried out by nanoparticle tracking analysis (○).

6.4 Conclusions

Nanoparticles contained in a commercially available disinfectant product have been detected and sized *via* anodic particle coulometry in both a standard electrolyte solution and authentic seawater media. Independent sizing analysis performed using NTA supports the accuracy of this method for sizing the silver particles in this consumer product. The nanoparticles studied here are a prime example of the typical nanoparticles that will leach into the environment from commercial goods and have potentially ecotoxic effects, making anodic particle coulometry an ideal method for detecting nanoparticles that have been released into water systems.

The limit of detection for this technique depends on the nature of the nanoparticles. However, as shown in chapter 4 silver nanoparticles have been detected at tens of pM. The experiments in this study provide a high number of signals in a time of just a few seconds so that with extended measurement times, limits of detection of up to two orders

of magnitude lower can be realistically expected. The following chapter describes an alternate method for nanoparticle detection known as a "sticking and stripping" technique that has the potential to offer significantly lower limits of detections for nanoparticles in a seawater sample.

Bibliography

[1] E. J. E. Stuart, K. Tschulik, D. Omanovi, J. T. Cullen, K. Jurkschat, A. Crossley and R. G. Compton, *Nanotechnology* **22** (2013) 444002.

[2] E. J. E. Stuart, N. V. Rees, J. T. Cullen and R. G. Compton, *Nanoscale* **5** (2013) 174–177.

[3] A. Pyatenko, M. Yamaguchi and M. Suzuki, *J. Phys. Chem. C* **111** (2007) 7910–7917.

[4] Y. G. Zhou, N. V. Rees and R. G. Compton, *Angew. Chem., Int. Ed.* **50** (2011) 4219–4221.

[5] G. V. Lowry, B. P. Espinasse, A. R. Badireddy, C. J. Richardson, B. C. Reinsch, L. D. Bryant, A. J. Bone, A. Deonarine, S. Chae, M. Therezien, B. P. Colman, H. Hsu-Kim, E. S. Bernhardt, C. W. Matson and M. R. Wiesner, *Environ. Sci. Technol.* **46** (2012) 7027–7036.

[6] J. Fabrega, S. N. Luoma, C. R. Tyler, T. S. Galloway and J. R. Lead, *Environ. Int..* **37** (2011) 517–31.

[7] S. Yu, Y. Yin and J. Liu, *Environ. Sci.: Processes Impacts* **15** (2013) 78–92.

[8] *Woodrow wilson international center for scholars, nanotechnology consumer product inventory available from: www.nanotechnproject.org/inventories/consumer/*, 2013.

[9] Y. Zhou, Y. Kong, S. Kundu, J. D. Cirillo and H. Liang, *J. Nanobiotechnology* **10** (2012) 19.

[10] W. R. Li, X. B. Xie, Q. S. Shi, H. Y. Zeng, Y. S. Ou-Yang and Y. B. Chen, *Appl. Microbiol. Biotechnol.* **85** (2010) 1115–22.

[11] A. G. Howard, *J. Environ. Monit.* **12** (2010) 135–142.

[12] A. D. Maynard, R. J. Aitken, T. Butz, V. Colvin, K. Donaldson, G. Oberdorster, M. A. Philbert, J. Ryan, A. Seaton, V. Stone, S. S. Tinkle, L. Tran, N. J. Walker and D. B. Warheit, *Nature* **444** (2006) 267–269.

[13] K. Kulthong, S. Srisung, K. Boonpavanitchakul, W. Kangwansupamonkon and R. Maniratanachote, *Part. Fibre Toxicol.* **7** (2010) 8.

[14] L. Geranio, M. Heuberger and B. Nowack, *Environ. Sci* **43** (2009) 8113–8118.

[15] J. Farkas, H. Peter, P. Christian, J. A. Gallego Urrea, M. Hassellv, J. Tuoriniemi, S. Gustafsson, E. Olsson, K. Hylland and K. V. Thomas, *Environ. Int.* **37** (2011) 1057–1062.

[16] T. M. Benn and P. Westerhoff, *Environ. Sci. Technol* **42** (2008) 4133–4139.

[17] S. E. Ward Jones, F. W. Campbell, R. Baron, L. Xiao and R. G. Compton, *J. Phys. Chem. C* **112** (2008) 17820–17827.

[18] E. J. E. Stuart, Y. G. Zhou, N. V. Rees and R. G. Compton, *RSC Adv.* **2** (2012) 6879–6884.

Chapter 7

Gold Electrodes from Recordable CDs for the Sensitive, Semi-Quantitative Detection of Commercial Silver Nanoparticles in Seawater Media

In this chapter the use of homemade disposable gold electrodes fabricated from commercial recordable CDs for the detection and quantification of silver nanoparticles from a consumer product in a seawater sample is reported. The CDtrode is immersed in a seawater sample containing silver nanoparticles for a certain amount of time during which the silver nanoparticles adsorb onto the CDtrode surface under open circuit conditions. The CDtrode is then transferred to an aqueous electrolyte and oxidative stripping is used to determine the amount of silver nanoparticles that have become stuck to the electrode surface. Depending on immersion time and silver nanoparticle concentration, up to a full monolayer coverage of silver nanoparticles on the CDtrode surface has been achieved.

This work has been published in *Sensors and Actuators B*[1] and was carried out in collaboration with Dr K. Tschulik, Dr D. Lowinsohn (Universidade Federal De Juiz de Fora, MG, Brasil)and Dr J. T. Cullen (University of Victoria, BC, Canada). Dr K. Tschulik helped with interpretation of experimental results, Dr D. Lowinsohn shared the

method for fabricating CDtrodes and Dr J. T. Cullen advised on oceanographic sampling.

7.1 Introduction

It has been described in the previous chapter that the detection of nanoparticles that have been released into the aquatic environment is a major challenge facing environmental scientists[2]. A possible solution to this analytical challenge, anodic particle coulometry, was outlined in chapters 5 and 6. However an alternate detection method is to use a simple electrochemical technique where a "sticky" electrode is introduced into a silver nanoparticles suspension and left for a certain amount of time during which the nanoparticles will stick to the electrode surface under open circuit conditions[3]. Any immobilised nanoparticles are then oxidatively stripped off the electrode allowing quantification of the silver nanoparticles not only on the electrode surface but also, with suitable calibration, in the solution of interest.

Proof-of-concept studies simulating the environmental detection of silver nanoparticles have validated the application of this sticking and stripping technique for the real-time detection of silver nanoparticles using disposable sticky carbon electrodes in real seawater media[3, 4]. The use of disposable electrodes is important for ensuring low cost field-based sampling and is ideal for long-term experiments where electrodes might need to be suspended in seawater for up to several days in order to ensure a sufficient signal can be gained for quantification due to the reportedly low concentrations of nanoparticles present in natural waters[5]. Previous studies testing the suitability of disposable electrodes for this application have used commercially available screen printed carbon electrodes that have been modified with cysteine to achieve a sticky surface reporting a maximum surface coverage of silver nanoparticles on the electrode surface of less than 1%[4]. Note

that the sticky electrodes provide a qualitative indication of the presence or absence of nanoparticles and also allow the approximate detection of concentration levels with order of magnitude estimates usually being adequate in this area of detection.

This technique offers advantages over anodic particle coulometry for the detection of silver nanoparticles in seawater (as described in chapters 5 and 6) as with anodic particle coulometry the very low concentrations of silver nanoparticles present in authentic seawater samples will require the user to wait a substantial period of time to observe a single impact spike. In contrast, sticking and stripping is an accumulative technique where the electrode can be left in the seawater to be tested, possibly by attaching it to buoy in the sampling area, for long durations to ensure that a signal is definitely observed during oxidative stripping of the adhered silver nanoparticles thereby providing the potential to detect lower concentrations of nanoparticles in solution.

A simple method to produce home-made disposable gold electrodes was first reported by Angnes et al.[6] who proposed using recordable compact discs (CDs) to achieve extremely versatile, commonly available one way use gold electrodes at low cost that behave almost identically to commercial gold macroelectrodes. The potential of these CDtrodes was soon recognised by the scientific community and they have since been used to study self-assembled monolayers[7], quantify mercury in both natural waters[8] and fish samples[9], in the determination of Selenium[10] and in the production of microfluidic devices[11]. Recently, Xiong et al.[12] reported a simple method for the construction of CDtrodes based on the thermal lamination construction technique proposed by Neudeck et al. in [13]. Thorough testing of the laminated CDtrodes revealed their ability to generate accurate and reproducible results for commonly used systems in both aqueous solutions and ionic liquids[12].

Howard[2] has suggested that the challenge of detecting nanoparticles in the aquatic environment is the lack of existence of analytical techniques capable of measuring dispersed nanoparticles in a liquid phase as opposed to dissolved species. Hitherto laminated CDtrodes have only been used to study the electrochemistry of dissolved species[12]. In this chaper the application of CDtrodes to the detection of silver nanoparticles from a consumer product in seawater media *via* the sticking and transfer stripping method described above and summarized in figure 7.1 is proposed. The aim is to use unmodified CDtrodes for the semi-quantitative analysis of silver nanoparticles giving the user an estimation of silver nanoparticle concentration to within an order of magnitude and improve upon the maximum surface coverage values reported in previous work for silver nanoparticle sticking at an electrode surface. The extent of silver nanoparticle adhesion observed at laminated gold CDtrodes in this study can reach full monolayer coverage on the electrode surface circumventing the need for the use of sticky electrodes as in [3, 4]. It is emphasised that this work is semi-quantitative due to the high variability associated with silver nanoparticle sticking at the gold CDtrodes, these typically large errors are a generic feature of nanoelectrochemistry caused by the increased sensitivity of nanoparticles to any adsorbed species present on the electrode surface thereby reducing the area available for nanoparticle sticking.

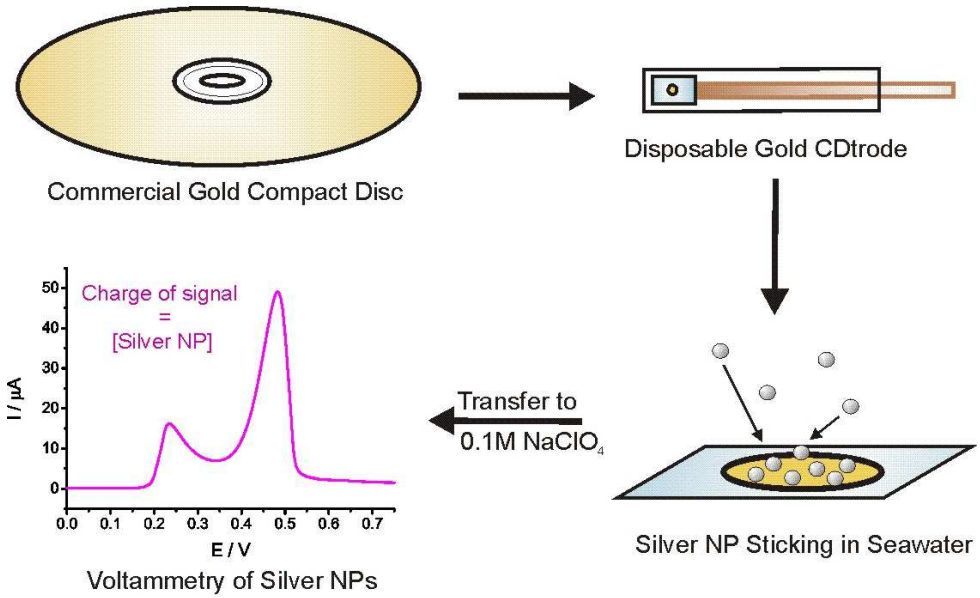


Figure 7.1: The production of a homemade disposable gold electrode from a recordable CD and how it can be used to quantify silver nanoparticles in seawater *via* a sticking and transfer stripping technique

7.2 Experimental Procedure

7.2.1 Reagents

Commercial Silver Nanoparticles

The silver nanoparticles used in this study are the same as that used in chapter 6. The particles are from a commercially available colloidal silver cleaning spray product (Higher Nature Ltd, East Sussex, UK) with a silver nanoparticle concentration of 47 pM. The nanoparticle concentration was determined by depositing 2 µL of the spray on the surface of a glassy carbon (GC) macroelectrode (r_e=1.5 mm), drying the electrode under nitrogen and oxidatively stripping off the dropcasted silver nanoparticles in 0.1 M $NaClO_4$, the concentration was then calculated from the charge of the anodic peak observed taking into consideration the size of the nanoparticles (r_{NP}=11 nm), determined *via* both anodic particle coulometry and NTA in chapter 6, the one electron oxidation of each silver atom,

as well as the density and molar mass of silver.

Seawater Sampling

Seawater samples were collect from Saanich Inlet, Victoria, Canada as described in section 5.2.1.

7.2.2 Fabrication of CDtrodes

The CD etching process is summarised in figure 7.2. The gold CD (MAM White Inkjet Gold Archive Disc) was first introduced into a bath of 0.6 M NaOH for a minimum of 20 min to fully remove the white inkjet printable surface. After rinsing with water and leaving to air-dry, the CD was placed into a bath of conc. HNO_3 as in [6]. It takes approximately 3 min for the polymer film to start to peel away from the gold surface; a water jet can then be used to fully remove the film before drying the newly exposed gold surface with nitrogen.

Scissors were used to cut the CD to the desired electrode size (8 mm × 8 mm) and an electrical connection to the CD piece was achieved with adhesive copper tape (Farnell element 14, Leeds, UK). A hole (r=1.0 mm) was punched in one page of a laminating film before positioning the CDtrode between the two pages of film ensuring that the gold was exposed through the punched hole. The laminating film was then passed through the laminator (Ativa AT-100A4) three times to ensure a sufficient seal. For experiments requiring the CDtrode to be in solution for long periods of time (>25 h) nail polish (Sabrina Cosmetics, Germany) was applied to the edges of the CDtrode to reinforce the laminated seal.

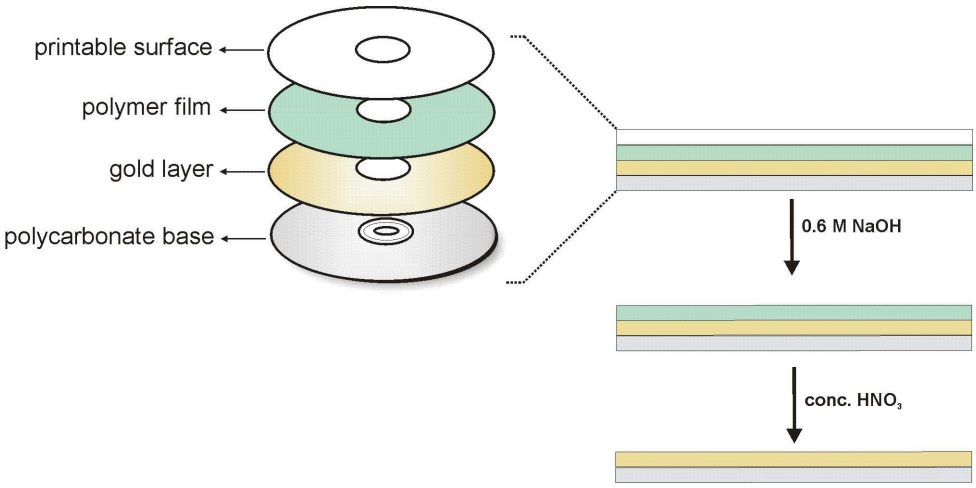


Figure 7.2: Schematic showing the components of a compact disc and the chemical treatment performed to remove the printable surface and protective polymer film in order to expose the gold layer

7.2.3 Silver Nanoparticle Sticking in Seawater at Gold CDtrodes

An aliquot of silver nanoparticles (6 mL) was added to 12 mL seawater so that the concentration of silver nanoparticles was 15.6 pM. The silver nanoparticle-seawater mixture was then sonicated for 5 min to ensure a homogeneous dispersion of nanoparticles in solution. CDtrodes were placed in the silver nanoparticle-seawater solution for the desired sticking time. Glassware used for nanoparticle sticking experiments was thoroughly cleaned with aqua regia (3:1, hydrochloric acid: nitric acid) between experiments. Sticking experiments were also performed with varying silver nanoparticle concentrations in the range of 1.1 pM to 15.6 pM for a fixed sticking time of 1 h.

7.2.4 Stripping of Silver Nanoparticles adhered to Gold CDtrodes

Upon completion of the desired sticking duration the CDtrodes were carefully transferred from the silver nanoparticle-seawater solution to 0.1 M $NaClO_4$. Either linear sweep voltammetry or cyclic voltammetry was then employed using the experimental set-up described in 3.3.2. The gold CDtrode (r_e=1.0 mm) was used as the working electrode, a

Ag/AgCl electrode was used as the reference electrode and a carbon rod acted as the counter electrode. Voltammetry was performed at a scan rate of $20\,\mathrm{mV\,s^{-1}}$ in 0.1 M $NaClO_4$ to oxidatively strip off the nanoparticles that had become immobilised on the CDtrode surface.

7.2.5 Reduction of $K_3Fe(CN)_6$ at Gold CDtrodes

A solution of 1 mM $K_3Fe(CN)_6$/0.1 M KCl was degassed with nitrogen for 15 min before studying the voltammetry of the $Fe(CN)_6^{3-}/Fe(CN)_6^{4-}$ redox couple using gold CDtrodes at a scan rate of $50\,\mathrm{mV\,s^{-1}}$.

7.2.6 Silver Nanoparticle Sticking and Stripping at a Gold Microelectrode

A gold microelectrode (r_e=4.2 µm) was suspended in a chloride free and chloride contaminated suspension of laboratory synthesised citrate capped silver nanoparticles (r_{NP}=11 nm) for 3 h. Details of the silver nanoparticle synthesis can be found in section 3.2.1, determination of the nanoparticle size was performed *via* NTA in chapter 10 and the concentration was determined as described in section 7.2.1 for the silver nanoparticle spray. Cyclic voltammetry was then used to study the oxidation of silver nanoparticles in a chloride free and chloride contaminated sample at a scan rate of $20\,\mathrm{mV\,s^{-1}}$. For the chloride free experiment, the gold microelectrode (r_e=4.2 µm) was suspended in the stock solution of silver nanoparticles (60 pM) before transferring to a 0.1 M solution of TraceSELECT Ultra nitric acid for stripping against a Hg/Hg_2SO_4 reference electrode and using a carbon rod counter electrode. A suspension of silver nanoparticles (3.6 pM) in 0.1 M $NaClO_4$ solution

containing $\leq 0.003\%$ chloride anions was used to investigate silver nanoparticle sticking and stripping in the presence of chloride ions. A Ag/AgCl reference electrode was used for this experiment meaning the leaking of chloride ions from the reference electrode could also contribute to the chloride contamination. Between experiments the gold microelectrode was polished with alumina (1.0, 0.3 and 0.1 µm) on soft lapping pads (micro cloth PSA, Buehler) and electrochemically cleaned by voltammetric cycling in 0.1 M H_2SO_4 at a scan rate of $100\,\mathrm{mV\,s^{-1}}$ until a stable voltammogram that no longer changed with scanning was obtained (approximately 10 scans).

7.3 Results and Discussion

7.3.1 Detection of Silver Nanoparticles at a CDtrode Immersed in a Silver Nanoparticle-Seawater Suspension for Varying Sticking Times

The materials chosen for this study were selected to simulate environmental detection in the aquatic environment; therefore authentic seawater was used with silver nanoparticles from a commercially available colloidal silver cleaning spray. To determine whether laminated CDtrodes can be applied to the detection of silver nanoparticles in seawater, a time study for silver nanoparticle sticking on the CDtrode surface was performed. Silver nanoparticles were added to an authentic seawater sample so that the concentration of nanoparticles in solution was equal to 15.6 pM (the method used to determine the concentration of silver nanonparticles in the colloidal silver spray is detailed in section 7.2.1). After sonication of the solution for 5 min to ensure homogeneous dispersion of the

nanoparticles, homemade CDtrodes were introduced in solution and left for varying times inside a thermostatted Faraday cage set to 25 °C under open circuit conditions to allow the silver nanoparticles to adhere to the electrode surface. The sticking times studied were 30 min, 1, 2, 3, 4.5, 6, 8, 9, 11, 13, 15, 25, 45 and 72 h. After the desired sticking duration, the CDtrodes were carefully removed from the silver nanoparticle-seawater solution, transferred to an electrochemical cell containing 0.1 M $NaClO_4$ and connected to the electrochemical set-up where they were to act as the working electrode. The CDtrodes were scanned to positive potentials to oxidatively strip off the silver nanoparticles that had become stuck to the electrode surface and the resulting voltammetric scans are shown in figure 7.3a (for clarity, voltammograms have not been shown for all time points studied). A well-distinguished oxidation peak with an approximate peak potential of +0.22 V *vs.* Ag/AgCl was observed and, depending on the sticking time, an additional oxidation peak could be seen at approximately +0.46 V *vs.* Ag/AgCl, a discussion of this can be found below. Occasionally, scans were resistive in appearance with the background current increasing across the scan (see voltammetric plot for the 5.2 pM concentration of silver nanoparticles (pink line) in figure 7.4a for an example) requiring baseline correction to be performed, this effect is most likely due to variation in electrical connection to the gold CD *via* the adhesive copper tape.

At longer sticking times, for the majority of electrodes tested, two oxidation peaks were observed (E=+0.22 V and +0.46 V *vs.* Ag/AgCl) as opposed to the single peak seen at short times (E=+0.22 V *vs.* Ag/AgCl). This phenomenon can be explained by the findings on the electrochemical detection of chloride levels using silver nanoparticles reported by Toh et al. in [14]. In brief, when two oxidation peaks are observed the first peak at a peak potential of +0.22 V *vs.* Ag/AgCl corresponds to reaction 7.1:

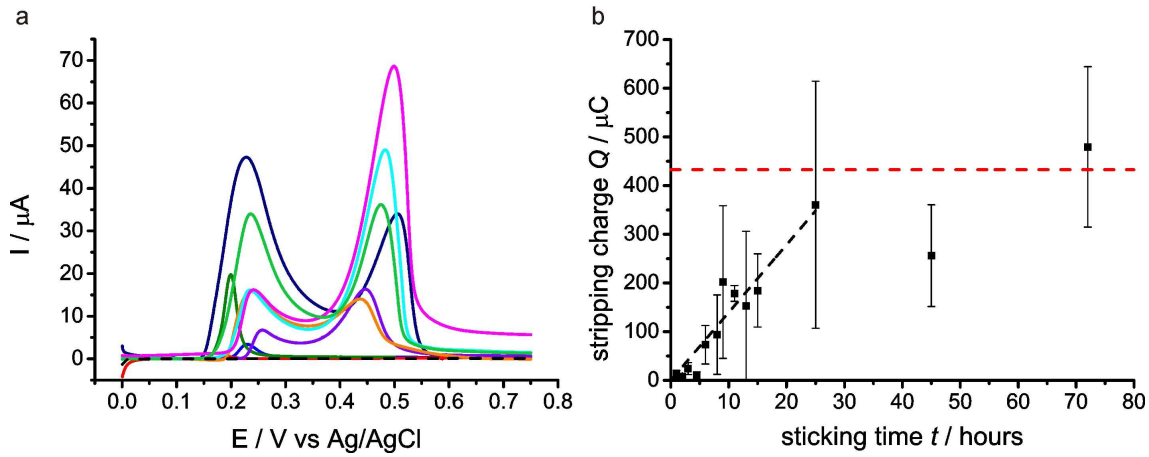


Figure 7.3: (a) Linear sweep voltammograms measured during the transfer stripping of silver nanoparticles 'stuck' to the surface of a gold CDtrode (r_e=1.0 mm) immersed in a 15.5 pM silver nanoparticle-seawater solution for 30 min (red line), 1 (blue line), 3 (dark green line), 6 (purple line), 11 (orange line), 15 (cyan line), 25 (pink line), 45 (light green line), 72 h (navy blue line) and then transferred to 0.1 M $NaClO_4$ for electrochemical measurement. The dotted black line shows the blank scan where a bare CDtrode is stripped in 0.1 M $NaClO_4$. (b) Plot of charge for the oxidative stripping of silver nanoparticles from the gold CDtrode surface against the time the CDtrode is immersed in the 15.6 pM silver nanoparticle-seawater solution. The dotted red line indicates the expected stripping charge for a full monolayer coverage of silver nanoparticle on the CDtrode surface.

$$Ag_{(s)} + Cl^-_{(aq)} \longrightarrow AgCl_{(s)} + e^- \tag{7.1}$$

with the source of chloride ions in this experiment being the seawater sample in which the working electrode had been suspended.

The second peak at +0.46 V *vs.* Ag/AgCl is caused by the formation of silver(I) cations from metallic silver as outlined in reaction 7.2:

$$Ag_{(s)} \longrightarrow Ag^+_{(aq)} + e^- \tag{7.2}$$

At shorter times only the Ag/AgCl peak is observed as there are less silver nanoparticles stuck on the surface meaning that there is a sufficient concentration of chloride ions present for the formation of silver chloride to be the only reaction recorded.

To measure the amount of silver nanoparticles stuck on the electrode surface, where there are two peaks the areas of both are considered to determine the stripping charge. A plot of the stripping charge, Q, as a function of sticking time, t, is shown in figure 7.33b. It can be seen that at sticking times <25 h there is an increase in stripping charge and therefore the number of nanoparticles stuck to the CDtrode surface with increasing sticking time. The expected stripping charge for a full monolayer coverage of silver nanoparticles on the electrode surface, $Q_{\text{monolayer}}$, was calculated to be 433 µC *via*:

$$Q_{\text{monolayer}} = \frac{Q_{\text{NP}} A_{\text{e}}}{A_{\text{NP}}} \tag{7.3}$$

where Q_{NP} is the expected charge for the full oxidation of a single spherical silver nanoparticles with a radius of 11 nm (5.24×10^{-14} C), A_{e} is the geometric area of the working electrode (3.16×10^{-6} m^2) and A_{NP} is the area of a silver nanoparticle with a radius of 11 nm (3.80×10^{-16} m^2). The dotted red line on the plot shown in figure 7.3b shows the charge expected for this full monolayer coverage and it can be seen that at the longer time points studied (45 and 72 h) the amount of nanoparticle sticking begins to level off when nanoparticle adhesion approximately reaches that of full monolayer coverage.

This full monolayer surface coverage is significantly larger than that observed by Cheng et al.[4] for sticking of the same concentration and type of silver nanoparticles in seawater at a cysteine modified sticky commercial disposable carbon electrode (r_{e}=1.0 mm) where the maximum coverage reported was approximately 0.2%. This value was similar to that reported by Tschulik et al.[3] for the adhesion of laboratory synthesised silver nanoparticles in 0.1 M $NaClO_4$ at a non-disposable glassy carbon electrode, also modified with cysteine to achieve a sticky surface. Therefore, with the full monolayer (100%)

coverage of nanoparticles achieved on the surface of the gold CDtrodes employed in this study, the use of CDtrodes can provide a 500% increase in silver nanoparticle sticking in comparison to previous work on carbon electrodes. One may suggest that it is the gold surface of the CDtrode that provides an increased affinity for the suspended silver nanoparticles over adhesion on carbon surfaces. However, in chapter 10 commercial non-disposable gold macroelectrodes modified with 2,3-dimercaptosuccinic acid are shown to give a maximum surface coverage of 2% for the adhesion of laboratory synthesised silver nanoparticles suspended in 0.1 M sodium citrate, not significantly larger than the sticking coverages observed at the modified carbon electrodes. In all studies, silver nanoparticle sticking at the corresponding unmodified electrode surface was found to be significantly smaller than that at the modified electrodes. Hence, it was unexpected that such high surface coverages can be achieved on a bare CDtrode surface that has not been chemically modified.

One possible explanation for the drastically increased silver nanoparticle affinity at the unmodified gold CDtrode surface may be the uneven surface of the CD resulting from the tracking trails on the polycarbonate base of the CD[15] which have an approximate depth of 0.1 µm[16]. The resulting surface roughness from these tracking trails increases the surface area available for nanoparticle sticking on the CD surface and a higher maximum surface coverage of silver nanoparticles can be achieved thereby suggesting that employing gold CDtrodes in silver nanoparticle sticking experiments provides an optimal surface for nanoparticle sticking in comparison to a flat gold electrode surface. Another possibility is that the chemical treatment performed during the CDtrode fabrication process where 0.6 M NaOH and conc. HNO_3 are used to remove both the printable surface layer and the polymer film in order fully expose the gold surface within the CD (see figure 7.2) removes

any impurities that may be present on the gold film resulting in a very clean surface that exhibits improved nanoparticle sticking capabilities. Alternatively, as suggested by Yu et al., the protective polymer layer of the CD helps to protect the gold surface from contamination in air[7].

7.3.2 Detection of Silver Nanoparticles at a CDtrode Immersed in a Silver Nanoparticle-Seawater Suspension of Varying Silver Nanoparticle Concentration

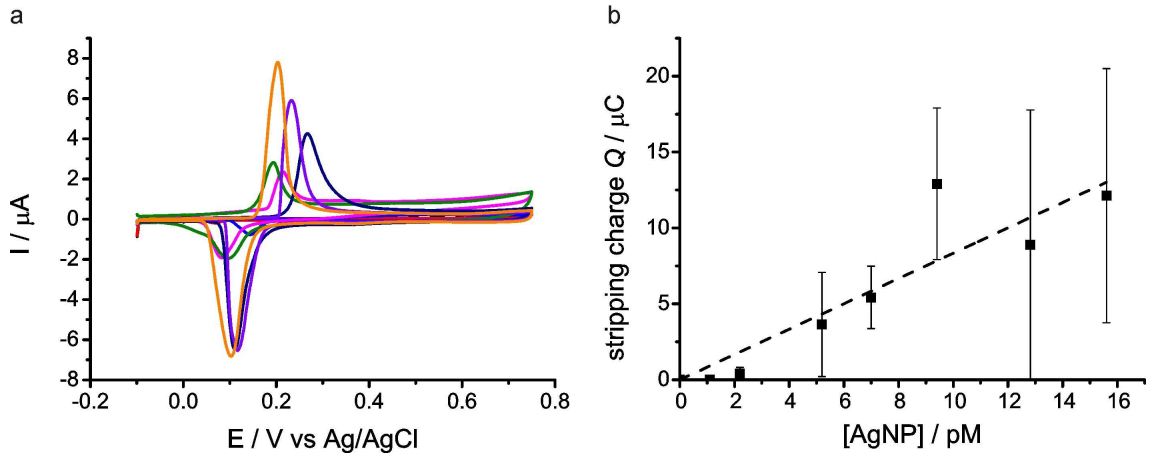


Figure 7.4: (a) Cyclic voltammograms recorded for the oxidation of silver nanoparticles that had become adhered on the surface of a gold CDtrode during 1 h immersion in a solution of 1.1(red line), 2.2 (blue line), 5.2 (pink line), 7.0 (green line), 9.4 (navy blue line) 12.8 (purple line) and 15.6 pM (orange line) silver nanoparticles in seawater. The CDtrode is then transferred to a solution of 0.1 M $NaClO_4$ and voltammetrically scanned at 20 mV s^{-1}. (b) Plot of charge for the oxidative stripping of silver nanoparticles from the gold CDtrode surface against the silver nanoparticle concentration in seawater after 1 h sticking time.

To further test the quantification of silver nanoparticles in seawater at CDtrodes, experiments were carried out as in the sticking time study described above, but with the sticking time being kept constant (1 h) while varying the concentration of silver nanoparticles added to the seawater sample. The silver nanoparticle concentrations tested were

1.1, 2.2, 5.2, 7.0, 9.4, 12.8 and 15.6 pM. Figure 7.4a shows the cyclic voltammograms measured during this concentration study, it can be seen that the silver nanoparticle stripping results in just one oxidation peak at an approximate peak potential of +0.2 V *vs.* Ag/AgCl due to the relatively low amount of silver nanoparticles on the electrode at the short sticking time of 1 h. In comparison, the concentration of chloride ions present is high due to transfer from the seawater to the stripping solution, therefore we can associate this oxidation peak with the formation of silver chloride (reaction 7.1). An approximately linear relationship between the charge of the silver oxidation peak and the silver nanoparticle concentration can be seen in figure 7.4b with no oxidation signal being observed for silver nanoparticle concentrations below 2.2 pM.

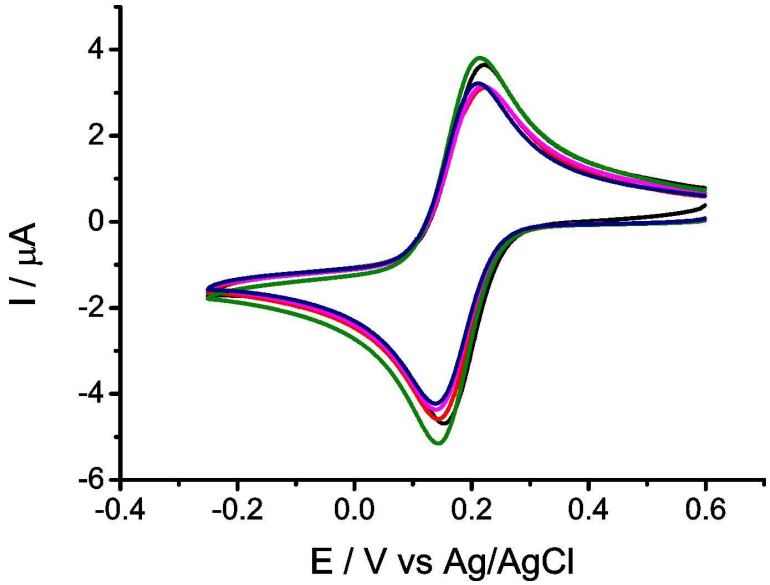


Figure 7.5: Voltammetric response of five different gold CDtrodes (r_e=1.0 mm) in 1 mM $K_3Fe(CN)_6$/0.1 M KCl at a scan rate of 50 mV s^{-1}.

Note the variation in silver nanoparticle sticking measurements shown by the error bars in figure 7.3b and 7.4b in comparison to the excellent agreement between voltammetric measurements for the reduction of the molecular species $K_3Fe(CN)_6$ at five different gold CDtrodes (r_e=1.0 mm) as shown in figure 7.5. This reflects an intrinsic issue with

nanoparticle voltammetry namely that greater variability between electrodes is observed along with a greater sensitivity to electrode blocking *via* adsorption for example of organic or other species on the electrode surface. In the case of molecular species only a very small part of the electrode needs to be unblocked for a full voltammetric signal to be seen since the diffusion zones around the active sites rapidly overlap[17–22]. In contrast with nanoparticles where the diffusion coefficients are significantly lower the role of blocking can be much enhanced. In addition, the increased size of nanoparticles compared to molecules means that they are unable to access some unblocked sites with which molecular species can react. For these reasons it is suggested that this approach is semi-quantitative; that said the lack of alternate techniques for the detection of dilute samples of nanoparticles should be noted[2].

7.3.3 Investigation of the Silver/Silver Chloride Redox Couple

Another observation that can be made from the voltammograms shown in figure 7.4a is the distinguishable reversible redox couple where the anodic peak current is equal to the cathodic peak current and the anodic peak has a peak potential of approximately +0.2 V *vs.* Ag/AgCl whilst the cathodic peak occurs at approximately +0.1 V *vs.* Ag/AgCl. The presence of this redox couple could be very helpful for the identification of silver nanoparticles in oceanographic samples.

It is possible that the cathodic peak observed in the back scan is caused by the reduction of AgCl. To test this hypothesis a silver nanoparticle sticking and stripping experiment was carried out using citrate capped silver nanoparticles that had been synthesised in the laboratory whilst ensuring that no chloride ions were present. A gold microelectrode (r_e=4.2 µm) was used as the working electrode, the electrolyte used to

strip the adhered silver nanoparticles was ultra pure 0.1 M HNO_3 and the reference electrode was changed to a Hg/Hg_2SO_4 electrode to ensure absolute chloride avoidance. A transfer stripping method was used as it is likely that the acid would cause aggregation of the silver nanoparticles during the sticking time due to protonation of negatively charged citrate capping groups. Therefore, the sticking experiment was carried out by placing the gold microelectrode directly in a stock solution of citrate capped, laboratory syntheised silver nanoparticles (60 pM) for 3 h and then placing the electrode in H_2O for 1 min to remove any adsorbed chloride ions before transferring to the HNO_3 solution for stripping. Figure 7.6a shows that under these chloride free conditions, no peak was seen in the backward scan with only a single anodic peak observed at a potential of +7 mV *vs.* Hg/Hg_2SO_4. This peak can be assigned to the one electron oxidation of metallic silver to silver ions (reaction 7.2), where the silver ions formed at the microelectrode surface diffuse away leaving a local $[Ag^+]$ of zero resulting in no deposition of Ag onto the surface and therefore no peak in the backward scan.

The redox couple observed in figure 7.4a was also observed at a gold microelectrode (r_e=4.2 µm) when suspended in 0.1 M $NaClO_4$ solution containing 3.6 pM citrate capped laboratory synthesised silver nanoparticles for a duration of 3 h. Figure 7.6b shows the first three scans for the voltammetric stripping of immobilised silver nanoparticles in the same silver nanoparticle containing 0.1 M $NaClO_4$ sticking solution. It was found that there was very little difference in charge between the oxidation and reduction signal in each cycle, with 94% of the oxidised silver species reducing back onto the CDtrode during the first scan, 87% in the second scan and 76% in the third scan. It can be concluded that the formation of silver(I) cations from metallic silver (reaction 7.2) is not the oxidation process observed here, since the formed silver(I) cations would rapidly diffuse

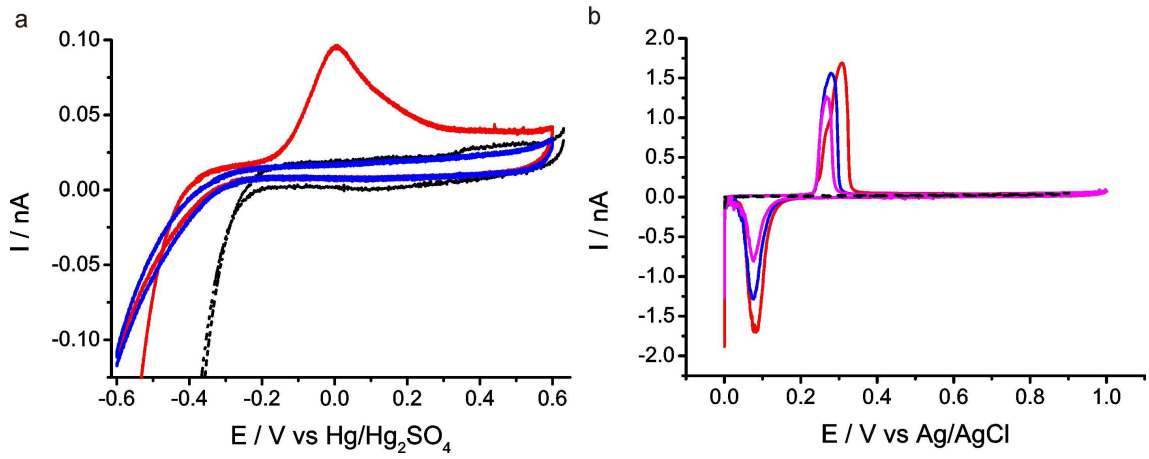


Figure 7.6: (a) Cyclic voltammograms to study the sticking of laboratory synthesised silver nanoparticles in the absence of chloride ions where a gold microelectrode (r_e=4.2 µm) is immersed in a silver nanoparticle stock solution (60 pM) for 3 h, soaked in H_2O for 1 min and then scanned in 0.1 M HNO_3. The first scan (red line) and second scan (blue line) are shown; the black dotted line shows the blank CV where a bare gold microelectrode was scanned in 0.1 M HNO_3. (b) Cyclic voltammograms for a gold microelectrode (r_e=4.2 µm) that had been suspended in 3.6 pM silver nanoparticles (laboratory synthesised)/0.1 M $NaClO_4$ for 3 h and then stripped in the same solution. The first scan (red line), second scan (blue line) and third scan (pink line) are shown; the black dotted line shows the blank CV where a bare gold microelectrode was scanned in 0.1 M $NaClO_4$

away from the electrode surface, due to convergent diffusion at a microdisc, resulting in little or no reduction feature being observed in the backward scan of the voltammogram. Alternatively, due to the high sensitivity of silver towards chloride ions, it would still be possible to observe the formation of AgCl in 0.1 M $NaClO_4$ as it contains $\leqslant$ 0.003% trace chloride anions and leaking of chloride ions from the reference electrode may also contribute to chloride contamination in the sample. The solid AgCl species formed in the presence of chloride ions is surface bound and would therefore be easily reduced back onto the gold surface, as observed in figure 7.6b[23].

Hence, the distinguishable redox couple observed for experiments at both the gold microelectrode and the gold CDtrode can be assigned to AgCl formation and reduction in the presence of chloride ions:

$$Ag_{(s)} + Cl^-_{(aq)} \leftrightharpoons AgCl_{(s)} + e^- \quad (7.4)$$

This discernible redox signal could be particularly useful to distinguish silver nanoparticles from a mixture of different types of nanoparticles which is likely to be the case in environmental samples.

7.4 Conclusions

The main aims of this chapter were to fabricate homemade disposable gold macroelectrodes *via* the thermal lamination of gold recordable CDs for use in the semi-quantitative detection of silver nanoparticles from a consumer product in real environmental samples and improve on the poor maximum surface coverage values that have been reported in previous work for the adhesion of nanoparticles on an electrode surface[3, 4].

A 500% increase in the maximum coverage of silver nanoparticles on the surface of the working electrode has been achieved *via* the use of gold CDtrodes when compared to previous work using chemically modified commercially purchased disposable screen-printed carbon electrodes for the detection of silver nanoparticles from the same consumer product in seawater[4]. The clear-cut oxidation peaks observed during the stripping of silver nanoparticles that have adhered to the CDtrode surface can be effectively analysed to give the user a good idea of the amount of silver nanoparticles in an oceanographic sample within the order of magnitude range. This technique is only semi-quantitative in nature due to the variability observed in silver nanoparticle sticking at the CDtrodes caused by the significant effect that any species that may be blocking the electrode surface will have on the slowly diffusing silver nanoparticles and the reduced number of active

sites that are available for nanoparticle sticking when compared to molecular species of a much smaller size that exhibit fast diffusion coefficients and overlapping diffusion zones rendering any electrode-blocking species insignificant.

The distinguishable redox couple associated with the formation of silver chloride from silver nanoparticles in the presence of chloride ions could be useful in distinguishing silver nanoparticles from environmental samples containing different types of nanoparticles. Additionally, it is likely that this technique is not just limited to silver nanoparticles and could also be used for the detection of other types of nanoparticles such as Ni or Fe_3O_4 and therefore in the analysis of a mixture of nanoparticles.

Bibliography

[1] E. Stuart, K. Tschulik, D. Lowinsohn, J. Cullen and R. Compton, *Sens. Actuators, B* **195** (2014) 223–229.

[2] A. G. Howard, *J. Environ. Monit.* **12** (2010) 135–142.

[3] K. Tschulik, R. G. Palgrave, C. Batchelor-McAuley and R. G. Compton, *Nanotechnology* **24** (2013) 295502.

[4] W. Cheng, E. J. . E. Stuart, K. Tschulik and R. G. Compton, *Nanotechnology* **24** (2013) 505501.

[5] N. C. Mueller and B. Nowack, *Environ. Sci. Technol.* **42** (2008) 4447–4453.

[6] L. Angnes, E. M. Richter, M. A. Augelli and G. H. Kume, *Anal. Chem.* **72** (2000) 5503–5506.

[7] H. Z. Yu, *Anal. Chem.* **73** (2001) 4743–7.

[8] M. A. Augelli, R. A. A. Munoz, E. M. Richter, A. Gouveia and L. Angnes, *Electroanalysis* **17** (2005) 755–761.

[9] M. C. Radulescu and A. F. Danet, *Sensors* **8** (2008) 7157–7171.

[10] C. F. Pereira, F. B. Gonzaga, A. M. Guarit-Santos and J. R. SouzaDe, *Talanta* **69** (2006) 877–881.

[11] C. K. Tang, A. Vaze and J. F. Rusling, *Lab Chip* **12** (2012) 281–286.

[12] L. H. J. Xiong, D. Lowinsohn, K. R. Ward and R. G. Compton, *Analyst* **138** (2013) 5444–5452.

[13] A. Neudeck and L. Kress, *J. Electroanal. Chem.* **437** (1997) 141–156.

[14] H. S. Toh, C. Batchelor-McAuley, K. Tschulik and R. G. Compton, *Analyst* **138** (2013) 4292–4297.

[15] D. Lowinsohn, E. M. Richter, L. Angnes and M. Bertotti, *Electroanalysis* **18** (2006) 89–94.

[16] H. Z. Yu, A. W. Rowe and D. M. Waugh, *Anal. Chem.* **74** (2002) 5742–5747.

[17] F. G. Chevallier, T. J. Davies, O. V. Klymenko, L. Jiang, T. G. J. Jones and R. G. Compton, *J. Electroanal. Chem.* **580** (2005) 265–274.

[18] B. A. Brookes, T. J. Davies, A. C. Fisher, R. G. Evans, S. J. Wilkins, K. Yunus, J. D. Wadhawan and R. G. Compton, *J. Phys. Chem. B* **107** (2003) 1616–1627.

[19] T. J. Davies, B. A. Brookes, A. C. Fisher, K. Yunus, S. J. Wilkins, P. R. Greene, J. D. Wadhawan and R. G. Compton, *J. Phys. Chem. B* **107** (2003) 6431–6444.

[20] T. J. Davies, R. R. Moore, C. E. Banks and R. G. Compton, *J. Electroanal. Chem.* **574** (2004) 123–152.

[21] T. J. Davies, B. A. Brookes and R. G. Compton, *J. Electroanal. Chem.* **566** (2004) 193–216.

[22] T. J. Davies, S. Ward-Jones, C. E. Banks, J. del Campo, R. Mas, F. X. Munoz and R. G. Compton, *J. Electroanal. Chem.* **585** (2005) 51–62.

[23] U. Hasse, K. Wagner and F. Scholz, *J. Solid State Electrochem.* **8** (2004) 842–853.

Chapter 8

Particle-impact Voltammetry: The Reduction of Hydrogen Peroxide at Silver Nanoparticles Impacting a Carbon Electrode

In previous chapters of this thesis the study of silver nanoparticle-electrode collisions has been performed using anodic particle coulometry where direct oxidation of the nanoparticle occurs upon impact. In this chapter, these stochastic nanoparticle collision events are instead observed by measuring the reduction of hydrogen peroxide occurring at the silver nanoparticle surface when it is in contact with a carbon electrode. It is shown that the charge passed during each nanoparticle-electrode impact can be approximated to the diffusion limited current at an isolated sphere, allowing the size of the impacting nanoparticle to be determined and providing new physical insight for modelling the contact environment.

This work has been published in *Chemical Physics Letters*[1] and was carried out in collaboration with Dr. N. V. Rees who helped with the interpretation of experimental results.

8.1 Introduction

The electrochemical observation of single nanoparticle-electrode collisions *via* the electrocatalytic amplification of a redox reaction occurring on the surface of a nanoparticle when it is in contact with an electrode has been introduced in chapter 2. Previous studies investigating this indirect nanoparticle detection technique have included measuring proton reduction[2], hydrazine oxidation[3, 4], sodium borohydride oxidation[5] and water oxidation[6] on varying nanoparticle types such as silver[2], gold[3], iridium oxide[6], titanium dioxide[7] and platinum [3, 8, 9] nanoparticles. It is vital that the reaction of interest only occurs on the surface of the nanoparticle and not on the electrode hence varying electrode materials have also been employed (carbon[2, 9], gold[6], platinum[5, 6], boron doped diamond[3] and mercury[7, 10–12]).

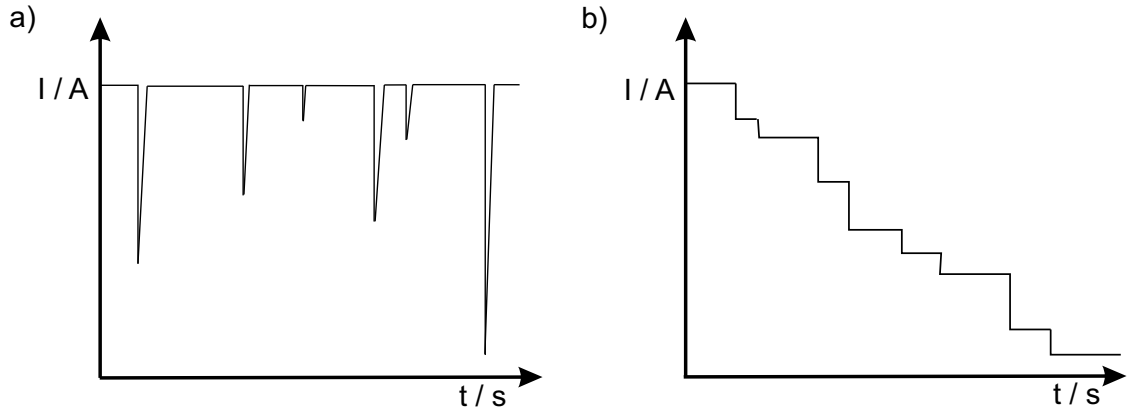


Figure 8.1: Schematic showing chronoamperometric profiles with a) spike-type transients and b) staircase-type transients in the current response caused by nanoparticle-electrode collisions where the nanoparticle rebounds from or is adsorbed to the electrode surface respectively

It is immediately apparent from studying the literature that there are large variations in the reported response observed when an electrocatalytic collision occurs between studies. The shape of the current response can differ significantly, with staircase[4] or

spike-type[6] transients being observed depending on whether the impacting nanoparticle is adsorbed or rebounded at the electrode surface (figure 8.1) thus resulting in significant variations in nanoparticle-electrode contact times. In order to explain the variability in previous reports and increase understanding of the underlying electrochemical processes that occur during a nanoparticle-electrode impact event it is important to develop new physical models of the contact environment.

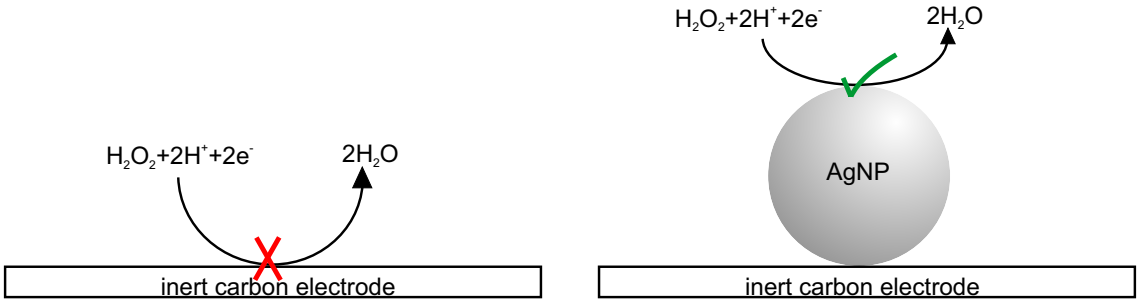


Figure 8.2: Schematic diagram demonstrating how the reduction of hydrogen peroxide can be electrocatalysed by an impacting silver nanoparticle

In this chapter the electrocatalytic reduction of hydrogen peroxide on silver nanoparticles impacting an inert carbon fibre microelectrode in acidic solution is studied (as shown in figure 8.2). The reduction of hydrogen peroxide on a silver nanoparticle array in the presence of protons has been reported previously and shown to proceed *via* the following reaction mechanism[13]:

$$\begin{aligned} \mathrm{H_2O_2 + H^+ + e^- \longrightarrow OH_{(ads)} + H_2O} \\ \mathrm{H^+ + OH_{(ads)} + e^- \longrightarrow H_2O} \end{aligned} \tag{8.1}$$

When reaction 8.1 occurs on the surface of an impacting silver nanoparticle spike-type transients are observed in the measured current response. It is found that the charge of these impact spikes can be approximated to the diffusion limited current at an isolated sphere of nanoscale dimensions thereby providing a method by which to size impacting

silver nanoparticles. This approximation also contributes new physical insight for the development of future models to increase understanding of the observed electrochemical response in electrocatalytic nanoparticle-electrode collision experiments.

8.2 Experimental Procedure

8.2.1 Silver Nanoparticle Synthesis

The silver nanoparticles used in this chapter were synthesised *via* the method outlined in section 3.2.1. The silver nanoparticle radius has been determined *via* anodic particle coulometry to be 13 nm and confirmed using SEM imaging (r_{NP}=14 ± 2 nm) in [2]. The concentration of the synthesised silver nanoparticle stock suspension was established using the method described in section 3.2.1.

8.2.2 Hydrogen Peroxide Titration

The exact concentration of H_2O_2 was determined by titrating the H_2O_2 with 0.01 M $KMnO_4$ in the presence of 0.1 M H_2SO_4. The stock H_2O_2 concentration was found to be 14.1% (w/w) in H_2O.

8.2.3 Cyclic Voltammetry

Cyclic voltammetry was carried out using the experimental set-up described in section 3.3.2. A glassy carbon (GC) macroelectrode (r_e=1.5 mm) was used as the working electrode while a saturated calomel electrode (SCE) and graphite rod were employed as the reference and counter electrodes respectively. The working electrode was modified with

6 µL of silver nanoparticles by dropcasting 3 × 2 µL of the synthesised silver nanoparticle suspension on the surface and dried under argon between each modification. Prior to modification the GC electrode was polished using 3.0, 1.0 and 0.1 µm diamond spray and then sonicated in H_2O for 1 min. All solutions were thoroughly degassed with argon before scanning and an oxygen-free environment was maintained during measurements. All scans were performed at a scan rate of 200 mV s^{-1}

8.2.4 Nanoparticle-impact Experiments

The set-up detailed in section 3.3.4 was utilised for all nanoparticle-impact experiments. The same reference and counter electrodes were used as in section 8.2.3 however the working electrode was a carbon fibre microelectrode (r_e=5.5 µm). The carbon fibre microelectrode was polished using the same method as above (section 8.2.3). The electrolyte used was thoroughly degassed with argon before scanning and an oxygen-free atmosphere was maintained throughout the duration of the experiment. The argon flow was also used to agitate the nanoparticles suspended in solution at regular intervals throughout the experiment. OriginPro 8.5.1 was used to analyse the observed impact spikes.

8.3 Results and Discussion

8.3.1 Cyclic Voltammetry of H_2O_2 on a Silver Nanoparticle-modified Electrode

As explained above it was vital that the reduction of H_2O_2 occurred only on the surface of the silver nanoparticles as opposed to on the bare carbon electrode. First, a GC macro-

electrode (r_e=1.5 mm) was scanned from 0.0 V to −1.0 V *vs.* SCE in 2.8 mM H_2O_2/0.1 M $HClO_4$ at a scan rate of 200 mV s^{-1} and it can be seen from figure 8.3 (dotted line) that no reduction feature was observed. The electrode was then modified with 6 µL of the synthesised silver nanoparticle stock suspension and scanned again in the same solution. Figure 8.3 (solid line) shows that the silver nanoparticles electrocatalyse the reduction of H_2O_2 with the observed reduction signal starting at approximately −3.0 V *vs.* SCE. This observed signal is in agreement with the literature[13].

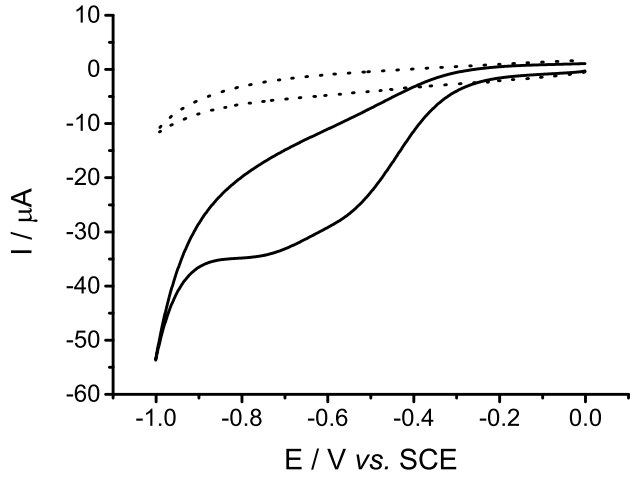


Figure 8.3: Reduction of 2.8 mM H_2O_2 in 0.1 M $HClO_4$ at a bare GC macroelectrode (r_e=1.5 mm, dotted line) and a GC macroelectrode (r_e=1.5 mm) that had been modified with silver nanoparticles (6 µL). All scans performed at a scan rate of 200 mV s^{-1}.

8.3.2 Particle-Impact Voltammetry of H_2O_2 on Impacting Silver Nanoparticles

Having determined the potential at which the reduction of H_2O_2 occurs on a silver nanoparticle-modified GC surface in acidic media, a carbon fibre microelectrode (r_e=5.5 µm) was immersed in a degassed solution of H_2O_2/0.1 M $HClO_4$ and held at a more negative potential than that of the observed reduction peak in figure 8.3 (−0.9 V

vs. SCE). Chronoamperomograms were recorded for 5 s in duration and an example of the observed response can be seen in figure 8.4(dotted line). An aliquot of the synthesised silver nanoparticle solution was then added to the H_2O_2 solution so that the concentration of nanoparticles in the electrochemical cell was equal to 43 pM. Post-addition of the nanoparticles reductive impact spikes in the current response were observed in the recorded chronoamperomograms (figure 8.4, solid line). The spike-type shape of the observed transients in the current response suggest that the silver nanoparticles rebound from the electrode surface upon impact with each spike resulting from the hydrogen peroxide reduction reaction occurring on the silver nanoparticle surface when it is contacting the carbon electrode.

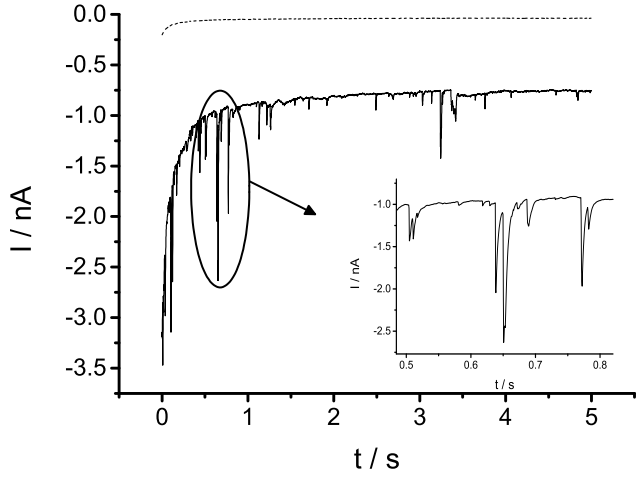


Figure 8.4: Typical chronoamperometric profile for a carbon fibre microelectrode (r_e=5.5 µm) potentiostatted at −0.9 V *vs.* SCE in a solution of 2.8 mM H_2O_2 in 0.1 M $HClO_4$ with (solid line) and without (dotted line) 43 pM silver nanoparticles added. Inset shows a zoomed image of the impact spikes observed in the presence of silver nanoparticles caused by nanoparticle-electrode collisions

The nanoparticle-impact experiment was repeated at varying potentials between 0.0 V and −0.9 V *vs.* SCE in order to determine the onset potential of the reductive impact spikes. The impact frequency at each of the measured potentials is plotted in figure

8.5a and overlaid with the cyclic voltammogram shown in figure 8.3 for the reduction of 2.8 mM H_2O_2 in 0.1 M $HClO_4$ on a silver nanoparticle-modified GC macroelectrode. The impact spikes appear to "switch-on" at -0.2 V *vs.* SCE which is earlier than the potential at which the reduction of H_2O_2 begins to occur in the cyclic voltammogram measured in 0.1 M $HClO_4$ (E=-0.3 V *vs.* SCE). Figure 8.5b shows that when the same plot of impact frequency *vs.* potential for the nanoparticle-impact experiments in acidic media is overlaid with a voltammetric profile for the reduction of 2.8 mM H_2O_2 in a pH 7 solution of 0.1 M $NaClO_4$ at a silver nanoparticle-modified GC macroelectrode there is a better agreement between the onset potential of impact spikes and the potential at which the reduction of hydrogen peroxide occurs in this solution of higher pH on the silver nanoparticle-modified surface. This improved agreement shows that the difference in potential observed between the voltammogram for the silver nanoparticle array and the onset of impact spikes in acidic solution (figure 8.5a) could be explained by a shift in the local pH at the single nanoparticle scale.

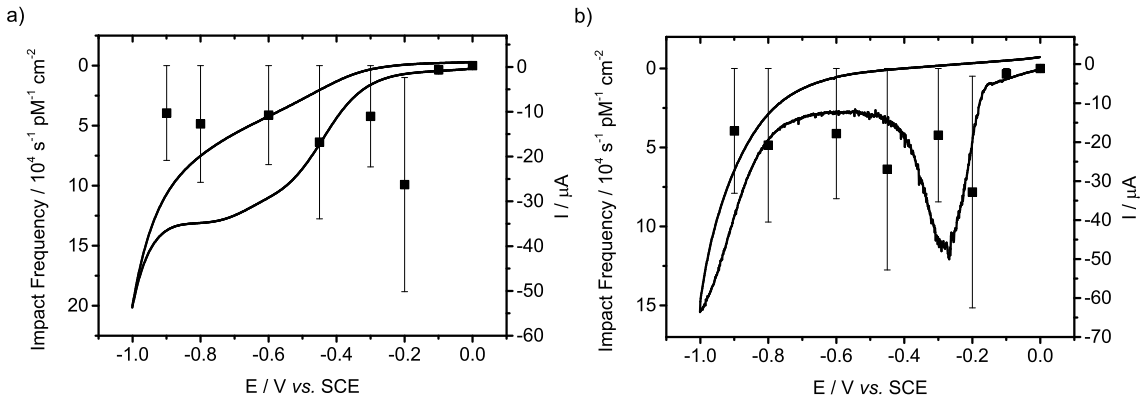


Figure 8.5: Frequency of impact spikes measured at a range of potentials between 0.0 V- -0.9 V *vs.* SCE in 43 pM silver nanoparticles/2.8 mM H_2O_2/0.1 M $HClO_4$ overlaid with the voltammetric profile of a silver nanoparticle-modfiied GC macroelectrode scanned at 200 mV s^{-1} in a) 2.8 mM H_2O_2/0.1 M $HClO_4$ and b) 2.8 mM H_2O_2/0.1 M $NaClO_4$

The next step was to the increase the concentration of silver nanoparticles added to the 2.8 mM H_2O_2/0.1 M $HClO_4$ solution. Figure 8.6 shows that as the concentration of

silver nanoparticles in the electrochemical cell is increased the observed impact frequency of spikes also increases, with 300-700 impact spikes having been measured per data point shown. The gradient of the linear fit shown in figure 8.6 was found to be 5.2×10^4 $s^{-1}cm^{-2}pM^{-1}$. This dependence on nanoparticle concentration is similar to that observed by Zhou et al. who studied the reduction of protons on the surface of impacting silver nanoparticles also at a carbon microelectrode (3.9×10^4 $s^{-1}cm^{-2}pM^{-1}$)[2]. The observed relationship between the frequency of nanoparticle impacts and silver nanoparticle concentration as well as its consistency with previous literature[2] suggests that the recorded impact spikes are caused by the reduction of H_2O_2 on the surface of a silver nanoparticle during individual nanoparticle-electrode collisions.

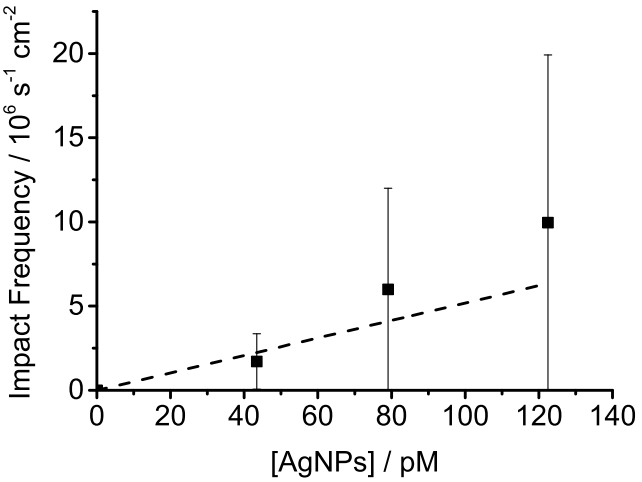


Figure 8.6: Frequency of observed impact spikes in 5 s chronomaperometric profiles measured at -0.9 V *vs.* SCE in a solution of 2.8 mM H_2O_2 in 0.1 M $HClO_4$ as a function of silver nanoparticle concentration.

Increasing the concentration of the redox species in solution is another method by which to confirm that spikes in the current-time transient are caused by the electrocatalytic amplification of nanoparticle impacts[2]. The silver nanoparticle-electrode impact experiment was performed in a solution of varying concentrations of H_2O_2. H_2O_2 concen-

trations of 2.8 mM, 5.6 mM, 11.2 mM and 22.5 mM in a solution of 0.1 M HCl with varying concentrations KCl added to ensure full support were tested, as when $NaClO_4$ was added to the 0.1 M $HClO_4$ solution used previously to ensure a sufficient support ratio of 100 : 1 it crystallised at the reference electrode at concentrations greater than 1 M. Figures 8.7a, b, c and d shows the charge distributions plotted for between 150 and 700 impact spikes measured at each H_2O_2 concentration tested and the maximum of each charge distribution is plotted against the concentrion of H_2O_2 in figure 8.7e. The charge of the impact spikes was found to increase linearly with concentration of H_2O_2 and the resulting plot has a gradient of 4.1×10^{-7} C $mol^{-1}cm^{-3}$.

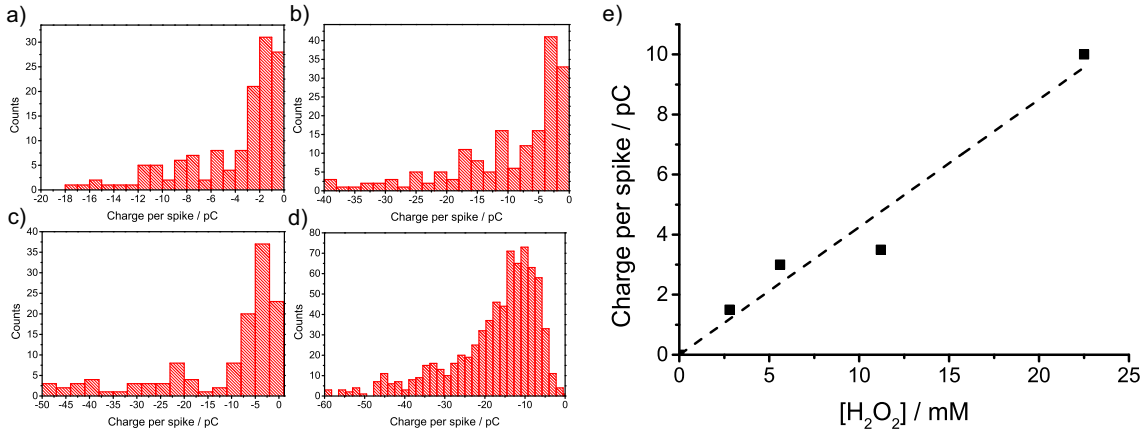


Figure 8.7: Charge distribution plots for impact spikes measured at H_2O_2 concentrations of a)2.8 mM, b)5.6 mM, c) 11.2 mM and d) 22.5 mM in 0.1 M HCl/KCl with 43 pM silver nanoparticles added and e) a plot of charge per spike *vs.* H_2O_2 concentration for which the value was taken from the maximum of the charge distributions shown in a)-d).

It can be seen from figure 8.7e that at a H_2O_2 concentration of 10 mM the impact spikes will have a charge of 4 pC which, if a full two electron reduction of every molecule of H_2O_2 is assumed, corresponds to the reduction of 1.6×10^7 H_2O_2 molecules during a single impact. If the impact is caused by a single spherical nanoparticle the maximum monolayer coverage of the formed $OH_{(ads)}$ species can be approximated to 2.5×10^5 molecules using an atomic radius of 60 pm for oxygen. Equation 8.2 can be applied if a

further assumption that the current at a conducting sphere is diffusion limited for the time duration of an impact (Δt) is made. This assumption is reasonable as the time required to establish steady state conditions is defined by Shoup and Szabo as r^2/D[14] which in this case has a value of the order of 10^{-7} s, much lower than the millisecond duration of an impact spike.

$$Q = I_{\text{lim}} \times \Delta t \tag{8.2}$$

Equation 8.2 can be rewritten to include the well known equation for the steady state current at a sphere[15] as shown in equation 8.3 if it is assumed that the current passed at the nanoparticle is equivalent to that at a sphere, although in reality where the nanoparticle is in contact with the electrode the plane of the electrode will block the diffusion of peroxide molecules to a portion of the nanoparticle surface.

$$\frac{Q}{[H_2O_2]} = 4\pi n F D r_{\text{NP}} \times \Delta t \tag{8.3}$$

Rearranging equation 8.3 it is possible to gain a value for the nanoparticle radius, r_{NP}, of 12.9 nm, where Δt=13 ms (the mean duration of 100 spikes), D is a typical diffusion coefficient (10^{-5} cm^{2}s^{-1}), F is the Faraday constant and n is the number of electrons transferred (2 electrons). The aim of this calculation is to show that the process is diffusional. The diffusion coefficient of hydrogen peroxide is not well known (values reported in the literature range between 1.07×10^{-5} cm^{2}s^{-1} and 1.80×10^{-5} cm^{2}s^{-1}[16–19]) and therefore it is necessary to approximate the value of D to that of a typical molecular diffusion coefficient viz. 10^{-5} cm^{2}s^{-1} noting that this might be in error by up to a factor of two. At the same time equation 8.3 assumes full unhindered spherical diffusion. In

reality partial shielding by the electrode will occur offering some compensation for any underestimation in D. The r_{NP} value of 12.9 nm determined *via* equation 8.3 is in very close agreement with the nanoparticle size obtained by Zhou et al. for the same silver nanoparticles *via* anodic particle coulometry (r_{NP}=13 nm) and SEM (r_{NP}=14 $\pm$ 2 nm) in [2] confirming that approximating the current response measured for a redox reaction at the surface of an impacting nanoparticle to the diffusion limited current at a conducting sphere is a reasonable approach.

8.4 Conclusions

In this chapter nanoparticle-impact experiments have been employed to study the reduction of hydrogen peroxide on the surface of silver nanoparticles impacting upon a carbon electrode. The silver nanoparticles electrocatalyse the reduction of hydrogen peroxide and spike-type transients are observed in the current response when a nanoparticle collides with the electrode surface. The charge of the resulting impact spikes can be used to provide information on the size of the silver nanoparticles by approximating the charge of the impact process to the diffusion limited current at an isolated sphere. The good agreement between the nanoparticle size obtained from this approximation and that determined using other methods (anodic particle coulometry and SEM)[2] suggests that this approximation is valid and provides new physical insight into the nanoparticle-electrode contact environment during indirect nanoparticle detection studies.

The work in this chapter compliments the work performed by Zhou et al.[2] where silver nanoparticles are sized from the charge of the impact spikes observed when the nanoparticles are directly oxidised and upon collision with a suitably potentiostatted

electrode as it has now been shown that the accurate sizing of silver anoparticles can be performed *via* both direct and indirect nanoparticle-electrode impact methods.

Bibliography

[1] E. J. E. Stuart, N. V. Rees and R. G. Compton, *Chem. Phys. Lett.* **531** (2012) 94–97.

[2] Y. G. Zhou, N. V. Rees and R. G. Compton, *Angew. Chem., Int. Ed.* **50** (2011) 4219–4221.

[3] D. Wakerley, A. G. Guell, L. A. Hutton, T. S. Miller, A. J. Bard and J. V. Macpherson, *Chem. Commun.* **49** (2013) 5657–5659.

[4] X. Xiao, F. F. Fan, J. Zhou and A. J. Bard, *J. Am. Chem. Soc* **130** (2008) 16669–16677.

[5] H. Zhou, F. F. Fan and A. J. Bard, *J. Phys. Chem. Lett.* **1** (2010) 2671–2674.

[6] S. J. Kwon, F. F. Fan and A. J. Bard, *J. Am. Chem. Soc* **132** (2010) 13165–13167.

[7] M. Heyrovsky, J. Jirkovsky and M. Struplovabartackova, *Langmuir* **11** (1995) 4300–4308.

[8] R. Dasari, D. A. Robinson and K. J. Stevenson, *J. Am. Chem. Soc.* **135** (2013) 570–573.

[9] X. Y. Xiao and A. J. Bard, *J. Am. Chem. Soc.* **129** (2007) 9610–9612.

[10] M. Heyrovsky, J. Jirkovsky and B. R. Muller, *Langmuir* **11** (1995) 4293–4299.

[11] R. Dasari, K. Tai, D. A. Robinson and K. J. Stevenson, *ACS Nano* **8** (2014) 4539–4546.

[12] R. Dasari, B. Walther, D. A. Robinson and K. J. Stevenson, *Langmuir* **29** (2013) 15100–15106.

[13] F. W. Campbell, S. R. Belding, R. Baron, L. Xiao and R. G. Compton, *J. Phys. Chem. C* **113** (2009) 9053–9062.

[14] D. Shoup and A. Szabo, *J. Electroanal. Chem. Interfacial Electrochem.* **140** (1982) 237–245.

[15] R. G. Compton and C. E. Banks, *Understanding Voltammetry* (Imperial College Press, London, 2011), second edition.

[16] V. Prabhu, L. Zarapkar and R. Dhaneshwar, *Electrochim. Acta* **26** (1981) 725–729.

[17] D. M. H. Kern, *J. Am. Chem. Soc* **76** (1954) 4208–4214.

[18] S. van Stroe-Biezen, F. Everaerts, L. Janssen and R. Tacken, *Anal. Chim. Acta* **273** (1993) 553–560.

[19] I. Katsounaros, W. B. Schneider, J. C. Meier, U. Benedikt, P. U. Biedermann, A. A. Auer and K. J. J. Mayrhofer, *Phys. Chem. Chem. Phys.* **14** (2012) 7384–7391.

Chapter 9

A Fickian Model for Nanoparticle Transport and the Importance of Determining the Sticking Coefficient

This chapter reports on a how a Fickian model for diffusion can be used to describe the observed frequency response of nanoparticle-electrode collisions for both direct and indirect nanoparticle detection methods where the experimental data reported in chapter 8 is used for the indirect study. Determination of the sticking coefficient is shown to be vital in applying this Fickian approach to the indirect detection method and the experimentally determined sticking coefficient of gold nanoparticles is also reported.

This work was performed in collaboration with Dr. N. V. Rees who helped with the interpretation of experimental results and derived equation 9.8 for the fitting of experimentally determined indirect nanoparticle-electrode impact data. The gold nanoparticles used in this chapter were synthesised by Dr. J. Pillay, Dr. S. Vilakazi and Dr. R. Tshikhudo at Mintek, South Africa. SEM imaging of the gold nanoparticles was performed by the Crossley Group, Dept. of Materials Science, University of Oxford and the gold nanoparticle concentration was determined *via* UV-vis spectroscopy by Dr. Y. Zhou. The work in this chapter has been published in RSC Advances[1] and Chemical Physics Letters[2].

9.1 Introduction

While recent progression in the area of nanoparticle-impact electrochemistry introduced in chapter 2 has identified a number of wide-ranging applications for this novel technique from the analysis of DNA[3] to the synthesis of core-shell nanoparticles[4, 5], it is important to develop a theoretical understanding behind this exciting technique.

Initially a kinetic theory approach was proposed by Bard et al. however it was found that this ballistic view over-estimated the frequency of observed nanoparticle-electrode collisions by at least three orders of magnitude[6]. Following this, Dickinson et al. simulated the direct oxidation of silver nanoparticles upon impact with a carbon electrode using a model where the nanoparticles are moving in solution *via* Brownian motion[7]. The same destructive system for silver nanoparticle impacts was investigated in chapter 4 and an approach based on Fickian diffusion proved to be useful in the accurate analysis of impact spike frequency, which was also found to be applicable to nickel nanoparticles[8].

This chapter provides further evidence to support the use of a Fickian diffusion model to interpret experimental nanoparticle-electrode impact data. It is shown that the transport of nanoparticles to the electrode surface can be explained, without the need for complex simulation, by this diffusional model for both direct nanoparticle detection, where the nanoparticle is destroyed upon impact at a suitably potentiostatted electrode surface, and indirect nanoparticle detection, whereby electrocatalytic amplication of the impact event occurs *via* the electrolysis of a redox species in solution on the nanoparticle surface. For the direct nanoparticle detection method the destructive oxidation of silver nanoparticles is studied while for the indirect method the reduction of hydrogen peroxide on impacting silver nanoparticles, as outlined in the previous chapter, is investigated.

Silver was chosen as the nanoparticle material as it has been thoroughly studied using the particle-impact method previously with information on silver nanoparticle sticking probability[9], aggregation[10], oxidation kinetics[11] and sizing[12] having been gained *via* this technique. It is proposed that a concentration gradient is established for both types of nanoparticle detection methods: for the direct nanoparticle detection method the nanoparticle sink is the destruction of the nanoparticle upon impact whereas in indirect nanoparticle detection the adhesion of nanoparticles to the carbon surface provides the drive for diffusion.

The silver nanoparticle sticking coefficient, a measurement of the proportion of impacts that result in adhesion, proved to be vital to the development of this Fickian model for indirect nanoparticle impacts. The value of this sticking coefficient had been determined previously by Zhou et al. in [9], the sticking coefficient of nickel nanoparticles on carbon has also been reported[2]. Further to this, the sticking coefficient of another nanoparticle type that is commonly used in indirect nanoparticle-electrode impact studies, gold nanoparticles[13, 14], is determined in this chapter, which will be useful in modelling the frequency response for indirect studies in which gold nanoparticles are employed in future work.

9.2 Experimental Procedure

9.2.1 Silver Nanoparticle Synthesis

Silver nanoparticles were synthesised according to the method described in section 3.2.1. The radius of the silver nanoparticles was found to be 13 nm *via* anodic particle coulometry and 14 $\pm$ 2 nm *via* SEM imaging[12]. The nanoparticle concentration was measured as

explained in section 3.2.1.

9.2.2 Direct Nanoparticle-Electrode Impact Experiments

Figure 9.1 shows the experimental set-up for the direct nanoparticle-electrode impact experiments. The electrochemical cell was surrounded by a heating coil through which heated water, provided by a thermostatted water bath, was pumped through a peristaltic pump. Cotton wool was wrapped around the cell to provide insulation.

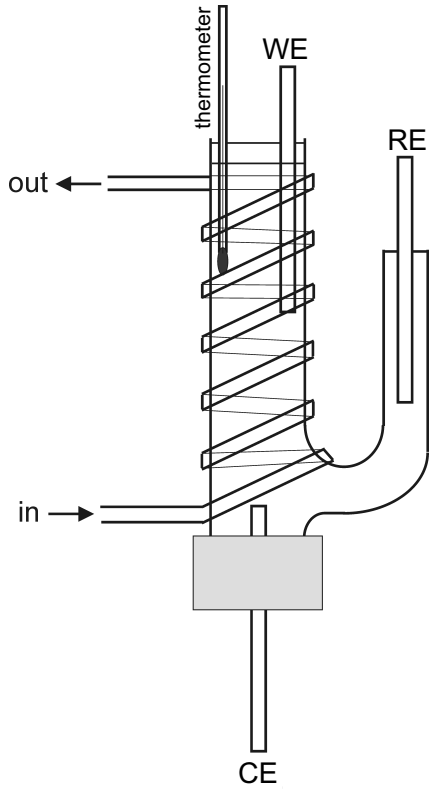


Figure 9.1: Schematic of the experimental set-up to carry out nanoparticle-impact experiments at varying temperatures showing a heating coil, thermometer and working, counter and reference electrodes (WE, CE and RE respectively).

The working electrode was a carbon fibre microelectrode (r_e=4.8 µm) while a saturated calomel electrode (SCE) and graphite rod acted as the reference and counter electrodes respectively. The working electrode was polished using 3.0, 1.0 and 0.1 µm diamond spray

before sonicating in H_2O for 1 min. Solutions were thoroughly degassed and agitated with argon. The observed impact spikes were analysed using OriginPro 8.5.1.

9.2.3 Indirect Nanoparticle-Electrode Impact Experiments

The experimental set-up used is described in section 3.3.4. The electrodes used were the same as that in section 9.2.2 however the carbon fibre working electrode was 5.5 µm in radius. The hydrogen peroxide concentration was determined *via* titration to be 14.1 % (w/w) in H_2O as detailed in section 8.2.2. Argon was used to degas the electrolyte and agitate the nanoparticles dispersed in solution. OriginPro 8.5.1 was used in the analysis of impact spikes.

9.2.4 Gold Nanoparticle Synthesis

Citrate-capped gold nanoparticles with a radius of 10 nm were synthesised by Mintek, South Africa. SEM measurements performed by Dr. K. Jurkschat, University of Oxford confirmed that the gold nanoparticle radius was 10 nm, in good agreement with the radius value determined using anodic particle coulometry by Zhou et al. in [15] (r_{NP}=10.5 nm).

9.2.5 Cyclic Voltammetry

Cyclic voltammetry was performed according to section 3.3.2. The working electrode was a gold nanoparticle modified-glassy carbon (GC) macroelectrode (r_e=1.5 mm) while the counter and reference electrode were a graphite rode and saturated calomel electrode (SCE) respectively. The working electrode was polished on diamond spray of three different grades (3.0, 1.0, 0.1 µm) and sonicated in H_2O for 1 min.

9.2.6 Anodic Stripping Voltammetry

Anodic stripping voltammetry was carried out according to section 3.3.3 and all scans were measured at a scan rate of $200\,\mathrm{mV\,s^{-1}}$. The working electrode was a carbon fibre microelectrode (r_e=5.9 µm), the reference electrode was a SCE and the counter electrode was a graphite rod. Before each use, the working electrode was polished using diamond spray (3.0, 1.0, 0.1 µm) and then sonicated in H_2O for 1 min.

9.3 Results and Discussion

9.3.1 Direct Electrochemistry of Nanoparticles

For the direct nanoparticle-electrode impact experiments, where the exhaustive oxidation of a nanoparticle occurs upon impact with a suitably potentiostatted electrode, the destruction of the nanoparticle provides a "sink" for the nanoparticles in solution resulting in a concentration gradient being established, along which Fickian diffusion can occur. If the transport of nanoparticles from the bulk solution to the electrode surface is diffusional the observed frequency of impact will be dependent on temperature.

The direct nanoparticle detection system studied in this chapter is the same as that in chapter 4 where the oxidation of silver nanoparticles (r_{NP}=13 nm) occurs when a nanoparticle comes into contact with a carbon fibre electrode surface. The carbon fibre electrode (r_{e}=4.8 µm) was placed in a solution of 50 pM silver nanoparticles/10 mM $NaC_6O_7H_7$/90 mM KCl and potentiostatted at a potential more positive than the oxidation potential of silver nanoparticles (+0.3 V *vs.* SCE). Chronoamperomograms of 5 s duration were recorded and oxidative impact spikes were observed in the current response.

A typical chronoamperometric profile can be seen in chapter 4. The impact experiment was performed at varying temperatures between 296K and 308K where the temperature of the electrolytic solution was controlled using the set-up shown in figure 9.1. Several hundred impact spikes were recorded at each temperature and the corresponding impact frequencies were determined.

If the transport of silver nanoparticles to the carbon microelectrode surface is diffusional then it would be expected that the observed impact frequency, f_s, is proportional to the diffusion coefficient, D, of the nanoparticles in solution

$$f_s \propto D \tag{9.1}$$

and therefore, according to the Stokes-Einstein equation, the frequency of nanoparticle-electrode collisions will be inversely proportional to the viscosity of the solution, η, in which the nanoparticles are suspended as in equation 9.2.

$$f_s \propto \frac{1}{\eta} \tag{9.2}$$

The expected impact frequencies for nanoparticles at the same temperatures tested experimentally were calculated using values for the viscosity of water taken from [16] and an Arrhenius-type analysis was performed giving an expected activation energy for nanoparticle transport of 24.6 KJ mol^{-1}. Figure 9.2 shows a logarithmic plot of impact frequency against inverse temperature for these calculated values (empty circles) and the experimentally determined impact frequencies (filled squares). The general trend of increasing impact frequency with increasing temperature suggests that the transport of nanoparticles to the electrode is indeed diffusional. The activation energy calculated from

the experimental data was 24.9 KJ mol^{-1} which is in good agreement with the expected activation energy. The vertical offset between the experimental and theoretical data points seen in figure 9.2 is due to the effects of aggregation as the concentration value used to calculate the expected impact frequency was that for single nanoparticles whereas, in reality, aggregation of the silver nanoparticles will occur over the experimental timeframe (10 minutes) with previous work demonstrating that the dominant silver nanoparticle species will be a cluster of four nanoparticles[10]. A four-fold decrease in concentration translates to a difference of 1.35 in the logarithmic impact frequency which is very similar to the difference between the experimental and theoretical data in figure 9.2.

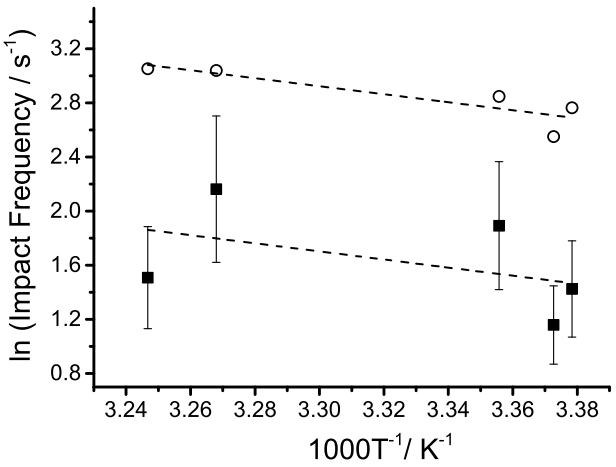


Figure 9.2: Arrhenius plots showing experimental data (filled squares) and theoretical data (empty circles) for the dependence of impact frequency on temperature for the destructive oxidation of silver nanoparticles (r_{NP}=13 nm) impacting a carbon microelectrode (r_e=5.5 µm) in 10 mM $NaC_6O_7H_7$/90 mM KCl.

9.3.2 Indirect Electrochemistry of Nanoparticles

While the driving force for Fickian diffusion to the electrode in the direct nanoparticle detection method is the concentration gradient established when the silver nanoparticles are oxidatively destroyed upon collision with the electrode surface, for indirect nanopar-

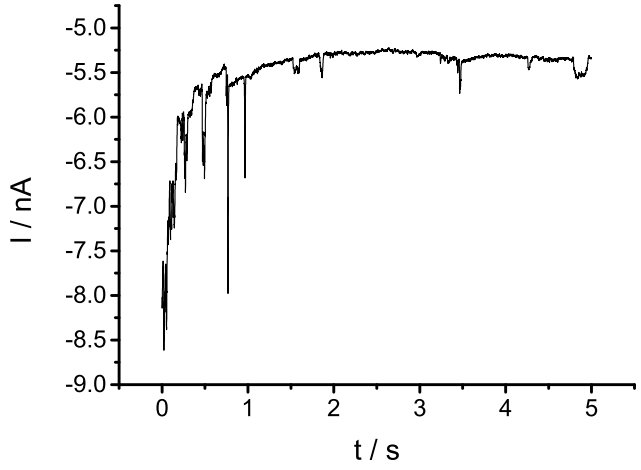


Figure 9.3: Reductive impact spikes observed for the reduction of H_2O_2 on the surface of impacting silver nanoparticles (r_{NP}=13 nm) at a carbon fibre microelectrode (r_e=4.8 µm) potentiostatted at −0.9 V *vs.* SCE in a solution of 2.8 mM H_2O_2/0.1 M HCl/0.3 MKCl at 295 K.

ticle detection the nanoparticles are not destroyed upon impact and therefore the "sink" for nanoparticle diffusion must be provided by another factor.

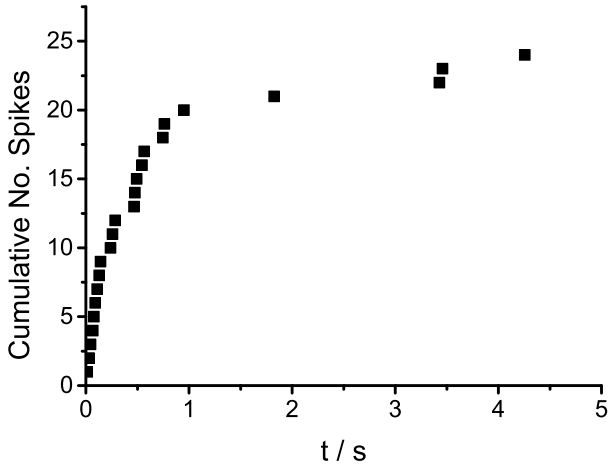


Figure 9.4: Plot of cumulative number of spikes as a function of time for the chronomaperogram shown in figure 9.3.

In order to study the impact frequency of nanoparticle-electrode collisions detected *via* this indirect technique the reduction of hydrogen peroxide on impacting silver nanoparticles was measured as described in chapter 8. A typical 5 s chronoamperometric profile

showing the reductive impact spikes observed can be seen in figure 9.3. Figure 9.4 shows a plot of the cumulative number of spikes measured in this scan as a function of time. It can be seen that the frequency of spikes is larger at the beginning of the scan. This observation was explained for the case of oxidative impact spikes for the destructive oxidation of colliding silver nanoparticles detected *via* the direct nanoparticle detection method in chapter 4 using an integrated form of the Shoup and Szabo expression (equation 9.3):

$$N = N_{\mathrm{A}} C r_{\mathrm{e}}^3 (\tau + 1.437\tau^{1/2} + 6.57 \times 10^{-2} ln\tau - 3.35 \times 10^{-3}\tau^{-1} + 3.43 \times 10^{-3}\tau^{-1/2} + 3.49 \times 10^{-4}\tau^{-3/2} \quad (9.3)$$

where N is the cumulative number of spikes, r_e is the electrode radius, N_{A} is the Avagadro constant and τ is the dimensionless time given by $\tau = 4Dt/r_{\mathrm{e}}^2$.

It has previously been found that silver nanoparticles adhere to the electrode surface and the sticking coefficient, s, for silver nanoparticles at carbon electrode is 0.15 ± 0.02 [9]. Sticking of nanoparticles to the electrode surface will not occur in the direct nanoparticle detection method as the potential applied to the working electrode during chronoamperometric scanning to measure the impact spikes is past the oxidation potential for silver nanoparticles hence any adhered nanoparticles will be oxidised upon the scanning required in nanoparticle-electrode impact experimrents. For the indirect nanoparticle detection, the oxidation of silver nanoparticles does not occur at the potential applied to the working electrode as the scanning potential is chosen to correspond to the reduction of hydrogen peroxide (E=−0.9 V *vs.* SCE) therefore the silver nanoparticles will be able to stick to the electrode surface. This nanoparticle adhesion provides a sink for nanoparticles and

therefore a concentration gradient down which Fickian diffusion can occur for the case of indirect nanoparticle detection. In order to take the influence of nanoparticle sticking into account for the indirect nanoparticle technique equation 9.3 can be rewritten as:

$$N = N_{\mathrm{A}} C s r_{\mathrm{e}}^{3} (\tau + 1.437\tau^{1/2} + 6.57 \times 10^{-2} ln\tau - 3.35 \times 10^{-3}\tau^{-1} + 3.43 \times 10^{-3}\tau^{-1/2} + 3.49 \times 10^{-4}\tau^{-3/2} \quad (9.4)$$

For a surface coverage, Γ, the rate at which colliding nanoparticles adsorb is given by:

$$\frac{d\Gamma}{dt} = ks(1-\Gamma)\frac{dN}{dt} \quad (9.5)$$

where k is a constant with dimensions of (no. of particles)$^{-1}$. Solving expression 9.5 gives:

$$\Gamma = 1 + Ce^{-skN} \quad (9.6)$$

Given that Γ=0 when N=0 the integration constant, C, can be evaluated to be -1.

The rate of *observable* impacts, N_{obs} can then be expressed as:

$$\frac{dN_{\mathrm{obs}}}{dt} = (1-\Gamma)\frac{dN}{dt} \quad (9.7)$$

If equation 9.6 is substituted into equation 9.7 and integrated with respect to time with the condition that N_{obs}=0 when N=0 the following expression is gained:

$$N_{\text{obs}} = \frac{1}{sk}(1 - e^{-skN}) \tag{9.8}$$

Equations 9.4-9.8 were derived by Dr. N. V. Rees. The value of k takes into account factors that influence the effective free area of the electrode surface that is available for a nanoparticle collision. Such factors could include the formation of depletion zones around each adsorbed nanoparticle on the electrode surface, nanoparticle aggregation in solution and the greater sticking coefficient for silver nanoparticle adhesion on a silver surface (s=0.70[17]) as opposed to a carbon surface (s=0.15[9]). The nature of these factors suggest that the value of k will be specific the nanoparticle system being studied and will be influenced by nanoparticle material, size and capping agent.

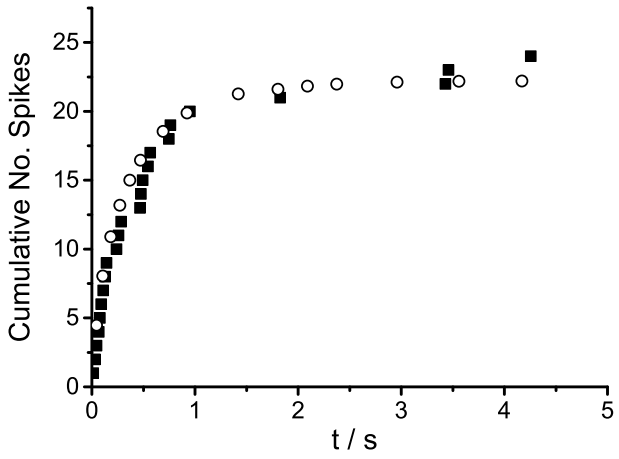


Figure 9.5: Plots showing the fit of equation 9.8 with k=0.30 particle^{-1} (empty circle) to experimentally gained (filled square) cumulative no. spikes *vs.* time plots for the reduction of H_2O_2 on impacting silver nanoparticles.

As described in chapter 4 where equation 9.3 was fitted to plots of the cumulative number of spikes *vs.* time for the destructive oxidation of impacting silver nanoparticles observed *via* the direct nanoparticle detection method, equation 9.8 can be used to fit plots of the same type where the impact spikes have been measured using the indirect

nanoparticle detection method. Figure 9.5 shows a plot of the cumulative number of impacts as a function of time for experimentally measured data overlaid with an analogous plot determined *via* equation 9.8 where N_{obs} is calculated at times where the value of N determined from equation 9.4 is an integer and the value for k=0.30 particle^{-1}. The good agreement between the N_{obs} and the cumulative number of impact spikes observed experimentally using the indirect nanoparticle detection method shows that a Fickian diffusion model can be used to effectively describe how the impact frequency varies with time, where the concentration gradient for diffusion is established when the adhesion of silver nanoparticles to the electrode surface provides a nanoparticle sink.

9.3.3 Determining the Sticking Coefficient of Gold Nanoparticles at a Carbon Electrode

Section 9.3.2 demonstrated the importance of the sticking coefficient as it provides the nanoparticle sink for Fickian diffusion of nanoparticles to the elecotrde surface and thus influences the number of impact spikes observed. Knowledge of the silver nanoparticle sticking coefficient on carbon was vital in developing a simple Fickian model to describe the observed impact frequency for the indirect nanoparticle detection technique. Gold nanoparticles are commonly used in the indirect, or electrocatalytic amplification, nanoparticle detection method where the nanoparticles are measured *via* the electrocatalysis of a redox species in solution on the nanoparticle surface[13, 14]. Therefore determination of the gold nanoparticle sticking coefficient will be useful in the future analysis of nanoparticle-electrode impact data.

The sticking coefficient is defined as:

$$s = \frac{\text{Rate of NPs sticking to surface } (P_{\text{ads}})}{\text{Rate of NP collisions with surface } (f_{\text{s}})} \tag{9.9}$$

It is determined experimentally by using the direct nanoparticle detection technique to measure the collision rate of nanoparticles with the electrode surface and anodic stripping voltammetry to electrochemically strip any adhered nanoparticles from the electrode surface after set exposure times.

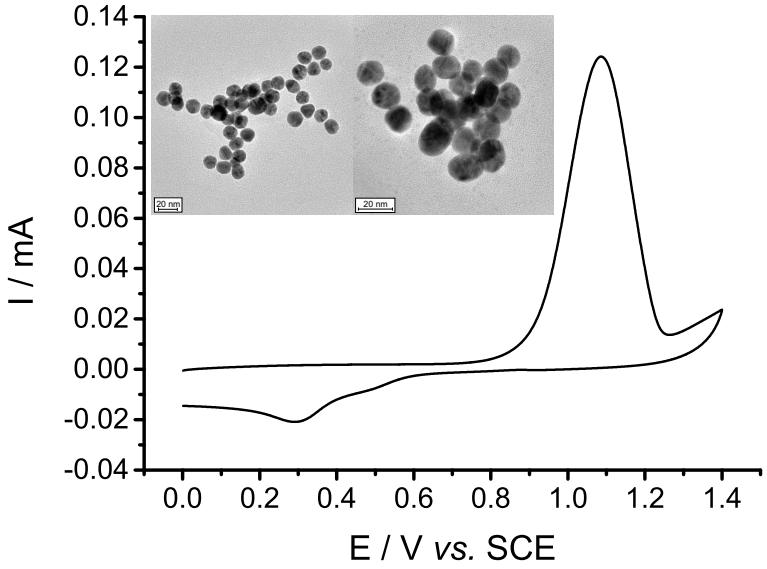


Figure 9.6: Cyclic voltammogram for a gold nanoparticle (r_{NP}=10 nm) modified-GC macroelectrode (r_{e}=1.5 mm) in 0.1 M HCl measured at a scan rate of 200 mV s^{-1}. Inset shows SEM images of gold nanoparticles with r_{NP}=10 nm.

First, cyclic voltammetry was used to measure the electrochemical response of a gold nanoparticle-modified GC electrode (r_{e}=1.5 mm) in 0.1 M HCl. The electrode was modified by dropcasting 2 µL gold nanoparticles (r_{NP}=10 nm) and drying in an argon atmosphere. It can be seen from figure 9.6 that the oxidation potential of gold nanoparticles is approximately +1.05 V *vs.* SCE. The same response was observed by Zhou et al. and it was found that 1.9 ± 0.1 electrons were transferred per gold atom[15]. The anodic dissolution of gold in the presence of chloride ions is facilitated by the formation of dichloroaurate

(I) and tetrachloroaurate (III) ions *via* [15, 18]:

$$\begin{aligned} \mathrm{Au} + 4\,\mathrm{Cl}^- &\rightleftharpoons \mathrm{AuCl_4}^- + 3\,\mathrm{e}^- \\ \mathrm{AuCl_4}^- + 2\,\mathrm{Au} + 2\,\mathrm{Cl}^- &\rightleftharpoons 3\mathrm{AuCl_2}^- \end{aligned} \tag{9.10}$$

Direct nanoparticle-electode impact experiments were then used to determine the collision frequency of gold nanoparticles. A carbon fibre microelectrode (r_e=5.9 µm) was potentiostatted in 0.1 M HCl at a potential past that of the gold nanoparticle oxidation potential (E=+1.20 V *vs.* SCE). An aliquot of gold nanoparticles was then added so that the concentration of nanoparticles in the electrochemical cell was equal to 89.1 pM and oxidative impact spikes were observed in the recorded chornoamperometric profiles (figure 9.7). The collision frequency, f_s, of gold nanoparticles with the carbon fibre microelectrode surface was found to be 2.8 ± 0.2 pM min^{-1}.

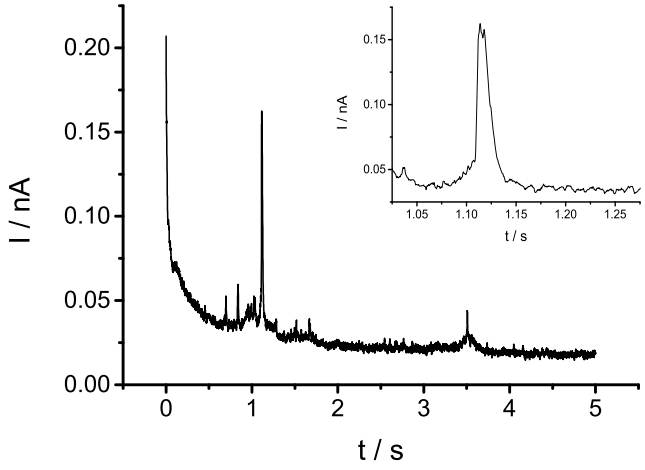


Figure 9.7: Typical 5 s chronoamperomogram showing oxidative spikes caused by gold nanoparticles (r_NP=10 nm) colliding with a carbon fibre microelectrode (r_e=5.9 nm) measured at a potential of +1.20 V *vs.* SCE in 0.1 M HCl with 89.1 pM gold nanoparticles added. Inset shows zoomed image of an oxidative impact spike.

In order to quantify the amount of nanoparticle collisions that result in adhesion at the electrode surface the same method used by Zhou et al. in determining the sticking

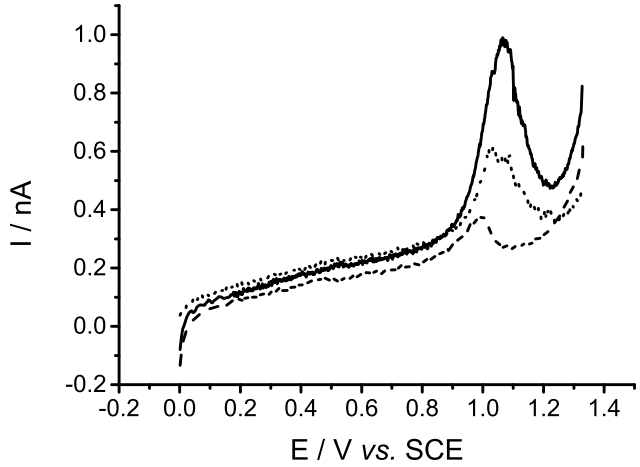


Figure 9.8: Anodic stripping voltammetry performed after sticking times of 15 (dashed line), 30 (dotted line) and 60 min (solid line) at an exposure potential of +0.1 V *vs.* SCE for a carbon microelectrode(r_e=5.9 µm) in a solution of 161.3 pM gold nanoparticles/0.1 MHCl. All scans performed at 200 mV s^{-1}.

coefficient of silver nanoparticles at a carbon electrode was employed[9]. A polished carbon fibre microelectrode (r_e=5.9 µm) was immersed in a 0.1 M HCl solution containing 161.3 pM gold nanoparticles and the exposure potential, E_{exp}, was set to +0.1 V *vs.* SCE. The carbon fibre microelectrode was exposed to the gold nanoparticle collisions for an exposure time, t, of 15, 30, 60 min before anodic stripping voltammetry was employed to quantify the number of nanoparticles that had 'stuck' to the electrode surface during this time period *via* measurement of the charge, Q, of the resulting oxidative stripping peak. Figure 9.8 shows the anodic stripping voltammetry profiles measured after varying exposure, or sticking, times while a plot of stripping charge as a function of sticking time can be seen in figure 9.9. The stripping charge increases linearly with time with a gradient of 6.5×10^{-12} C min^{-1}.

Equation 9.11 can be used to determine the number of adsorbed gold atoms per minute, N_{ads}, from the gradient measured in figure 9.9:

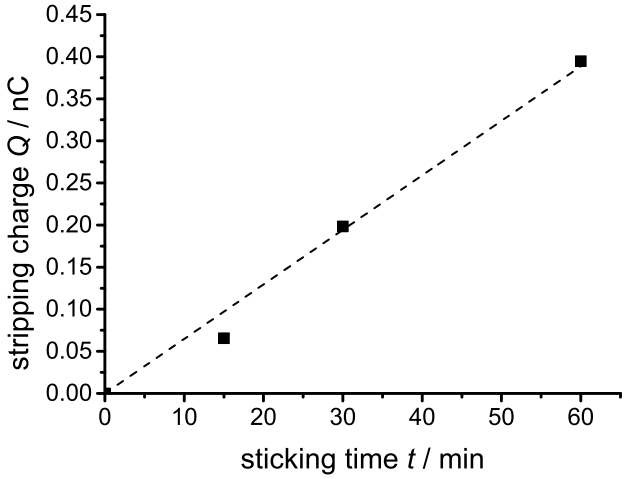


Figure 9.9: Plot of stripping charge Q as a function of sticking time t from which s=0.19 was derived (gradient=6.5$\times$ 10^{-12} Cmin^{-1}, R^2=0.993).

$$\frac{Q}{t} = N_{ads} n e \tag{9.11}$$

where e is elementary charge (C) and n is the number of electrons transferred per gold atom (determined in [15] to be 1.9).

The number of adsorbed nanoparticle per minute, P_{ads}, can be determined by:

$$P_{\mathrm{ads}} = \frac{N_{\mathrm{ads}}}{N_{\mathrm{NP}}} \tag{9.12}$$

where N_{NP} is the number of atoms in a colliding gold nanoparticle of radius 10 nm.

The sticking coefficient can then be determined *via* equation 9.13 which is rewritten from equation 9.9.

$$\mathrm{s} = \frac{P_{\mathrm{ads}}}{f_{\mathrm{s}}} = 0.19 \pm 0.01 \tag{9.13}$$

In order to confirm that the sticking coefficent measured for a gold nanoparticle at

a carbon fibre electrode is not influenced by the exposure potential the experiment described above was repeated at E_{exp}=+0.30 and +0.60 V *vs.* SCE. The sticking coefficients determined at these potentials were found to be s=0.16 ± 0.04 and s=0.21 ± 0.06 respectively suggesting that there is no systematic variation in sticking coeffient with exposure potential. The sticking coefficients of silver [9] and nickel nanoparticles [8] were also found to be independent of the exposure potential.

9.4 Conclusions

In this chapter it has been shown that the transport of nanoparticles to the electrode surface in both direct and indirect nanoparticle-electrode impact experiments can be described by a Fickian diffusion model. A concentration gradient is established in both types of impact experiment with the nanoparticle sink in the direct nanoparticle detection technique provided by the destructive oxidation of the nanoparticle upon contact with a suitably potentiostatted electrode surface while, for the indirect method, the sink results from the adhesion of nanoparticles on the electrode surface. This chapter builds upon the work presented in chapter 4 where a Fickian model was used to describe the cumulative number of spikes as a function of time for the direct impact processes by demonstrating that the same Fickian approach is also applicable to indirect nanoparticle impact experiments providing that the sticking probability is known. With the sticking coefficients of silver and nickel nanoparticles at a carbon electode having been calculated previously[8, 9], the sticking coefficient of gold nanoparticles at a carbon electrode was also determined in this chapter.

Bibliography

[1] E. J. Stuart, Y.-G. Zhou, N. V. Rees and R. G. Compton, *RSC Adv.* **2** (2012) 12702–12705.

[2] Y.-G. Zhou, E. J. Stuart, J. Pillay, S. Vilakazi, R. Tshikhudo, N. V. Rees and R. G. Compton, *Chem. Phys. Lett.* **551** (2012) 68–71.

[3] J. Liu, M. Tian and Z. Liang, *Electrochim. Acta* **113** (2013) 186–193.

[4] Y. G. Zhou, N. V. Rees and R. G. Compton, *Chem. P* **511** (2011) 183–186.

[5] Y.-G. Zhou, N. V. Rees and R. G. Compton, *ChemPhysChem* **12** (2011) 2085–2087.

[6] S. J. Kwon, H. Zhou, F.-R. F. Fan, V. Vorobyev, B. Zhang and A. J. Bard, *Phys. Chem. Chem. Phys.* **13** (2011) 5394–5402.

[7] E. J. Dickinson, N. V. Rees and R. G. Compton, *Chem. Phys. Lett.* **528** (2012) 44–48.

[8] E. J. E. Stuart, Y. G. Zhou, N. V. Rees and R. G. Compton, *RSC* **2** (2012) 6879–6884.

[9] Y. G. Zhou, N. V. Rees and R. G. Compton, *Chem. Phys. Lett.* **514** (2011) 291–293.

[10] N. V. Rees, Y. G. Zhou and R. Compton, *ChemPhysChem* **12** (2011) 1645–1647.

[11] Y.-G. Zhou, B. Haddou, N. V. Rees and R. G. Compton, *Phys. Chem. Chem. Phys.* **14** (2012) 14354–14357.

[12] Y. G. Zhou, N. V. Rees and R. G. Compton, *Angew. Chem., Int. Ed.* **50** (2011) 4219–4221.

[13] J. M. Kahk, N. V. Rees, J. Pillay, R. Tshikhudo, S. Vilakazi and R. G. Compton, *Nano Today* **7** (2012) 174–179.

[14] H. Zhou, F. Fan and A. Bard, *J. Phys. Chem. Lett.* **1** (2010) 2671–2674.

[15] Y. G. Zhou, N. V. Rees, J. Pillay, R. Tshikhudo, S. Vilakazi and R. G. Compton, *Chem. Comm.* **48** (2012) 224–226.

[16] R. C. Weast, *CRC Handbook of Chemistry and Physics* (CRC Press, Boca Raton, FL, USA, 1974), fifty-fifth edition.

[17] R. F. Benck, C. Crisco and H. L. Spies, *J. Vac. Sci. Technol.* **10** (1973) 562–563.

[18] A. Kolics, A. E. Thomas and A. Wieckowski, *J. Chem. Soc., Faraday Trans.* **92** (1996) 3727–3736.

Chapter 10

Improving the Rate of Silver Nanoparticle Adhesion to "Sticky Electrodes": Stick and Strip Experiments at a DMSA-modified Gold Electrode

The previous chapter described the use of a technique involving the immobilisation of nanoparticles from solution at a solid surface followed by anodic stripping voltammetry to determine the sticking coefficient of gold nanoparticles. The same sticking and stripping technique is also useful in the analysis of nanoparticle concentrations and identity as outlined in chapter 7. In this chapter it is shown that the modification of gold electrodes with meso-2,3-dimercaptosuccinic acid (DMSA) shows a useful increase in the adsorption rate of silver nanoparticles on a gold substrate demonstrating that chemical modification of the electrode is analytically advantageous.

This work was carried out in collaboration with Miss J. Ellison who carried out the NTA shown in figure 10.2 and Dr. K. Tschulik who helped with the interpretation of experimental results and carried out the SEM imaging also shown in figure 10.2 with the help of Dr. K. Hennig at IFW, Dresden, Germany. The results included this chapter have been published in *Electroanalysis*[1].

10.1 Introduction

The surface immobilisation of silver particles can be studied using a number of different experimental techniques. Most commonly, it is SEM and AFM that are employed to establish the coverage of particles on a solid substrate. An alternate approach is to use electrochemical techniques, for example anodic stripping voltammetry, to oxidatively strip off silver nanoparticles that have become stuck to a substrate electrode before measuring the charge of the stripping peak observed to determine a surface coverage value provided the size of the nanoparticles and the electrode is known[2, 3]. The use of "sticky electrodes" for the analytical determination of nanoparticles in aqueous samples have been proposed[2, 3] where a sticky electrode is immersed in a nanoparticle containing solution for varying time durations before anodic stripping voltammetry is used to quantify the amount of silver nanoparticles that have become stuck to the electrode surface. Sticky electrodes offer improved nanoparticle detection capabilities due to the increased immobilisation of nanoparticles on the modified electrode surface.

Typical molecules used to make the surface "sticky" include those that contain thiol[2], carboxylic acid[4] and amino groups[5, 6] where modification can be performed *via* electrochemical[2] or chemisorption[5, 7] methods at substrate electrodes of varying materials e.g. gold[5], carbon[2, 4] and indium tin oxide[6]. Depending on the molecule selected to act as the sticking agent, the trapping of nanoparticles in solution can occur *via* chemical[2] or electrostatic interactions[5, 6]. Physisorption can also be used to trap nanoparticles from solution, bypassing the need for chemical modification[8](as in chapter 7).

It has been shown that the electrochemical modification of a carbon substrate electrode with cysteine can significantly increase the reproducibility and the number of silver

nanoparticles that stick to a carbon electrode surface when compared to the nanoparticle coverage achieved at an unmodified carbon electrode after the same sticking time[2, 3].

The aim of this chapter is to increase the adsorption rate of silver nanoparticles on a gold substrate using sticky gold electrodes. Modification of the gold substrate with meso-2,3-dimercaptosuccinic acid (DMSA) *via* chemisorption according to reaction 10.1 is performed to achieve this desired sticky gold surface[7]. The structure of a DMSA molecule is shown in Figure 10.1.

$$\mathrm{RSH} + \mathrm{Au} \longrightarrow \mathrm{RS{-}Au} + \tfrac{1}{2}\,\mathrm{H_2} \tag{10.1}$$

where R=$SHCO_2HCHCHCO_2H$.

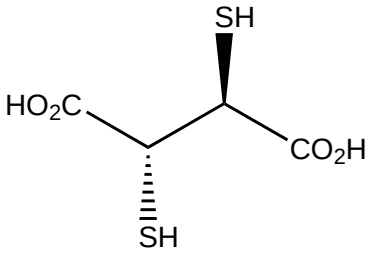


Figure 10.1: Structure of *meso*-2,3-dimercaptosuccinic acid (DMSA).

DMSA has been used in the past for the detection of copper (II) ions[9, 10], uric acid[7, 11] and epinephrine[11] however this is the first time it has been used to achieve a sticky surface to capture nanoparticles from solution.

10.2 Experimental Procedure

10.2.1 Electrochemical Set-Up

All electrochemical experiments were performed as described in section 3.3.2. For the three electrode set up a graphite rod acted as the counter electrode, a gold substrate electrode (r_e=0.5 mm or 1.5 mm) was used as the working electrode while potentials applied were measured against a leakless silver/silver chloride (Ag/AgCl) reference electrode, saturated calomel electrode (SCE) or a platinum mesh quasi reference electrode.

10.2.2 Preparation of the Electrode Surface

Thorough cleaning of the electrode is imperative for effective surface modification, this involved both mechanical and electrochemical cleaning methods. First, the working electrode was polished on alumina (1.0 µm, 0.3 µm and then 0.01 µm powder) using soft lapping pads (micro cloth PSA, Buehler) prior to the ultrasonic removal of any Al_2O_3 particles remaining on the gold substrate in H_2O for 1 min. Electrochemical cleaning was then employed where the gold electrode was voltammetrically cycled in 0.1 M H_2SO_4 at a scan rate of 100 mV s^{-1}[12]. Measurements were made across a potential range of 0 V to +1.5 V *vs.* Ag/AgCl until a stable voltammogram that no longer changed with scanning was obtained (approximately 10 cycles).

10.2.3 Modification of the Gold Electrode with DMSA

Post cleaning, the gold electrode was suspended in 5 mM *meso*-2,3-dimercaptosuccinic acid (DMSA) for 1 h. The DMSA solution had been degassed with nitrogen prior to addition of the electrode in order to prevent oxidation of the thiol groups to disulfides and the

pressure was kept on throughout the modification time. Once modification was complete, the gold electrode was removed from the DMSA solution and rinsed thoroughly with water in order to remove any physisorbed species. To test for a successful modification, the DMSA-gold electrode was scanned to negative potentials in a fully degassed 0.15 M phosphate buffer solution (pH 6.8) to observe the reductive stripping of the thiol from the golf substrate.

10.2.4 Silver Nanoparticle Sticking Experiments

The DMSA-modified gold electrode was prepared prior to sticking experiments *via* the methods specified in both sections 10.2.2 and 10.2.3 above while the unmodified gold electrode was cleaned according to the methods outlined in section 10.2.2. To prepare the sticking solution a known volume of silver nanoparticle stock solution with a concentation of 60 pM (determined as explained in section 3.2.1) was added to a sodium citrate solution (0.1 M) and the solution was sonicated for 5 min to disperse the nanoparticles. The gold electrode was then suspended in the silver nanoparticle solution for the desired time duration where it was held at open circuit potential (OCP).

10.2.5 Electrochemical Stripping of Adsorbed Silver Nanoparticles

Upon completion of the desired sticking time, anodic stripping voltammetry was employed to observe the oxidation of silver nanoparticles that had become stuck to the working electrode surface. Electrochemical stripping of the adsorbed nanoparticles was performed in the nanoparticle sticking solution i.e. 0.1 M sodium citrate with the added

silver nanoparticles. All measurements were performed at a scan rate of $20\,\mathrm{mV\,s^{-1}}$.

10.2.6 Recycling the Silver Nanoparticle/Sodium Citrate Solution

When silver nanoparticles are suspended in 0.1 M sodium citrate they are susceptible to agglomeration rather than aggregation. That is the reversible clustering of nanoparticles as opposed to irreversible clustering[13]. Therefore, it was possible to reuse the silver nanoparticle/sodium citrate solutions used in this investigation. In order to reverse the agglomeration process affecting the nanoparticles, the silver nanoparticle suspension was sonicated for 5 min before the addition of the gold electrode for the sticking experiment. After both the sticking and stripping experiments had been performed, the silver nanoparticle/citrate solution was covered with Parafilm (Bemis Company, Inc.) and stored in the dark when not in use. It was found that the same solution should only be used for a maximum of 4 d as the citrate was observed to degrade at long times.

10.3 Results and Discussion

This section outlines nanoparticle sticking at an unmodified gold electrode, before describing the modification of the electrode with DMSA *via* chemisorption and the increase in the rate of nanoparticle adhesion observed at this chemically modified electrode surface.

The silver nanoparticles used in this investigation were 22 nm in diameter. Figure 10.2 shows the characterisation data for silver nanoparticle sizing using NTA, SEM imaging was also used to confirm the size of the silver nanoparticles (shown in the inset of figure 10.2).

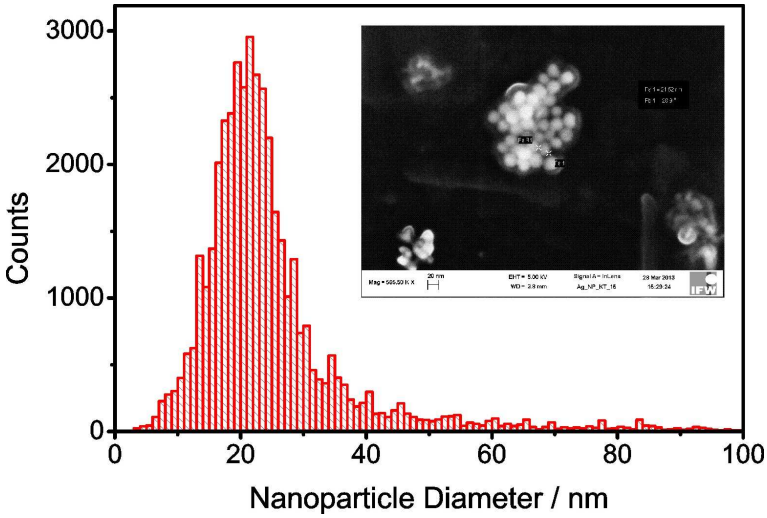


Figure 10.2: Size distribution of silver nanoparticles determined *via* nanoparticle tracking analysis giving a modal nanoparticle size of 22 nm diameter. Sizing was confirmed using SEM imaging (inset).

10.3.1 Nanoparticle Sticking at Unmodified Gold Electrodes

To monitor silver nanoparticle sticking at unmodified gold surfaces, electrodes were submerged in a silver nanoparticle containing sodium citrate solution with a silver nanoparticle concentration of 9.6 pM at OCP for time durations of 3, 4.5, 6, 9, 12, 14 and 15 h, before anodic stripping voltammetry was performed to oxidatively strip off adhered silver nanoparticles. Integration of the area of the silver nanoparticle stripping peaks in figure 10.3 reveals the charge of the oxidation process and therefore the silver nanoparticle coverage on the gold substrate. For nanoparticle adsorption at unmodified gold electrodes there was a general trend for larger stripping peaks at longer sticking times (inset of figure 10.3), although it is likely that an upper limit would be reached at very long times. The variation in the data shown in the inset of figure 10.3 provides the drive to develop superior electrodes as described below. The observed variability in the potential of the silver nanoparticle stripping peak is due to the instability of the platinum quasi-reference electrode used in the electrochemical set-up.

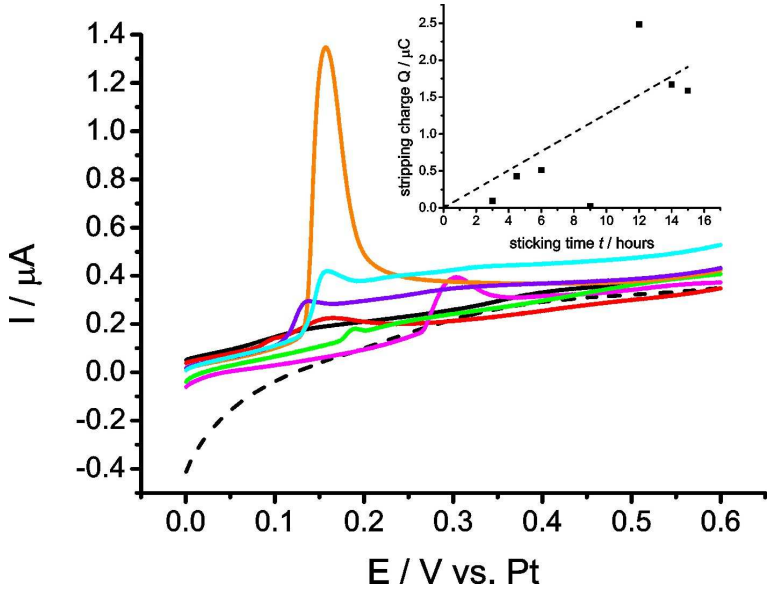


Figure 10.3: Voltammograms for the oxidative stripping of silver nanoparticles that had become adhered to an unmodified gold electrode (r_e=0.5 mm) immersed in a 9.6 pM silver nanoparticle/0.1 M sodium citrate solution for 3 (black), 4.5 (red), 6 (magenta), 9 (green), 12 (orange), 14 (purple) and 15 h (cyan). The black dotted line shows the anodic stripping voltammogram for the blank experiment where a bare gold electrode was scanned to positive potentials in 0.1 M sodium citrate solution. All scans performed at 20 mV s^{-1}. Figure inset shows a plot of the stripping charge for the oxidation of adhered silver nanoparticles as a function of time.

10.3.2 DMSA modification of gold electrode

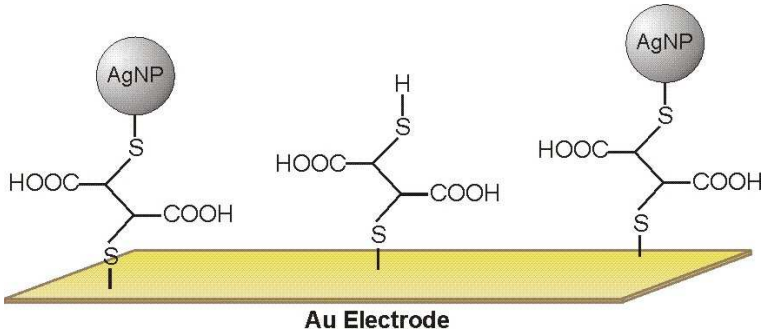


Figure 10.4: Schematic diagram showing silver nanoparticle "sticking" at a DMSA modified gold electrode

A gold electrode was modified *via* the chemisorption of DMSA over a 1 h modification time. We assume one thiol bond is used to link the DMSA to the gold electrode surface and the other to the target nanoparticle, as shown in figure 10.4. In order to verify that DMSA adsorption at the gold electrode occurs within 1 h, cyclic voltammetry was employed to reductively strip the thiol from the gold surface. As can be seen in figure 10.5, a clear reductive peak is observed at -0.72 V *vs.* SCE corresponding to the cleavage of the gold-thiol bond suggesting that a successful modification has been achieved[14]. While the oxidation peak in the reverse scan is caused by oxidative readsorption onto the gold surface[15].

The surface coverage of DMSA on the gold electrode surface can be determined by integrating the area of the reductive stripping peak seen in figure 10.5 to establish the charge, Q, before substituting this value into equation 10.2[16]:

$$\frac{m}{A_e} = \frac{Q}{n.F} \times \frac{1}{A_e} \tag{10.2}$$

where A_e is the geometric area of the working electrode ($7.068 \times 10^{-6} m^2$), n is the number of electrons transferred assumed to be one[12], F is the Faraday constant and m

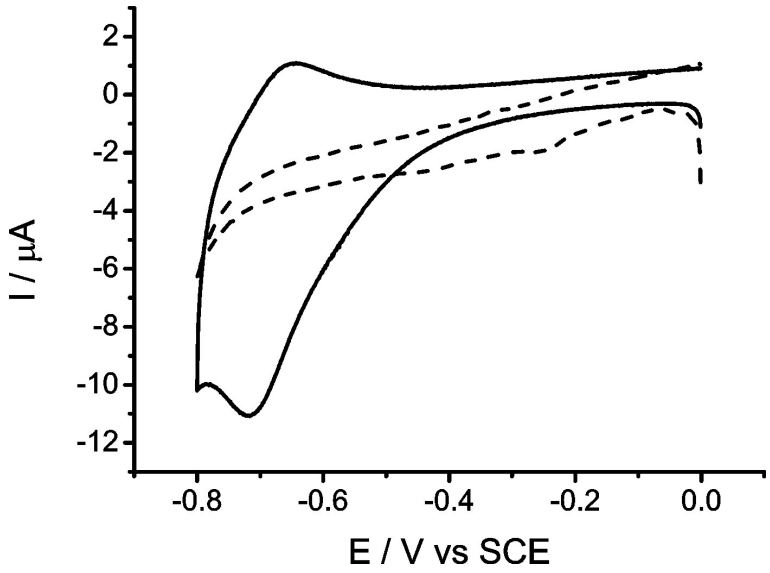


Figure 10.5: Cyclic voltammogram showing the reductive cleavage of the gold-thiol bond in oxygen-free pH 6.8 phosphate buffer after 1 h modification of gold electrode (r_e=1.5 mm) in 5 mM DMSA. The black dotted line shows the cyclic voltammogram for an unmodified gold electrode (r_e=1.5 mm) in pH 6.8 phosphate buffer. All scans performed at 100 mV s^{-1}.

is the number of moles of DMSA. The surface coverage of DMSA after a 1 h modification time was found to be 1.2 × 10^{-9} mol cm^{-2}. From this value it can be approximated that each DMSA molecule is occupying an area of the electrode measuring 0.136 nm^2 suggesting a molecular size of ca. 3.6 Å × 3.6 Å and therefore a probable full monolayer coverage of DMSA on the electrode surface[17].

10.3.3 Nanoparticle Sticking at DMSA Modified Gold Electrodes

After fabrication of DMSA-gold sticky electrodes, nanoparticle sticking experiments were performed as described in section 10.3.1 for 2 min, 5 min, 7 min, 15 min, 30 min, 1 h, 2 h, 3 h, 4 h, 5.5 h, 12 h and 14 h. Figure 10.6 shows the resulting silver nanoparticle stripping peaks, however for clarity not all anodic stripping voltammetry profiles have been included, and a plot of the silver nanoparticle stripping charge as a function of time for all measurements can be seen in the inset of figure 10.6. As opposed to the general in-

crease in silver nanoparticle sticking with increasing time observed at the unmodified gold electrodes, nanoparticle adsorption at the modified electrode surface almost immediately reaches saturation coverage. As with the unmodified gold surface, the variability in the peak potential measured for silver nanoparticle stripping at the DMSA-gold electrode is due to the use of a quasi-reference electrode.

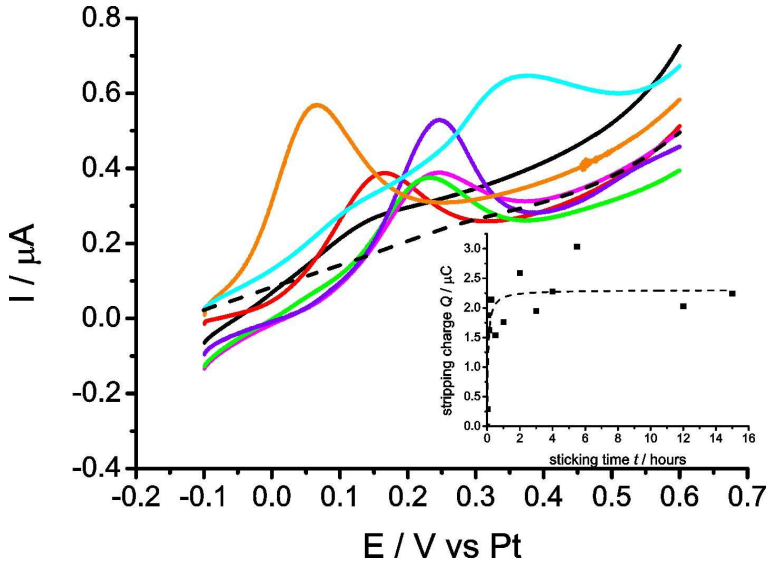


Figure 10.6: Stripping of silver nanoparticles that had adsorbed onto a DMSA modified gold electrode (r_e=0.5 mm) after 2 min (black), 5 min (red), 7 min (magenta), 30 min (green), 2 h (orange) and 15 h (cyan) sticking in a 9.6 pM silver nanoparticle/0.1 M sodium citrate solution. The black dotted line shows the blank experiment where a DMSA modified gold electrode was scanned to positive potentials in 0.1 M sodium citrate solution. All scans performed at 20 mV s^{-1}. Figure inset shows a plot of the stripping charge for the oxidation of adhered silver nanoparticles at the DMSA-modified gold electrode as a function of time.

Assuming a saturation coverage of silver nanoparticles on the electrode surface occurs at a stripping charge of approximately 2.25 µm (Q_s), the average maximum charge in the inset of figure 10.6, the surface coverage (Γ) of nanoparticles on the gold substrate can be established using:

$$\Gamma = \frac{Q_s A_{NP}}{Q_{NP} A_e} \times 100 \tag{10.3}$$

where A_e is the geometric area of the working electrode (7.85×10^{-7} m^2), A_{NP} is the area of a silver nanoparticle with radius 11 nm calculated using πr^2 (3.8×10^{-16} m^2) where the silver nanoparticle size was determined using NTA as shown in figure 10.2, and Q_{NP} is the expected charge for the full oxidation of a single spherical nanoparticle (5.24×10^{-14} C).

For this experiment the nanoparticle saturation coverage (Γ_{max}) at the DMSA modified gold electrode is approximately 2 %. This can be compared to nanoparticle coverage results achieved in similar studies performed previously where the maximum coverage (Γ_{max}) for silver nanoparticle sticking at a cysteine modified disposable carbon electrode in seawater was found to be 0.23 %[3] and levelling off appeared to start occurring when an approximate coverage of 0.17 % for silver nanoparticle sticking at a glassy carbon electrode also modified with cysteine in 0.1 M $NaClO_4$ was reached[2]. The larger coverage achieved in this study suggests DMSA modification of the electrode provides a stickier surface for nanoparticle adhesion as opposed to a cysteine modified surface. However, the coverage values achieved in these systems are still very low, this is most likely due to electrostatic repulsion between nanoparticles that have become stuck onto the electrode surface and incoming nanoparticles, with the negatively charged citrate molecules in solution also contributing to repulsion effects. The carboxylic acid groups of the DMSA molecules on the electrode surface may also repel approaching negatively charged citrate capped silver nanoparticles.

10.3.4 Analysing the Rate of Nanoparticle Sticking

In order to make a more detailed comparison between nanoparticle sticking at unmodified and DMSA-modified gold electrodes to evaluate how nanoparticle adsorption kinetics are

changed when chemical modification of the electrode surface is performed, it was necessary to gain stripping charge data before Γ_{max} is reached for the sticking experiments at the DMSA modified electrode. This was easily achieved by lowering the silver nanoparticle concentration in the sticking solution so it was equal to one third of the original concentration used. In these results a more stable reference electrode was used because, as seen in figures 10.3 and 10.6, the potential of the silver nanoparticle oxidation peak was found to shift considerably when using the quasi-reference platinum electrode and potential stability was found to be particularly poor when thiols were present in the system (figure 10.5).

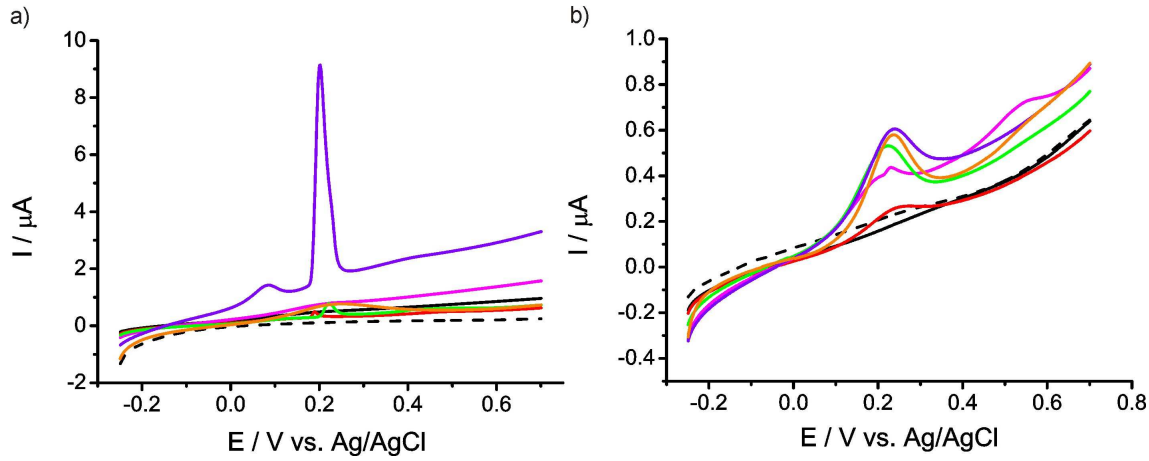


Figure 10.7: (a) Voltammograms for the oxidative stripping of silver nanoparticles in 0.1 M sodium citrate solution that had become adhered to an unmodified gold electrode (r_e=1 mm) that had been immersed in a 3.2 pM silver nanoparticle/0.1 M sodium citrate solution for 3 (black), 6(red), 15 (magenta), 24 (green), 48 (purple) and 96 h (orange). (b) Stripping of silver nanoparticles that had adsorbed onto a DMSA modified gold electrode (r_e=0.5 mm) after 3 (black), 6(red), 15 (magenta), 24 (green), 48 (purple) and 96 h (orange) sticking in a 3.2 pM silver nanoparticle/0.1 M sodium citrate solution. All scans performed at 20 mV s^{-1}. The black dotted lines show the stripping profile for the blank experiments where the unmodified and DMSA modified gold electrodes were scanned to positive potentials in 0.1 M sodium citrate solution.

As before, the DMSA-modified and unmodified gold electrodes were immersed in the sticking solution but this time the concentration of silver nanoparticles in solution was 3.2 pM. Sticking experiments under OCP at various time intervals were carried out (figure

10.7) and figure 10.8a shows the linear relationship that was observed for silver nanoparticle adsorption at both the DMSA-modified (red squares) and unmodified (black squares) electrodes. As expected, the DMSA-gold electrode exhibited much better sticking capabilities in comparison to the unmodified gold surface. At longer times beyond 24 h, the stripping charge for the oxidation of silver nanoparticles on the electrode surface levelled off at approximately 2.0 µC (figure 10.8b). This value corresponds to a saturation coverage of 1.9 % (calculated using equation 10.3). The almost identical saturation coverage values achieved for both silver nanoparticle concentrations tested confirms the reliability of silver nanoparticle sticking experiments at DMSA modified gold electrodes. For silver nanoparticle adhesion at the unmodified electrode, the linear relationship observed up until 24 h did not continue and variable values for the stripping charge at 48 h and 96 h were gained (Q_{48h}=12.0 µC,Q_{96h}=6.4 µC) however, this was not unexpected as silver nanoparticle sticking at an unmodified glassy carbon substrate was also found to be irreproducible[2], this is probably due to co-adsorption of impurities in the solvent.

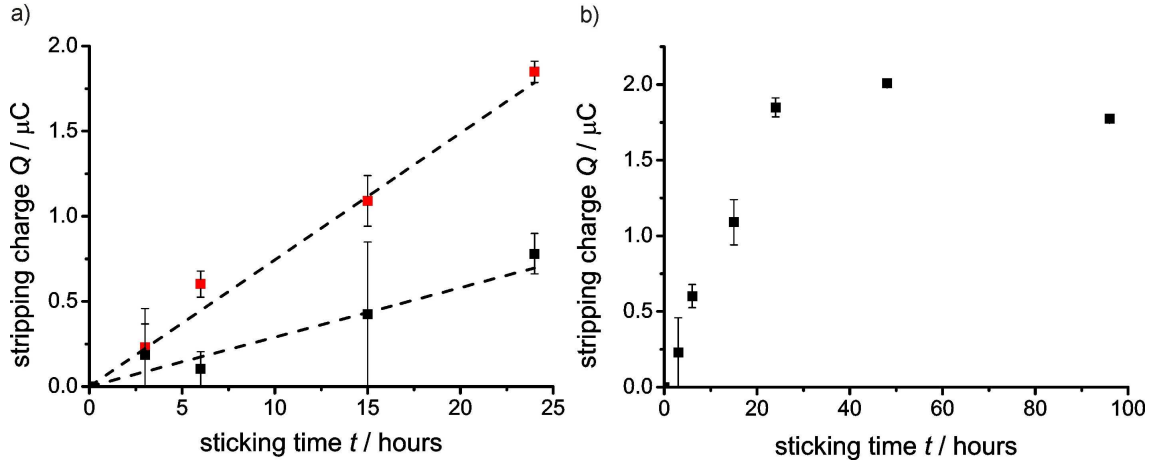


Figure 10.8: (a) Charge of stripping peaks observed as a function of sticking time (¡24 h) at an unmodified (black squares) and DMSA-modified (red squares) gold electrode (r_e=0.5 mm) that had been immersed and then stripped in 3.2 pM silver nanoparticle/0.1 M sodium citrate solution (b) stripping charge at a DMSA-modified gold electrode (r_e=0.5 mm) that had been immersed and then stripped in 3.2 pM/0.1 M sodium citrate solution including longer sticking times of 48 and 96 h.

The stripping charge data can be reinterpreted in terms of percentage coverage to extract kinetic information regarding nanoparticle sticking rates. If it is assumed that the irreversible uptake of nanoparticles from solution onto the substrate is occurring equation 10.4 can be used to describe the system:

$$\Gamma_{\mathrm{t}}=\Gamma_{\max}[1-exp(-kt)] \tag{10.4}$$

where at short times:

$$\Gamma_{\mathrm{t}}=\Gamma_{\max}kt \tag{10.5}$$

Thereby, plotting surface coverage Γ *vs.* time (figure 10.9) for silver nanoparticle sticking experiments at both an unmodified and DMSA-modified gold electrode, it is possible to extract values for the kinetic adsorption constants (k) assuming a $\Gamma_{\max}$ value of 1.9 %(determined from the maximum stripping charge value observed in figure 10.8b, Q_s=2.01 µC).

For silver nanoparticle sticking at a DMSA-modified gold electrode the adsorption rate constant (k_{mod}) was found to be $0.037\,\mathrm{h}^{-1}$, more than double the rate of silver nanoparticle adhesion at the bare gold electrode surface ($k_{\mathrm{unmod}} = 0.015\,\mathrm{h}^{-1}$), demonstrating the extent to which modifying a gold electrode with thiol groups using DMSA can increase the silver nanopartcle sticking at the substrate.

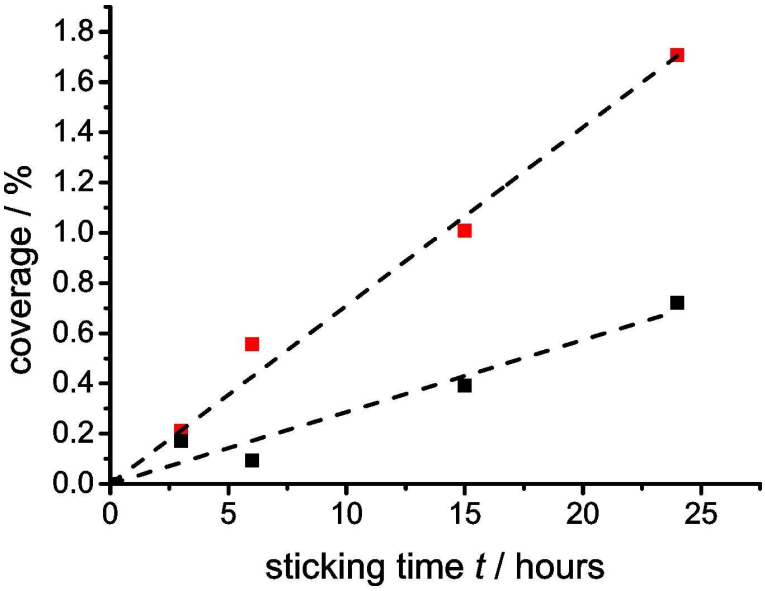


Figure 10.9: Percentage coverage of nanoparticles on electrode surface as a function of sticking time for sticking times <24 h at a DMSA modified gold electrode (red squares) and a bare gold electrode (r_e=0.5 mm)(black squares).

10.4 Conclusions

In this chapter, the kinetics of silver nanoparticle sticking at a DMSA modified "sticky" gold electrode surface and an unmodified gold electrode have been investigated. A comparison of the rate adsorption constants measured for nanoparticle sticking at the surfaces of unmodified and DMSA modified gold electrodes revealed increased nanoparticle sticking rates at the modified substrate demonstrating that chemical modification of the electrode is advantageous for silver nanoparticle immobilisation at a gold surface.

Bibliography

[1] E. J. E. Stuart, K. Tschulik, J. Ellison and R. G. Compton, *Electroanalysis* **26** (2014) 285–291.

[2] K. Tschulik, R. G. Palgrave, C. Batchelor-McAuley and R. G. Compton, *Nanotechnology* **24** (2013) 295502.

[3] W. Cheng, E. J. . E. Stuart, K. Tschulik and R. G. Compton, *Nanotechnology* **24** (2013) 505501.

[4] X. Wei, W. Tong, V. Fidler and M. B. Zimmt, *J. Colloid Interface Sci.* **387** (2012) 221–227.

[5] D. R. Reyes, G. I. Mijares, B. Nablo, K. A. Briggman and M. Gaitan, *Appl. Surf. Sci.* **257** (2011) 8373–8377.

[6] O. S. Ivanova and F. P. Zamborini, *J. Am. Chem. Soc.* **132** (2009) 70–72.

[7] L. Mei Niu, H. Qun Luo and N. Bing Li, *Instrum. Sci. Technol.* **35** (2007) 59–73.

[8] H. Li, X. Gui, L. Zhang, S. Wang, C. Ji, J. Wei, K. Wang, H. Zhu, D. Wu and A. Cao, *Chem. Comm.* **46** (2010) 7966–7968.

[9] A. Mohadesi and M. A. Taher, *Talanta* **72** (2007) 95–100.

[10] P. D. Ding, L. M. Niu, H. Q. Luo and N. B. Li, *Croat. Chem. Acta* **80** (2007) 61–66.

[11] N. Bing Li, L. Mei Niu and H. Qun Luo, *Microchim. Acta* **153** (2006) 37–44.

[12] L. M. Fischer, M. Tenje, A. R. Heiskanen, N. Masuda, J. Castillo, A. Bentien, J. mneus, M. H. Jakobsen and A. Boisen, *Microelectron. Eng.* **86** (2009) 1282–1285.

[13] A. D. McNaughty and A. Wilkinson, *IUPAC. Compendium of Chemical Terminology (the "Gold Book")* (Blackwells, Oxford), second edition.

[14] J. Mason, C. Batchelor-McAuley and R. G. Compton, *Phys. Chem. Chem. Phys.* **15** (2013) 8362–8366.

[15] G. Hager and A. G. Brolo, *J. Electroanal. Chem.* **550** (2003) 291–301.

[16] S. Ernst, L. Aldous and R. G. Compton, *Chem. Phys. Lett.* **511** (2011) 461–465.

[17] Y. Wu, M. Song, Z. Xin, X. Zhang, Y. Zhang, C. Wang, S. Li and N. Gu, *Nanotechnology* **22** (2011) 225703.

Chapter 11

Electrochemical Observation of Single Collision Events: Fullerene Nanoparticles

The previous chapters of this thesis have dealt with the characterisation of metallic nanoparticles in aqueous solution. In this chapter a type of non-metallic nanoparticle, fullerene nanoparticles, are detected and sized in a non-aqueous solvent *via* cathodic particle coulometry where the direct, quantitative reduction of single nanoparticles is achieved upon collision with a potentiostatted gold electrode. This is the first time that the nanoparticle-impact technique has been shown to work in a non-aqueous electrolyte and utilised to coulometrically size carbonaceous nanoparticles. Contrast is drawn between single nanoparticle electrochemistry and that seen using nanoparticle ensembles *via* modified electrodes.

This work has been published in *ACS Nano*[1] and was performed in collaboration with Dr. Kristina Tschulik and Dr. Christopher Batchelor-McAuley who helped with the interpretation of experimental results. Dr. Kristina Tschulik also carried out the SEM imaging that is included in this chapter with the help of Dr. Kerstin Hennig at IFW, Dresden, Germany.

11.1 Introduction

Electrochemical techniques have been invaluable in the investigation of fullerene molecules with the most studied being buckminsterfullerene, C_{60}[2]. C_{60} has been found to undergo both oxidation and reduction[3]. Up to six successive one electron reductions of C_{60} in solution have been reported under certain conditions[4]. While the electrochemistry of C_{60} molecules, C_{60} molecular films and other colloidal carbon-based materials[5] have been studied in detail the electrochemical properties of C_{60} nanoparticles, or nano-C_{60}, remains unexplored[6, 7]. The nanoparticulate form of C_{60} has gained increasing attention due to the spontaneous aggregation of C_{60} molecules in environmental waters to form nano-C_{60}[8]. Significant environmental exposure to C_{60} and thus nano-C_{60} formation is likely given the mass production of C_{60} for manifold applications ranging from cosmetics[9] to photovoltaics[10] while C_{60} has also been found to occur naturally in the environment[11, 12]. Reports that nano-C_{60} is bactericidal[13] and toxic to human cell lines[14] have resulted in a need to monitor these carbonaceous nanoparticles.

A method to detect individual nanoparticles has been developed where an electrocatalytic reaction occurs exclusively on nanoparticles in contact with an inert electrode surface thereby resulting in an amplification of the current response upon a nanoparticle-electrode collision[15–20]. Chapter 8 demonstrated how this indirect technique can be used to study silver nanoparticle collisions *via* the reduction of hydrogen peroxide on the nanoparticle surface. The detection of single walled carbon nanotubes (SWCNTs) has also been achieved using this non-coulometric nanoparticle-impact technique *via* investigation of increasing electrode area and therefore amplified currents for ferrocenemethanol oxidation upon SWCNT collision[21]. One drawback of this electrocatalytic amplification

method for nanoparticle detection is that the types of nanoparticle and electrode materials that can be studied are limited as the electrode needs to be inert while the nanoparticle needs to catalyse the redox reaction of interest.

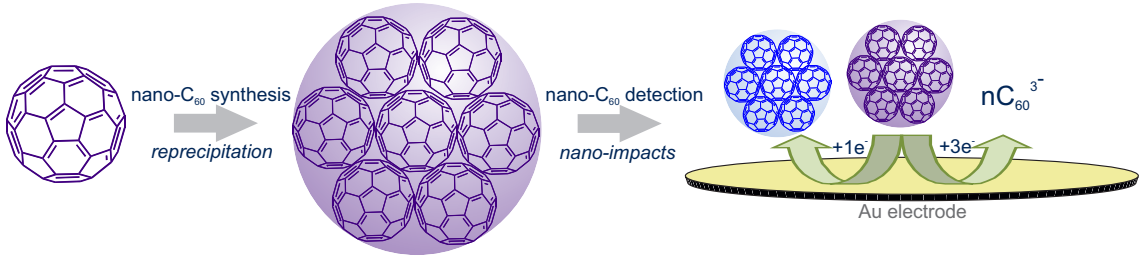


Figure 11.1: Schematic diagram for the synthesis and electrochemical detection of impacting nano-C_{60} particles at a gold microelectrode where nano-C_{60} is reduced upon collision *via* the transfer of one (represented by the colour change from purple to blue) or three electrons resulting in dissolution of the generated C_{60}^{3-} anions.

Particle coulometry is an alternate technique to detect individual nanoparticles that is not limited by nanoparticle and electrode materials[22]. In this thesis it has been demonstrated that anodic particle coulometry can be used to detect metallic nanoparticles in aqueous solution *via* their direct oxidation during stochastic collision events at a potentiostatted electrode. This technique has been further adapted to study systems where the nanoparticles are reduced upon contact with an electrode and termed cathodic particle coulometry. Cathodic particle coulometry has previosuly been used to size both metal oxide[23] and organic nanoparticles[24]. In the work reported in this chapter the cathodic particle coulometry method not only provides an analytical methodology but it also allows direct investigation of the morphology dependency of the redox properties of the C_{60}.

This chapter demonstrates that cathodic particle coulometry can be used to electrochemically size individual nano-C_{60} particles impacting upon a gold electrode. It is shown for the first time that this coulometric nanoparticle sizing technique can be employed not

only for the detection of carbonaceous nanoparticles but also in non-aqueous conditions. The morphological influence of transitioning from a molecular microcrystal-ensemble to a nanoparticle-ensemble to isolated nanoparticles on the electrochemical response of C_{60} is also investigated and contrasts drawn between single nanoparticle and nanoparticle ensemble studies.

11.2 Experimental Procedure

11.2.1 Nano-C_{60} Particle Synthesis

The experimental method used to synthesise nano-C_{60} particles is described in section 3.2.2.

11.2.2 Dynamic Light Scattering

DLS measurements were performed as detailed in section 3.4.1.

11.2.3 Scanning Electron Microscopy

SEM imaging was performed by Dr. Kerstin Hennig and Dr. Kristina Tschulik at IFW, Dresden, Germany. Section 3.4.3 describes the experimental set-up used for imaging.

11.2.4 Electrode Modification

Modification of the gold macroelectrode was performed by drop casting 4×5 µL layers of C_{60} solution/nano-C_{60} suspension before drying at 35 ± 0.2 °C. To prepare a solution of 0.15 mM C_{60} in CH_2Cl_2, the solution was stirred in the dark for 24 hours. Due to the low

surface tension of the solvents used solution run off onto the insulator surrounding the electrode surface could not be prevented and therefore quantification of the amount of C_{60} immobilised on the electrode was not possible.

11.2.5 Cyclic Voltammetry

Cyclic voltammetry was employed to study the micro- and nano-C_{60} ensembles using the experimental set-up outlined in 3.3.2. The three electrodes used were a macro-gold working electrode (r_e=0.8 mm), a silver wire pseudo-reference electrode and a graphite rod counter electrode. All measurements were performed at 25 ± 0.2 °C in 0.1 M NBu_4PF_6 at a scan rate of 100 mV s^{-1}. Ferrocene (2 mM) was added to the electrolyte solution to act as an internal redox marker for voltammetric measurements. An oxygen-free environment was maintained throughout the experiment by purging with nitrogen.

The working electrode was polished with alumina power (1.0, 0.3 and 0.01 µm) and then sonicated in water for 1 min prior to each experiment. All glassware was oven-dried post-cleaning to remove any traces of water. The nitrogen flow used to degas solutions was purged with acetonitrile that had been dried with molecular sieves to ensure no water was introduced to the system.

11.2.6 Cathodic Particle Coulometry

Cathodic particle coulometry was performed as described in section 3.3.4. The electrodes used were the same as in section 11.2.5 however a micro-gold electrode (r_e=4.2 µm) was employed as the working electrode. Experiments were performed in an oxygen-free solution of 0.1 M NBu_4PF_6 at a scan rate of 100 mV s^{-1}. A temperature of 25 ± 2 °C was maintained throughout the experiments. As described in section 11.2.5 care was taken to

ensure no water was introduced to the system. SignalCounter was employed to analyse the observed impact spikes.

11.3 Results and Discussion

11.3.1 Characterisation of nano-C_{60} Particles

Nano-C_{60} particles were synthesised *via* the reprecipitation method[25] and DLS was used to gain a size distribution for the nanoparticle radius which had a maximum at 16 nm(figure 11.2), a size that was confirmed with SEM (r_{NP}=19±4 nm).

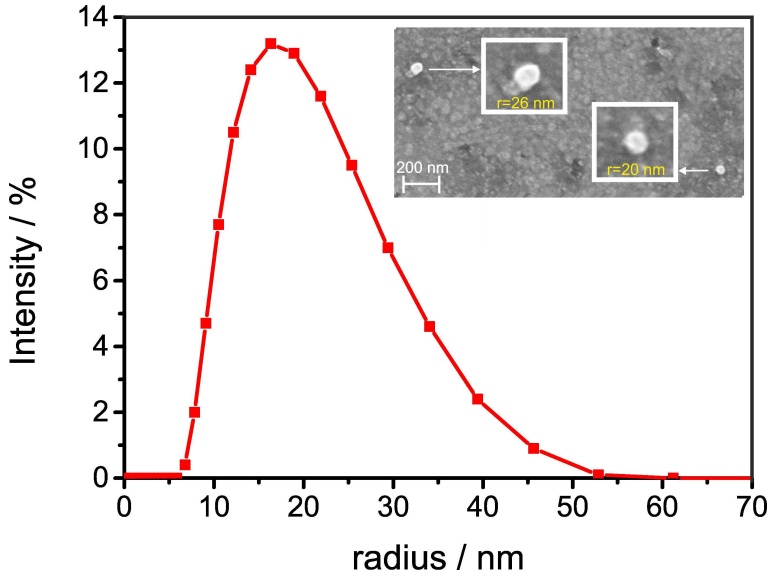


Figure 11.2: Size distribution for the synthesised stock suspension of nano-C_{60} particles measured *via* DLS and SEM image (shown inset) of the same nano-C_{60} stock suspension.

11.3.2 Cyclic Voltammetry of Molecular C_{60}

The electrochemistry of molecular C_{60} was investigated prior to the electrochemical characterisation of the synthesised nano-C_{60} particles. This approach was chosen as the electrochemical response of molecular C_{60} films has been previously explored in the

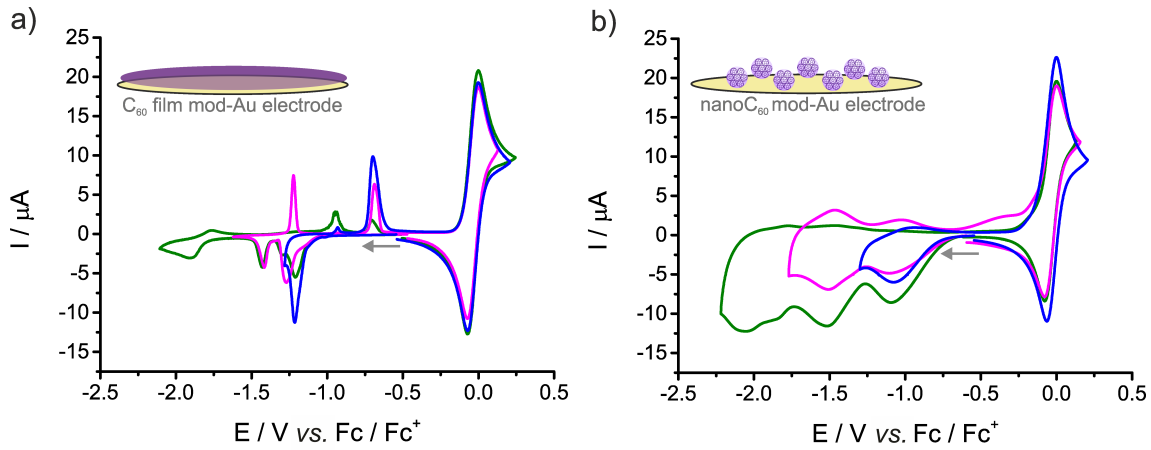


Figure 11.3: Voltammetric profiles for a gold macroelectrode (r_e=0.8 mm) modified with a) 20 µL solution of 0.15 mM C_{60} in CH_2Cl_2 and b) 20 µL suspension of 0.1 mM nano-C_{60} particles in 10% NMP:90% MeCN to observe the one (blue line), two (pink line) and three (green line) electron reductions of the C_{60} ensembles. All measurements were performed in MeCN (2 mM $Fe(C_5H_5)_2$, 0.1 M NBu_4PF_6) at a scan rate of 100 mV s^{-1}. The redox couple observed at ~0 V is Fc/Fc^+. Arrows represent scan direction.

literature[26–28]. Therefore the voltammetry of these well-studied molecular C_{60} films provides a useful comparison for the electrochemistry of the synthesised nanoparticulate nano-C_{60}. Figure 11.3a shows the voltammetric response of a molecular C_{60} film in 0.1 M NBu_4PF_6/MeCN where a gold electrode has been modified with 0.15 mM C_{60} in CH_2Cl_2 as in the work of Tan et al.[26]. Molecular C_{60} microcrystals form on the electrode surface upon evaporation of the solvent[26]. Ferrocene (2 mM) was added as an internal redox marker for voltammetric experiments and all potentials are referenced to the ferrocene/ferrocenium redox couple (Fc/Fc^+). Cathodic waves were observed for the first three electron reductions of the molecular C_{60} microcrystals at −1.21 V, −1.43 V and −1.90 V *vs.* Fc/Fc^+. The large potential separation between the cathodic and corresponding anodic peaks observed for the molecular C_{60} microcrystal ensemble has been explained by structural reorganisation on the electrode surface to accommodate cation insertion[27, 28]. As reported by Jehoulet et al., scanning the potential over the third reduction resulted in the first and second re-oxidation waves being significantly altered.[28]

This observed change suggests that C_{60}^{3-} is soluble and hence dissolution of the C_{60} microcrystals occurs after the third electron transfer[28, 29]. Dissolution of the third reduction product of the molecular C_{60} microcrystals was confirmed by holding the potential past the third reduction wave for 20 s and then scanning backwards revealing the loss of all re-oxidation peaks (figure 11.4a).

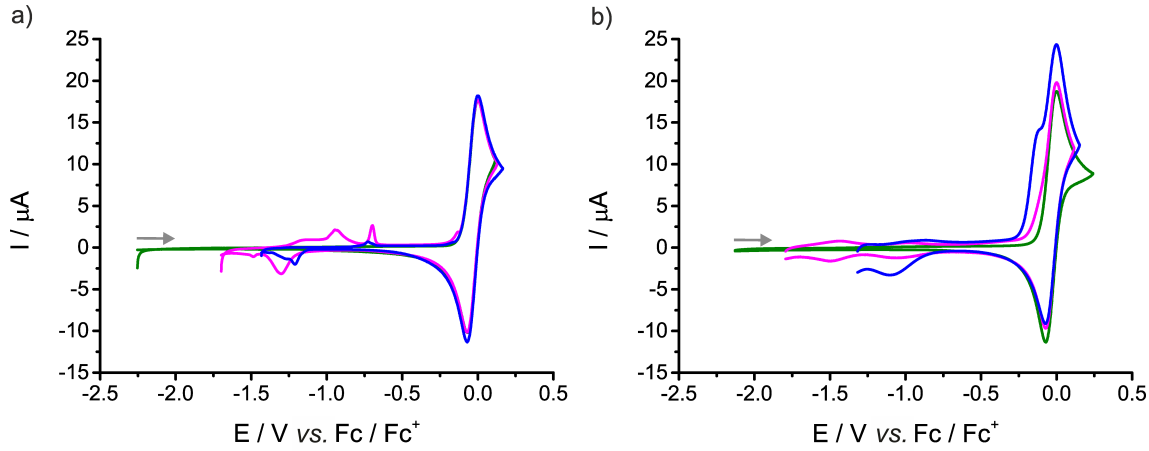


Figure 11.4: Voltammetric profiles in 2 mM Fc/0.1 M NBu_4PF_6/MeCN for a gold macroelectrode (r_e=0.8 mm) modified with (a) 20 µL 0.15 mM C_{60} in CH_2Cl_2 measured post 20 s chronoamperomograms where the potential applied was −1.43 V (blue), −1.70 V (pink) and −2.25 V (green) *vs.* Fc/Fc^+ (b) modified with 20 µL 0.1 mM nano-C_{60} particles in 10% NMP:90% MeCN measured post 20 s chronoamperomograms where the potential applied was −1.32 V (blue), −1.80 V (pink) and −2.14 V (green) *vs.* Fc/Fc^+. All measurements were performed at a scan rate of 100 mV s^{-1}. The arrow infers the direction of scanning.

11.3.3 Cyclic Voltammetry of nano-C_{60} Particles

Having observed the same voltammetric response for a C_{60} microcrystal film as reported in the literature[26], electrochemical characterisation was performed on an ensemble of the nano-C_{60} particles sized in figure 11.2. A gold electrode was modified by dropcasting of the nano-C_{60} stock suspension (nano-C_{60} as-synthesised in the absence of electrolyte) and cyclic voltammetry was performed in 2 mM Fc/0.1 M NBu_4PF_6/MeCN (figure 11.3b). Three reduction waves were observed at −1.09 V, −1.51 V and −2.06 V *vs.* Fc/Fc^+. The

redox response was found to be markedly different from that of the molecular C_{60} microcrystal film. In contrast to the large separation between cathodic and anodic peaks for the C_{60} microcrystal ensemble, the nano-C_{60} modified electrode exhibited a much smaller peak to peak splitting reflecting voltammetry reported for molecular C_{60}[4] and C_{60} Langmuir-Blodgett Films[28]. This difference in electrochemical response demonstrates that a change in the morphology of C_{60} on the electrode surface markedly affects electron transfer. The only similarity between the responses at the microcrystal and nano-C_{60} ensembles is that the third electron reduction of nano-C_{60} is also irreversible as evidenced by the absence of oxidative features in the reverse scan. The dissolution of nano-C_{60} on the third electron reduction was confirmed *via* the same potential holding method used for the microcrystal ensemble study above (figure 11.4b). A scan rate study of the three electron reduction of nano-C_{60} (figure 11.5) demonstrated that it is the dissolution of the generated C_{60}^{3-} anions as opposed to the electron transfer that is the irreversible step in this third electron reduction as the proportion of material being reoxidised back onto the electrode surface following the transfer of three electrons increases with increasing scan rate.

11.3.4 Detection of nano-C_{60} Particles *via* Cathodic Particle Coulometry

Having investigated the change in C_{60} electrochemistry when transitioning from a molecular C_{60} microcrystal ensemble to a nanoparticulate nano-C_{60} ensemble, cathodic particle coulometry was subsequently employed to study the electrochemistry of nano-C_{60} nanoparticles at the single nanoparticle scale. Cathodic particle coulometry detects and

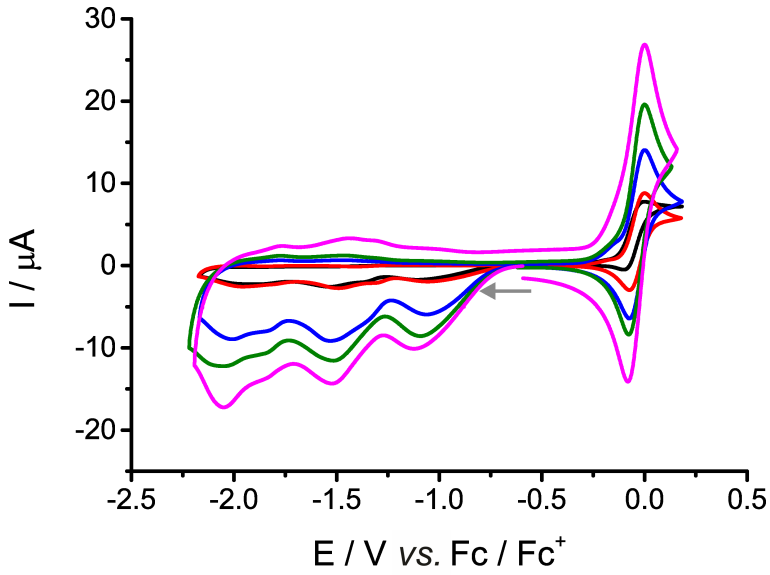


Figure 11.5: Voltammetric profiles for a gold macroelectrode (r_e=0.8 mm) modified with (a) 20 µL 0.1 mM nano-C_{60} particles measured in 2 mM Fc/0.1 M NBu_4PF_6/MeCN at a scan rate of 10 (black), 20 (red), 50 (blue), 100 (green) and 200 mV s^{-1} (pink). The arrow infers the scanning direction.

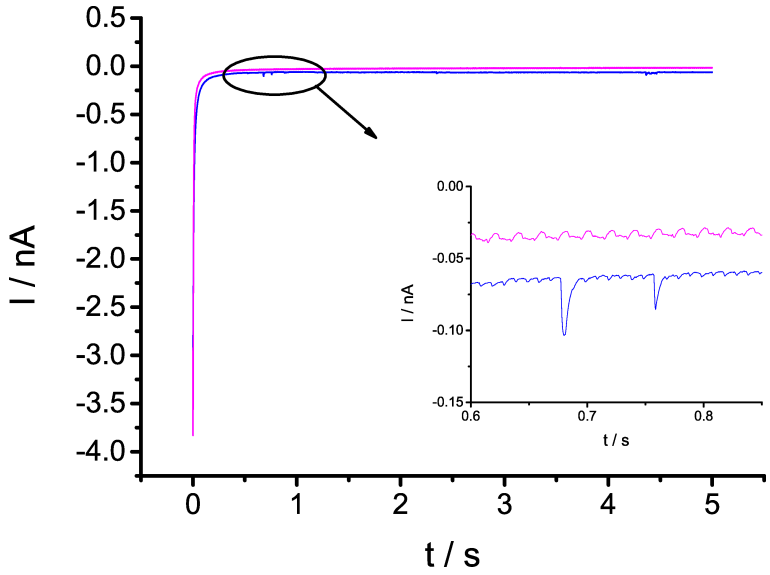


Figure 11.6: 5 s chronoamperogram for a gold microelectrode (r=4.2 µm) immersed in a 0.1 M NBu_4PF_6/MeCN solution containing 116 pM nano-C_{60} particles measured at E=−1.27 V *vs.* Fc/Fc^+ (blue line) and E=−0.655 V *vs.* Fc/Fc^+ (pink line).

sizes individual particles in solution. An aliquot of nano-C_{60} was added to a thoroughly degassed solution of 0.1 M NBu_4PF_6 in MeCN resulting in a nano-C_{60} concentration of 116 pM before a gold microelectrode (r_e=4.2 µm) suspended in solution was potentiostatted to −1.27 V *vs.* Fc/Fc^+. This chosen potential corresponds to the one electron reduction of nano-C_{60} as inferred from figure 11.3. The reductive spikes that were observed in the 5 s chronoamperometric scans measured post addition of nano-C_{60} particles are shown in figure 11.6 (blue line). Note that no impact spikes were observed in solutions pre addition of nano-C_{60}. Each of the reductive spikes observed results from the charge transfer upon a collision between nano-C_{60}, moving *via* Brownian motion in solution, and the gold microelectrode. Increasing the electrode potential to one at which the reduction of nano-C_{60} does not occur (−0.655 V *vs.* Fc/Fc^+) caused the observed spikes to disappear (figure 11.6, pink line).

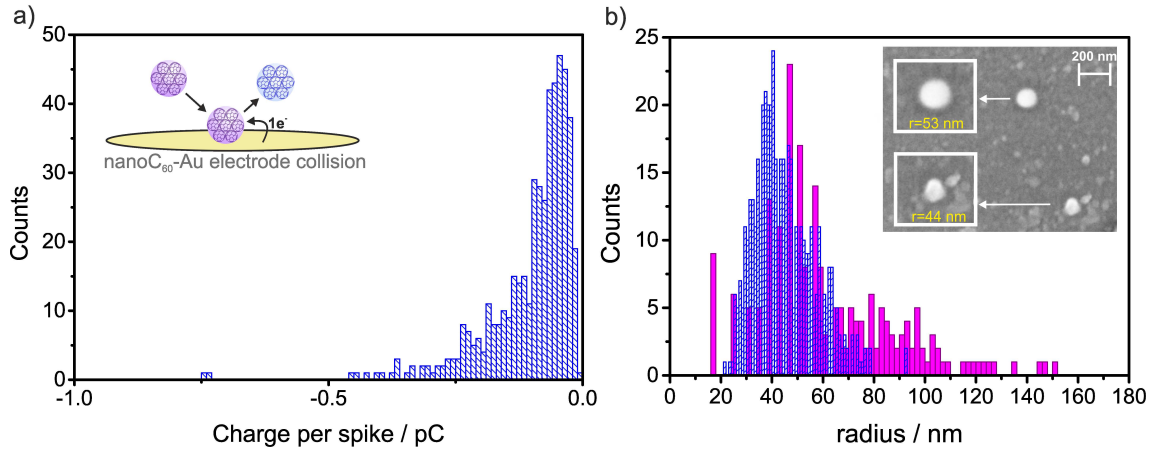


Figure 11.7: a) Charge distribution with a bin size of 0.01 pC for the one electron reduction of nano-C_{60} (116 pM) impacting a gold microelectrode (r_e=4.2 µm) in MeCN (0.1 M NBu_4PF_6) b) Size distribution with a bin size of 1 nm for the one electron reduction of nano-C_{60} (116 pM) impacting a gold electrode (r_e=4.2 µm) in MeCN (0.1 M NBu_4PF_6) (blue) overlaid with the size distribution determined by SEM imaging of nano-C_{60} particles dispersed in 0.1 M NBu_4PF_6/MeCN (pink, bin size=2 nm) and SEM image shown inset.

A total of 481 impact spikes were recorded for the one electron reduction of impacting

nano-C_{60} (E=−1.27 V *vs.* Fc/Fc^+) and the area under each current-time spike was integrated to give the charge for the reduction of each impacting nanoparticle. The charge distribution for the impact events recorded where one electron is exchanged is shown in figure 11.7a and the mean charge of the spikes observed was -0.102 ± 0.004 pC (where the error of the mean charge is the standard error of the mean given by $(S.D.)/(\sqrt{n_s})$ where $S.D.$ is the standard deviation and n_s is the sample number, in this case the number of spikes). If the whole nanoparticle is reduced upon impact and a spherical particle shape is assumed the Faradaic charge measured for the observed nanoparticle-electrode collisions can be reinterpreted to determine the radius of each impacting nanoparticle *via* equation 11.1:

$$r_{NP}=\sqrt[3]{\frac{3MQ}{4Fn\pi\rho}} \tag{11.1}$$

where M is the molar mass of C_{60} in kg mol^{-1}, Q is the charge measured in coulombs (C), F is the Faraday constant in C mol^{-1}, n is the number of electrons transferred and ρ is the density of C_{60} measured in kg m^{-3}.

The nanoparticle size distribution determined using equation 11.1 is shown in figure 11.7b (blue) and the mean radius was 45 ± 12 nm (where the error is given by the $S.D.$), significantly larger than the size of nano-C_{60} in the synthesised stock nanoparticle suspension measured using DLS and SEM (r_{NP} ≈20 nm). It is well known that nano-C_{60} particles are prone to aggregation upon the addition of salt,[8, 30] therefore we suggest that the larger nanoparticle size determined from the cathodic particle coulometry experiment is due to the aggregation of nano-C_{60} particles when dispersed in a 0.1 M NBu_4PF_6/MeCN solution. A size distribution of nano-C_{60} in the presence of the electrolyte could not

be measured *via* DLS as the aggregating particles resulted in a very high polydispersity within the sample. SEM analysis of nano-C_{60} particles in 0.1 M NBu_4PF_6/MeCN was performed to determine if the nanoparticles aggregate in the presence of the electrolyte used for the cathodic particle coulometry experiments. The measurements were carried out by dropcasting a sample of the nano-C_{60} particles suspended in electrolyte on a SEM sample holder that had been modified with a transmission electron microscopy grid in order to minimise nanoparticle aggregation during sample preparation. SEM analysis showed that nanoparticle size increased upon nano-C_{60} dispersion in NBu_4PF_6/MeCN and relatively good agreement was found between the nano-C_{60} size distributions measured *via* SEM and cathodic particle coulometry in the presence of electrolyte (figure 11.7b). There is an increased occurrence of larger particles ($r_{NP} \approx$ 80-150 nm) in the SEM determined nanoparticle size distribution which could be due to the aggregation of nano-C_{60} during preparation of the SEM sample despite steps having been taken to minimise this effect. Another possible explanation for the discrepancy between the cathodic particle coulometry and SEM determined size distributions is that slower diffusion coefficients of larger nanoparticles will result in a reduced collision probability during impact experiments and therefore larger nanoparticles are less likely to be measured *via* particle coulometry; this phenomenon has been investigated using silver nanoparticles by Lees at al.[31]

The accurate sizing of nano-C_{60} from impact events observed when the electrode is held at the potential for a one electron reduction, as determined from the voltammetric response of the nano-C_{60} ensemble (figure 11.3b), demonstrates that there is no change in the potential at which this first electron transfer occurs when changing from a nanoparticle ensemble to individual nanoparticles. In contrast changes are observed for the third electron reduction of nano-C_{60} when the electrochemical response of the nanoparticle

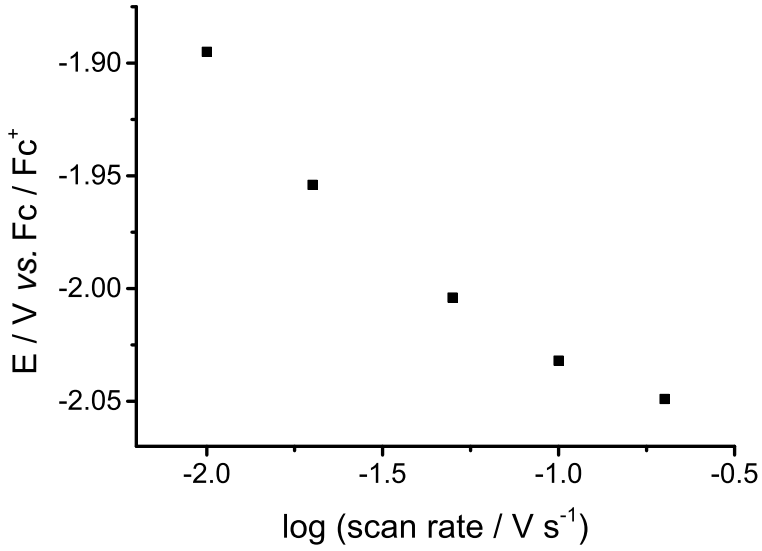


Figure 11.8: Plot of potential for the third electron reduction peak of nano-C_{60} against log(scan rate) for a 20 µL nano-C_{60} modified gold macroelectrode (r_e=0.8 mm) in a solution of 2 mM $Fe(C_5H_5)_2$, 0.1 M NBu_4PF_6 in MeCN. Voltammograms are shown in Figure 11.5.

ensemble is compared to single collision events. It is known that peak potentials can shift by up to hundreds of millivolts when the voltammetry of a nanoparticle ensemble with strongly overlapping nanoparticle diffusion layers is compared to a case where the nanoparticles are isolated and therefore diffusionally independent[32]. The voltammetric response shown in Figure 11.3b for the nanoparticle ensemble, where the nanoparticle diffusion layers will be overlapping, demonstrates that the second electron reduction of nano-C_{60} is a reversible process whilst the third cathodic wave observed is irreversible and results in the formation of the soluble C_{60}^{3-} product that will diffuse away from the electrode[28, 29]. For single collision events, a shift in potential occurs only for the irreversible third electron transfer as the ease of nano-C_{60} dissolution at the isolated nanoparticle scale lowers the potential required for the third electron reduction and results from the strong divergent diffusion of products away from individual nanoparticles as compared to the semi-infinite, planar diffusion seen for high coverage layers on electrode surfaces. Figure 11.8 demonstrates that as the scan rate for nano-C_{60} ensemble studies is

decreased, the third electron reduction of C_{60} becomes more favourable and is observed at increasingly positive potentials (voltammograms are shown in figure 11.5).

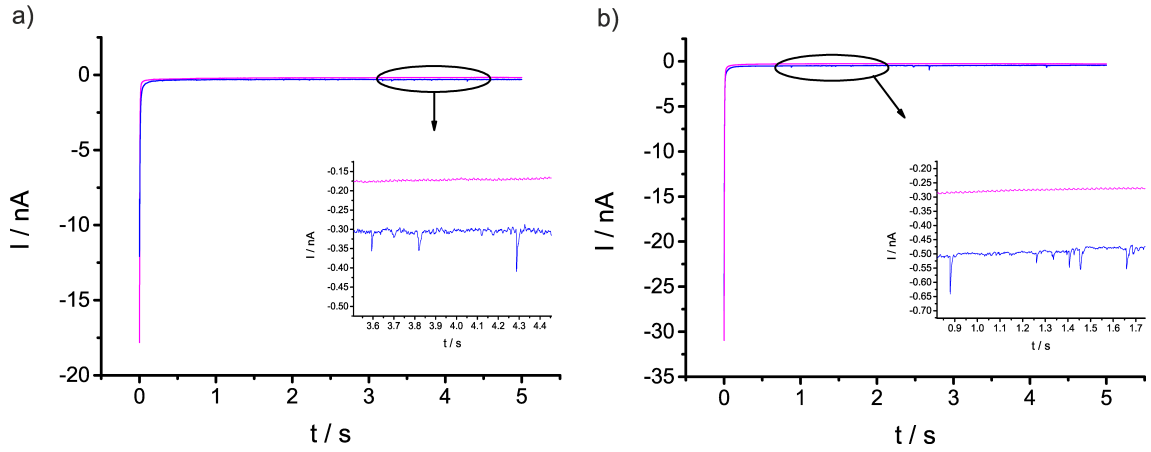


Figure 11.9: 5 s chronoamperograms measured at a) E=−1.74 V *vs.* Fc/Fc^+ and b)E=−2.22 V *vs.* Fc/Fc^+ for a gold microelectrode (r_e=4.2 µm) immersed in 0.1 M NBu_4PF_6/MeCN solution with (blue line) and without (pink line) 116 pM nano-C_{60} nanoparticles.

Cathodic particle coulometry experiments performed at potentials corresponding nominally to the second (E=−1.74 V *vs.* Fc/Fc^+) and third (E=−2.22 V *vs.* Fc/Fc^+) electron transfers as inferred from the ensemble studies (figure 11.3b) show a shift in potential at the single nanoparticle scale. Scans showing the impact spikes observed at each of these potentials can be seen in figure 11.9 and the resulting charge and radius distributions are shown in figure 11.10. For impact events measured at the former potential the mean charge was -0.360 ± 0.016 pC, this charge transfer is identical to the mean charge for current-time spikes observed for C_{60} particles undergoing a three electron reduction upon collision (-0.360 ± 0.015 pC). This similarity in charge suggests that a three electron reduction is observed for impacting nanoparticles held at the potentials where the nanoparticle ensemble shows a two and three electron reduction of nano-C_{60} should be occurring. This change in redox behaviour is due to the study of isolated nanoparticles *via* particle coulometry as opposed to a nanoparticle ensemble.

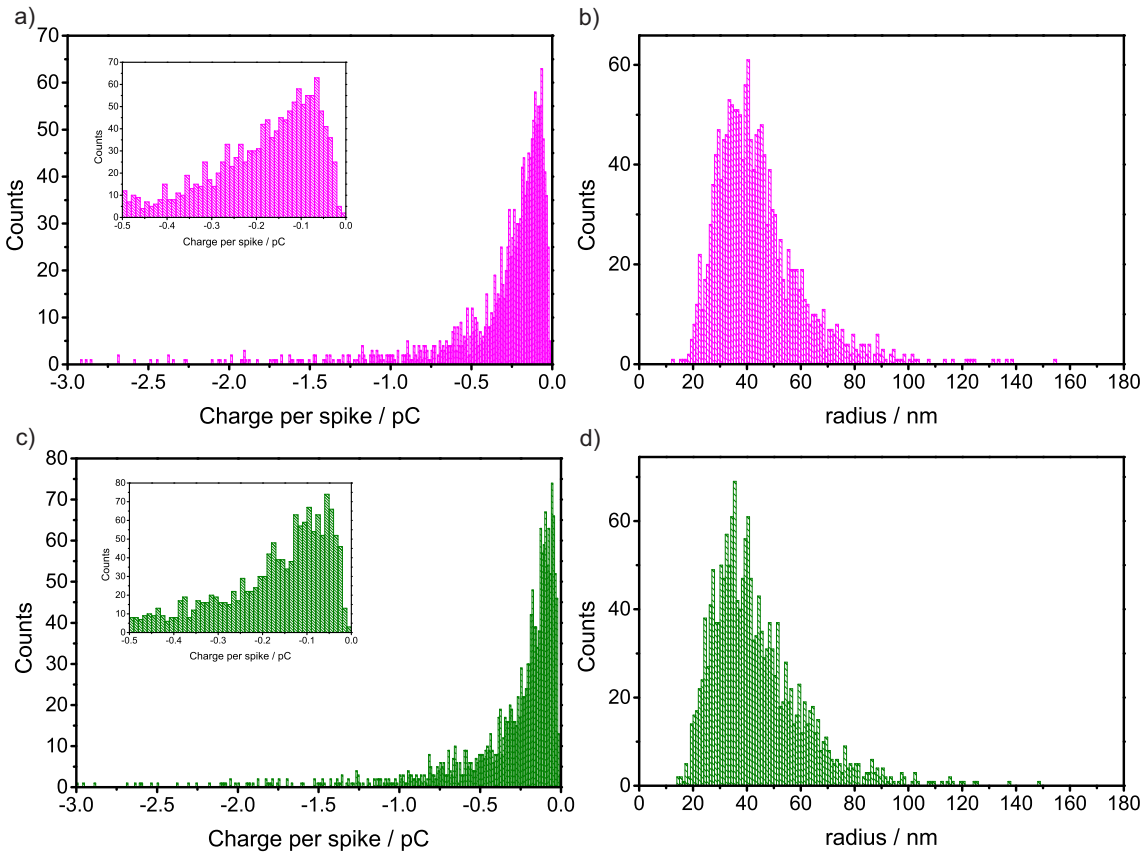


Figure 11.10: Charge distribution (a) and size distribution assuming n=3 (b) of 1581 spikes recorded for the reduction of nano-C_{60} (116 pM) impacting a gold microelectrode (r_e=4.2 µm) in MeCN (0.1 M NBu_4PF_6) at a potential of −1.74 V *vs.* Fc/Fc^+. Charge distribution (c) and size distribution assuming n=3 (d) of 1714 spikes recorded for the reduction of nano-C_{60} (116 pM) impacting a gold microelectrode (r_e=4.2 µm) in MeCN (0.1 M NBu_4PF_6) at a potential of −2.22 V *vs.* Fc/Fc^+. For clarity spikes with a charge above −3.0 pC have not been included in the charge distribution plots.

Figure 11.11 shows that if the charge transfer for a one electron reduction of a single impacting nano-C_{60} particle is fixed at $-0.10\,\mathrm{pC}$, the value observed for the cathodic particle coulometry experiment performed at E=$-1.27\,\mathrm{V}$ *vs.* Fc/Fc^+, we can make the assumption that a three electron transfer occurs for cathodic particle coulometry experiments at both $-1.74\,\mathrm{V}$ and $-2.22\,\mathrm{V}$ *vs.* Fc/Fc^+ as the mean charge measured at these potentials ($-0.36\,\mathrm{pC}$) is approximately three times the value of that for a one electron reduction at the single nanoparticle scale. This is further supported by reinterpretation of the charge transfer data measured at E=$-1.74\,\mathrm{V}$ *vs.* Fc/Fc^+ in terms of radius *via* equation 11.1 with the assumption n=3 giving a mean radius of $44 \pm 17\,\mathrm{nm}$ (figure 11.10b), in good agreement with mean radius values determined for the other two potentials studied (r_{NP}=$45 \pm 12\,\mathrm{nm}$ at E=$-1.27\,\mathrm{V}$ *vs.* Fc/Fc^+, r_{NP}=$44 \pm 17\,\mathrm{nm}$ at E=$-2.22\,\mathrm{V}$ *vs.* Fc/Fc^+). Hence for single nanoparticle studies, the third electron reduction of nano-C_{60} occurs at an earlier potential than that observed for the nanoparticle ensemble demonstrating that the electrochemical response of nano-C_{60} can differ when a nanoparticle ensemble is examined as opposed to an isolated nanoparticle.

11.4 Conclusions

This chapter reports on the electrochemical detection and sizing of individual nano-C_{60} nanoparticles demonstrating for the first time that nanoparticle-electrode impact studies can be performed in non-aqueous systems and cathodic particle coulometry can be applied to size carbonaceous nanoparticles. It is shown that a potential shift of the third electron transfer process occurs at the single nanoparticle scale when compared to the peak potential at which this process is observed in the voltammetry of a nano-C_{60} en-

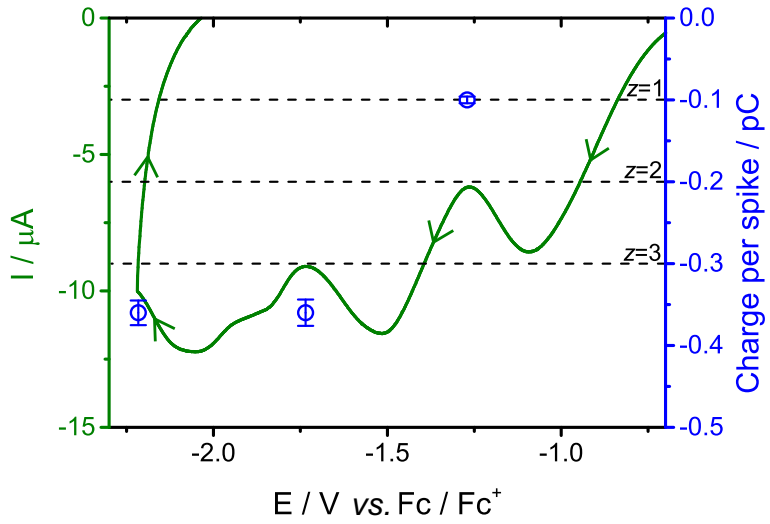


Figure 11.11: Voltammogram of a gold macroelectrode (r_e=0.8 mm) modified with 20 µL 0.1 mM nano-C_{60} particles scanned in MeCN (2 mM $Fe(C_5H_5)_2$, 0.1 M NBu_4PF_6) at a scan rate of 100 mV s^{-1} (green line) overlaid with a plot of potential against the mean charge transfer per impacting nano-C_{60} particle (blue symbols) where the error bars are determined by the standard error of the mean.

semble. Thus the electrochemical response is altered when changing from an ensemble of nano-C_{60} nanoparticles present on an electrode surface to an isolated nanoparticle scenario. Another factor that was found to strongly influence C_{60} electron transfer is the morphology of C_{60} on the electrode surface with significant changes in the voltammetric response observed between micro- and nano-C_{60} ensembles.

Bibliography

[1] E. J. E. Stuart, K. Tschulik, C. Batchelor-McAuley and R. G. Compton, *ACS Nano* DOI: 10.1021/nn502634n.

[2] H. W. Kroto, J. R. Heath, S. C. Obrien, R. F. Curl and R. E. Smalley, *Nature* **318** (1985) 162–163.

[3] C. Jehoulet, A. J. Bard and F. Wudl, *J. Am. Chem. Soc.* **113** (1991) 5456–5457.

[4] Q. S. Xie, E. Perezcordero and L. Echegoyen, *J. Am. Chem. Soc.* **114** (1992) 3978–3980.

[5] A. Y. S. Eng and M. Pumera, *Electrochem. Comm.* **43** (2014) 87–90.

[6] S. Barazzouk, S. Hotchandani and P. V. Kamat, *J. Mater. Chem.* **12** (2002) 2021–2025.

[7] P. V. Kamat, S. Barazzouk, K. G. Thomas and S. Hotchandani, *J. Phys. Chem. B* **104** (2000) 4014–4017.

[8] J. Brant, H. Lecoanet, M. Hotze and M. Wiesner, *Environ. Sci. Technol.* **39** (2005) 6343–6351.

[9] Z. G. Zhou, R. Lenk, A. Dellinger, D. MacFarland, K. Kumar, S. R. Wilson and C. L. Kepley, *Nanomedicine* **5** (2009) 202–207.

[10] G. Li, V. Shrotriya, J. S. Huang, Y. Yao, T. Moriarty, K. Emery and Y. Yang, *Nat. Mater.* **4** (2005) 864–868.

[11] P. R. Buseck, S. J. Tsipursky and R. Hettich, *Science* **257** (1992) 215–217.

[12] T. K. Daly, P. R. Buseck, P. Williams and C. F. Lewis, *Science* **259** (1993) 1599–1601.

[13] D. Y. Lyon, L. K. Adams, J. C. Falkner and P. J. J. Alvarez, *Environ. Sci. Technol.* **40** (2006) 4360–4366.

[14] C. M. Sayes, J. D. Fortner, W. Guo, D. Lyon, A. M. Boyd, K. D. Ausman, Y. J. Tao, B. Sitharaman, L. J. Wilson, J. B. Hughes, J. L. West and V. L. Colvin, *Nano Lett.* **4** (2004) 1881–1887.

[15] X. Y. Xiao and A. J. Bard, *J. Am. Chem. Soc.* **129** (2007) 9610–9612.

[16] X. Y. Xiao, F. R. F. Fan, J. P. Zhou and A. J. Bard, *J. Am. Chem. Soc.* **130** (2008) 16669–16677.

[17] S. J. Kwon, F. R. F. Fan and A. J. Bard, *J. Am. Chem. Soc.* **132** (2010) 13165–13167.

[18] R. Dasari, D. A. Robinson and K. J. Stevenson, *J. Am. Chem. Soc.* **135** (2013) 570–573.

[19] R. Dasari, B. Walther, D. A. Robinson and K. J. Stevenson, *Langmuir* **29** (2013) 15100–15106.

[20] R. Dasari, K. Tai, D. A. Robinson and K. J. Stevenson, *ACS Nano* **8** (2014) 4539–4546.

[21] J. H. Park, S. N. Thorgaard, B. Zhang and A. J. Bard, *J. Am. Chem. Soc.* **135** (2013) 5258–61.

[22] Y. G. Zhou, N. V. Rees and R. G. Compton, *Angew. Chem. Int. Ed.* **50** (2011) 4219–4221.

[23] K. Tschulik, B. Haddou, D. Omanovic, N. V. Rees and R. G. Compton, *Nano Res.* **6** (2013) 836–841.

[24] W. Cheng, X. F. Zhou and R. G. Compton, *Angew. Chem. Int. Ed.* **52** (2013) 12980–12982.

[25] H. Kasai, H. S. Nalwa, H. Oikawa, S. Okada, H. Matsuda, N. Minami, A. Kakuta, K. Ono, A. Mukoh and H. Nakanishi, *Jpn. J. Appl. Phys., Part 2* **31** (1992) L1132–L1134.

[26] W. T. Tan, E. B. Lim and A. M. Bond, *J. Solid State Electrochem.* **7** (2003) 134–140.

[27] M. F. Suarez, F. Marken, R. G. Compton, A. M. Bond, W. J. Miao and C. L. Raston, *J. Phys. Chem. B* **103** (1999) 5637–5644.

[28] C. Jehoulet, Y. S. Obeng, Y. T. Kim, F. M. Zhou and A. J. Bard, *J. Am. Chem. Soc.* **114** (1992) 4237–4247.

[29] A. M. Bond, W. J. Miao and C. L. Raston, *J. Phys. Chem. B* **104** (2000) 2320–2329.

[30] S. Deguchi, R. G. Alargova and K. Tsujii, *Langmuir* **17** (2001) 6013–6017.

[31] J. C. Lees, J. Ellison, C. Batchelor-McAuley, K. Tschulik, C. Damm, D. Omanovic and R. G. Compton, *ChemPhysChem* **14** (2013) 3895–3897.

[32] H. S. Toh, C. Batchelor-McAuley, K. Tschulik, M. Uhlemann, A. Crossley and R. G. Compton, *Nanoscale* **5** (2013) 4884–4893.

Chapter 12

Conclusions

This thesis has investigated the use of electrochemistry in the detection and characterisation of nanoparticles. Original results have been presented from experiments where an electrode is immersed in a nanoparticle containing solution where the nanoparticles move *via* Brownian motion and, from time to time, collide with the electrode. The nanoparticle collisions can be monitored directly, where the electrode is held at a potential to bring about the oxidation or reduction of the nanoparticle when it impacts, or indirectly, where the reduction or oxidation of a species in solution is electrocatalysed by an impacting nanoparticle. A progression of this method is the nanoparticle sticking and stripping technique, where nanoparticles that adsorb rather than rebound from the electrode upon collision accumulate over time before stripping voltammetry is employed to quantify the number of adhered nanoparticles.

The motivation behind a significant proportion of the work presented in this thesis is the increasing prominence of nanomaterials resulting in inevitable leaching into the environment and unknown associated risks. There are few techniques currently available to detect and characterise nanoparticles in the environment and electrochemistry offers a simple, portable and low cost route to nanoparticle sampling. It has been concluded that the nanoparticle impact technique can be used to quantify nanoparticles in solution

with a new methodology by which nanoparticle-impact data was analysed using the integrated flux equation and found to accurately determine unknown silver nanoparticle concentrations. The same direct detection method was proven to be suitable for use in seawater with accurate sizing of laboratory synthesised nanoparticles and those contained in a consumer product achieved in this environmental matrix. The sticking and stripping technique was also found to be applicable to the monitoring of nanoparticles in the environment with homemade electrodes used to detect commercial silver nanoparticles in seawater giving rise to a promising, semi-quantitative technique for monitoring nanoparticles that are present in low concentrations as the nanoparticles can be left to accumulate over time. This method has potential wide application in the cheap and easy measurement of nanoparticles of varying materials in different environmental waters e.g. rivers, streams.

Nanoparticle-electrode collisions of another environmentally important nanoparticle type, carbon, was studied *via* the direct method and it was concluded that this technique can be used to study the influence of scale on electrochemistry with an altered response observed for fullerene nanoparticles when trasitioning from a micro-ensemble to a nano-ensemble to an individual nanoparticle. Further work has focussed on improving the fundamental understanding behind this novel technique; a diffusional model was found to be appropriate for describing nanoparticle transport to the electrode surface while an investigation into indirect nanoparticle-electrode impacts, where the reduction of hydrogen peroxide was examined on impacting silver nanoparticles, provided new physical insight into the contact environment and was found to give complementary results to the direct method for silver nanoparticle sizing. Optimisation of the sticking and stripping technique was also carried out with an observed increase in the rate of nanoparticle sticking

at a DMSA modified "sticky" gold electrode giving rise to the conclusion that chemical modification of the electrode surface is beneficial and impacting on future analysis using this technique.

These original findings contribute significantly to the relatively unexplored area of nanoparticle detection *via* electrochemical methods providing a basis for further investigation into the value of this novel and promising nanoparticle-electrode impact technique.